Assessment of Chronic Toxicity of Petroleum and Produced Water Components to Marine Organisms

FINAL TECHNICAL SUMMARY

FINAL STUDY REPORT

PROJECT 6

Principal Investigators:

Gary N. Cherr
Richard M. Higashi
Jon M. Shenker

Co-Investigator

Teresa W.-M. Fan

The research leading to this report was supported by the Minerals Management Service as part of the Southern California Educational Initiative under Cooperative Agreement No. 14-35-0001-30471

May 31, 1993

ASSESSMENT OF CHRONIC TOXICITY OF PETROLEUM AND PRODUCED WATER COMPONENTS TO MARINE ORGANISMS

FINAL TECHNICAL SUMMARY

Principal Investigators:

Gary N. Cherr[1]
Richard M. Higashi[1]
Jon M. Shenker[2]

[1]University of California Davis-Bodega Marine Laboratory,
Bodega Bay, CA 94923

[2]Florida Institute of Technology, Melbourne, FL 32901

Co-Investigator:

Teresa W.-M. Fan
Department of Land, Air and Water Resources
University of California, Davis
Davis, CA 95616

May 31, 1993

STUDY TITLE: Southern California Educational Initiative

REPORT TITLE: Assessment of Chronic Toxicity of Petroleum and Produced Water Components to Marine Organisms

CONTRACT NUMBER: Cooperative Agreement No. 14-35-0001-30471

SPONSORING OCS REGION: Pacific

APPLICABLE PLANNING AREA: Pacific

FISCAL YEARS OF PROJECT FUNDING: 1990, 1991, 1992

COMPLETION DATE OF REPORT: April, 1993

COSTS: FY 1990: $78,000; FY 1991: $82,000; FY 1992: $82,000
CUMULATIVE PROJECT COST: $242,000

PROJECT MANAGER: G.N. Cherr

AFFILIATTION: Unuversity of California-Davis Bodega Marine Laboratory

ADDRESS: PO Box 247, Bodega Bay, CA 94923

PRINCIPAL INVESTIGATORS: G.N. Cherr, R.M. Higashi, and J.M. Shenker

KEY WORDS: Produced water; embryonic development, toxicity, sea urchin, mussel, kelp, shrimp, nuclear magnetic resonance spectroscopy, stress proteins

BACKGROUND: The largest discharge associated with offshore oil and gas production is produced water. In the Santa Barbara Channel, produced water is discharged into the coastal environment in 10-15 meters of water. As long-term effects on reproduction and development of marine organisms can often be subtle, it is difficult to assign cause-and-effect relationships amid the background of natural variability, particularly in an environment such as the Santa Barbara Channel where multiple complicating factors are present. Such high level of variations limits our ability to detect subtle impacts of contaminants. However, if the mechanism of action of toxicants under controlled laboratory conditions are better understood, the observed pattern of bioeffects in the natural environment can be more directly linked with specific contaminant(s). Such a marriage of laboratory and field studies must take place in order to achieve scientifically valid information that is also environmentally relevant. Among the myriad of effects that can be measured, gametogenesis and embryonic development are catagories that deserve special attention because of their relevance to effects at the population level. A mechanistic understanding of contaminant effects on cellular functioning during gametogenesis and embryonic development are generally unclear; understanding these is required for linking laboratory bieffects with field observations. Biological field surveys alone may not detect the cause of population changes in polluted environments due to the presence of other complicating factors. It has been suggested that the most promising approach would be to relate molecular and cellular alterations to individual-level physiological changes that lead to perturbations of reproduction and embryonic development. These effects are then relatable to potential impacts at the population level.

OBJECTIVES: 1) To determine the effects of produced water exposure in early life stages of marine plants and animals, at the cellular, subcellular, and physiological levels; 2) To determine

the effects of produced water exposure on reproduction in marine organisms, and to develop non-invasive approaches for assessing reproductive impairment.

DESCRIPTION: The effects of produced water (PW) was assessed on development in three ecologically and economically important species, the purple sea urchin (*Strongylocentrotus purpuratus*), the giant kelp (*Macrocystis pyrifera*), and the California mussel (*Mytilus californianus*). To determine the basis for effects of PW on these developing organisms, some fundamental studies were prerequisite. In the sea urchin embryo, a morphological study was conducted to elaborate the extent of the extracellular matrix during gastrulation. The effects of PW on this matrix and on embryonic development were then assessed. In the kelp, the development of gametophytes was elucidated at the subcellular level for the first time, and subsequent studies will define the perturbation of these events by PW. In the mussel embryo, the effects of PW on shell development was investigated. Furthermore, eggs and embryos from adults which were outplanted near the discharge were also studied. Finally, the biochemical response of embryos to PW was also defined.

To complement the research on early life stages described in the previous section, we also investigated the impact of PW on reproduction and health of adult organisms indigenous to the California coast. To assess reproductive success and organismal health, we developed a noninvasive approach utilizing nuclear magnetic resonance (NMR) spectroscopy and imaging. This technology has originally been developed for biomedical research and are now routinely used in clinical dignostics. We studied the utility of such approach for diagnosing the functioning of indigenous organisms. The principal advantages of the NMR approach are 1) long-term metabolic changes can be monitored on the same individual without interferences from intrinsic organismal differences; 2) metabolic information central to our understanding of organismal functioning and yet difficult to acquire with invasive approach can be obtained; 3) detailed structure information on important functional indicators are readily obtained. These advantages were illustrated in four separate studies on three marine invertebrates, *Mytilus edulis* (blue mussel), *M. californianus* (Calinfornia mussel), and *Syciona ingentis* (ridgeback prawn). Three of the studies emphasized on the development of NMR methodologies while the fourth applied the methodologies to investigating the chronic effect of PW on mussel reproduction.

SIGNIFICANT RESULTS AND CONCLUSIONS: Based on results using sea urchin embryos, it appears that embryos possess a much more extensive extracellular matrix than was previously thought. Furthermore, PW may perturb the later stages of embryonic development through affecting the quantity of the blastocoelic extracellular matrix. This is also manifested in the presence of abnormal spicules. These embryos also express a specific protein in response to PW, and it is not similar to the heat shock response; we speculate that this may be an extracellular matrix component. In kelp gametophytes, germination and nuclear events are temporally and spatially distinct. Furthermore, thsy are mechanistically distinct as well, with germination requiring actin microfilament integrity, while nuclear events require microtubule integrity. We are testing the hypothesis that PW specifically perturbs microtubule-based events. In mussel embryos, PW inhibits normal shell calcificationm, possibly due to the presence of competing divalent cations (i.e. barium). Furthermore, eggs from outplanted adults often possess abnormal chromosome morphologies; this results in their lack of viability. Embryos from these adults appear to show a decreased sensitivity to subsequent exposure to PW, indicating that a tolerance may have developed during gamete formation. A stress protein-like response was also observed in mussel embryos, but the protein expressed is not a typical stress protein with respect to molecular weight. Embryos derived from eggs from outplanted adults express this protein in the absence of PW, suggesting a protective role in subsequent PW response.

In adult mussels, non-invasive techniques were sucessfully developed to monitor biochemical responses and reactions *in vivo*. Important metabolites, energy compounds, and morphology were monitored *in situ*; these included intracellular pH, phosphoarginine, ATP, arginine kinase reaction kinetics, glycerophosphororylcholine (GPC), and ^{1}H imaging of

reproductive tissues. This research demonstrated that the noninvasive NMR approaches (^{31}P NMR spectroscopy and ^{1}H NMR imaging), together with correlative histological analysis, provided reliable assessments of gender-specific gametogenesis in mussels. Specifically, *in vivo* ^{31}P NMR revealed a specific phosphodiester indicator for oogenesis, in addition to providing information on gonadal energy budget. In a complementary fashion, ^{1}H NMR imaging enabled the distribution density of developing gametes across the entire gonad to be monitored.

When applied to follow the effect of PW exposure on mussel, both methods revealed the dynamics of chronic ovarian perturbations on the same individual, thus eliminating interferences arising from intrinsic heterogeneities in oogenesis of this species. Consequently, reliable conclusions could be drawn from a much smaller sample size. The changes observed suggest that PW exposure perturbed ovarian energy balance and caused ovarian degeneration in *M. californianus*. To the best of our knowledge, this is the first direct demonstration of perturbations in reproduction of organisms chronically exposed to PW under controlled laboratory conditions.

STUDY PRODUCTS:

Baldwin, J.D., M.C. Pillai, and G.N. Cherr. 1992. The reponse of sea urchin (*Strongylocentrotus purpuratus*) embryos to aqueous petroleum wastes includes the expression of a high molecular weight glycoprotein. *Mar. Biol.*, 114: 21-30

Cherr, G.N., R.G. Summers, J.D. Baldwin, and J.B. Morrill. 1992. Preservation and visualization of the sea urchin blastoceolic extracellular matrix. *Micr. Res. Tech.*, 22**:** 11-22

Fan, T.W-M., R.M. Higashi, G.N. Cherr, and M.C. Pillai. 1991. Aqueous petroleum wastes perturb reproduction in mussels as monitored *in vivo* by NMR spectroscopy and imaging. *Proc. of 12th annual SETAC Meeting,* Seattle, WA. pp. 221

Fan, T.W-M., R.M. Higashi, G.N. Cherr, and Pillai, M.C. (1992). Use Of Noninvasive NMR Spectroscopy And Imaging For Assessing Produced Water Effects On Mussel Reproduction. In: *Produced Water: Technological/Environmental Issues and Solutions.* J.P. Ray and F.R. Engelhardt, eds., Plenum Publishing, NY. pp. 403-414

Fan, T.W-M. and Lane, A.N. 1992. Identification Of Glycerophosphorylcholine In Mussel Ovarian Extracts By Two-Dimensional NMR. *Analyt. Biochem.*, 206:251-255

Fan, T.W.-M., R.M. Higashi, and Lane, A.N. 1992. Temperature Dependence of Arginine Kinase Reaction in the Tail Muscle of Live Sycionia ingentis as Measured In Vivo by ^{31}P NMR Driven Saturation Transfer. *Biochem. Biophys. Acta*, 1135:44-49

Fan, T.W.-M., R.M. Higashi, and Macdonald, J.M. 1991. Emergence and Recovery Response of Phosphate Metabolites and Intracellular pH in Intact Mytilus edulis as Examined In Situ by In Vivo ^{31}P NMR. *Biochim. Biophys. Acta* 1092:39-47

Garman, G.D., M.C. Pillai, and G.N. Cherr. 1991. Nuclear migration as an indicator of toxic response in the development of giant kelp gametophytes. *Proc. of 12th annual SETAC Meeting,* Seattle, WA. pp. 222

Higashi, R.M., G.N. Cherr, C.A. Bergens, T.W-M. Fan, D.G. Crosby. 1991. Toxicant isolation from aqueous petroleum wastes from the Santa Barbara Channel. *Proc. of 12th annual SETAC Meeting,* Seattle, WA. pp. 193

Higashi, R.M., G.N. Cherr, C.A. Bergens, T.W-M. Fan, and D.G. Crosby. 1993. Toxicant isolation from a produced water source in the Santa Barbara Channel. In: *In: Produced Water: Technological/Environmental Issues and Solutions*, J.P. Ray, ed., Plenum Publishing, New York, pp. 223-234

Pillai, M.C. , Baldwin, J.D. and Cherr, G.N. 1992a. Early development in an algal gametophyte:regulation of germination and nuclear events by cytoskeletal elements. Protoplasma, 170:34-45.

Pillai, M.C., Garman, G.D., Goff, L.J. and Cherr, G.N. 1992b. Nuclear events during early gametophytic development in a brown alga. *Mol. Biol. Cell*, 3:18a.

ASSESSMENT OF CHRONIC TOXICITY OF PETROLEUM AND PRODUCED WATER COMPONENTS TO MARINE ORGANISMS

FINAL STUDY REPORT

Principal Investigators:

Gary N. Cherr[1]
Richard M. Higashi[1]
Jon M. Shenker[2]

[1]University of California Davis-Bodega Marine Laboratory,
Bodega Bay, CA 94923

[2]Florida Institute of Technology, Melbourne, FL 32901

Co-Investigator:

Teresa W.-M. Fan
Department of Land, Air and Water Resources
University of California, Davis
Davis, CA 95616

May 31, 1993

TABLE OF CONTENTS

GENERAL INTRODUCTION

This research project focused on the toxicological effects of produced water (PW), a principal waste from oil production, on reproduction and early development of the California mussel, *Mytilus californianus,* the purple sea urchin, *Strongylocentrotus purpuratus,* and the giant kelp, *Macrocystis pyrifera.* As long-term effects on reproduction and development of organisms can often be subtle, it is difficult to assign cause-and-effect relationships amid the background of natural variability, particularly in an environment such as the Santa Barbara Channel where multiple complicating factors are present. Such high level of variations limits our ability to detect subtle impacts of contaminants. However, if the mechanism of action of toxicants under controlled laboratory conditions are better understood, the observed pattern of bioeffects in the natural environment can be more directly linked with specific contaminant(s). Such a marriage of laboratory and field studies must take place in order to achieve scientifically valid information that is also environmentally relevant. Among the myriad of effects that can be measured, gametogenesis and embryonic development are catagories that deserve special attention because of their relevance to effects at the population level. A mechanistic understanding of contaminant effects on cellular functioning during gametogenesis and embryonic development are generally unclear; understanding these is required for linking laboratory bieffects with field observations.

Biological field surveys alone may not detect the cause of population changes in polluted environments due to the presence of other complicating factors. It has been suggested that the most promising approach would be to relate molecular and cellular alterations to individual-level physiological changes that lead to perturbations of reproduction and embryonic development (Spies, 1987). Indeed, recent findings from the Southern Califoria Educational Initiative (SCEI) program have shown that PW discharges from Carpenteria impact reproductive development and growth of mussels (Osenberg and Schmitt, 1991; Osenberg et al., 1992; Fan et al., 1992), early embryonic development in sea urchins (Baldwin et al., 1992; Krause et al., 1992), larval settlement and metamorphosis in abalone (Raimondi and Schmitt, 1992), and development in giant kelp (Cherr et al., 1991; Garman et al., 1991). These effects are relatable to impacts at the population level.

The following is a final report on the research conducted under the proposal entitled "Assessment of Chronic Toxicity of Petroleum and Produced Water Components to Marine Organisms", G.N. Cherr, R.M. Higashi, and J.M. Shenker, Principal Investigators, T. W-M. Fan, Co-Investigator. It is organized into two main sections dealing with effects of PW on developing marine organisms (Section I), and effects on reproduction in adult organisms (Section II). For the applied investigations described below, considerable basic research in the areas of methods

development and establishment of the biological systems was prerequisite; as such, each section includes the description of this research as background for the work with PW. Seven peer reviewed publications have resulted from this research project, and largely contribute to the results described below. Each publication will be referenced as appropriate.

SECTION I

Effects of Produced Water on Developing Marine Animals and Plants

Introduction

Since the effects of pollutants at the most sensitive stages of the life cycle of any species provides a key to the biological success or failure of that species in polluted environments, it is particularly important to investigate the toxiclogical effects on early life stages. Presently, very little information is available regarding, the effects of PW on reproductive life stages of marine organisms, which is a vital link between impacts on individuals and on populations. We have utilized early life stages of key marine invertebrates and algae to investigate the impacts of produced water discharge in the marine environment.

The species utilized were important both ecologically and economically, and included the purple sea urchin, *Strongylocentrotus purpuratus*, the California mussel, *Mytilus californianus*, and the giant kelp, *Macrocystis pyfifera*. The early life stages of all three of these organisms have been utilized previously for assessing effects of pollutants; however, the studies described here focused on details of the toxic response which were previously unknown for any tocxicant, much less produced water. It should be noted that three of the four studies (sea urchin and kelp) described in this section have been published in the peer reviewed literature. The data presented here for the fourth (mussel) is currently being continued as part of an on-going SCEI-funded project ("Chronic Toxicological Effects of Produced Water on Reproduction and Development in Marine Organisms", G.N. Cherr and T. W-M. Fan, Principal Investigators), and will be submitted for publication this year.

Since it was necessary to investigate the cellular and subcellular details of the produced water responses in the different systems utilized, studies on the basic structures and functions were a prerequisite to the more applied toxicological investigations. Some of these more applied investigations are being completed as part of the above on-going SCEI-funded project, but were critically dependent on the research presented here.

STUDIES WITH THE SEA URCHIN

Analysis of Embryonic Development

One of the developmental processes most affected by produced water is early development, including gastrulation and spicule formation. Thus, the following study was a prerquisite to characterization of subsequent produced water effects on the subcellular events of early development. This research was published in *Microscopy Research Technique* (Cherr et al., 1992) and was an invited paper as part of a series on the ultrastructure of development.

It has been known for many years that the cleavage cavity and blastocoel of the sea urchin embryo are filled by a semi-solid extracellular matrix (ECM) containing glycoprotein and/or proteoglycan molecules ("blastocoelic jelly"; Monne and Slautterback, 1950; Monne and Harde, 1951; Strathman, 1989). The importance of the matrix and its component molecules in gastrulation events (including primary mesenchyme cell ingression, migration and adhesion, archenteron elongation, and secondary mesenchyme cell motility) has also been established by extensive experimental investigation (see reviews by Solursh, 1985; Galileo and Morrill, 1985; McClay and Ettensohn, 1987a,b).

However, the blastocoelic matrix has proven difficult to preserve using conventional aqueous chemical fixatives; thus differing views of its structure appear in various investigations (compare Kawabe, et al., 1981; Spiegel et al., 1989; Katow and Solursh, 1979; Morrill and Santos, 1985; Amemiya, 1989). Frequently it is preserved only partially and is often either extracted or collapsed onto the perimeter of the blastocoelic cavity. It is difficult to preserve because of its extreme hydration and the delicacy of its structural components. Many aqueous chemical fixatives and solvents used in ultrastructural protocols are known to extract ECM molecules (Sturgess et al., 1978).

Proper structural preservation of the blastocoelic matrix and its components is essential to an understanding of its assembly and spatial relationships in embryogenesis. The use of cytochemical probes to ECM molecules (eg. lectins, antibodies to fibronectin, laminin, CAM's, collagens and glycosaminoglycans, and regionally distributed ECM constituents, as well as embryonic cell types [McClay and Ettensohn, 1987a]) relies upon preservation protocols which retain the positions and reactivities of the substances comprising the ECM.

We present several techniques for the improved preservation and visualization of a blastocoelic matrix structure for light and electron microscopy and new information on blastocoelic matrix structure that we acquired with these methods. For the first time rapid freezing and freeze-substitution fixation have been used in combination with TEM and SEM in an investigation of the sea urchin blastocoelic matrix. Confocal microscopy has been employed in conjunction with lectin labelling to obtain optical sections of *intact* blastocoelic isolates.

These improved structural preservation methods and the use of confocal microscopy will permit a more meaningful *in situ* analysis of the blastocoelic ECM in sea urchin development.

Materials and Methods

Embryo Culture and Preparation

Purple sea urchins (*Strongylocentrotus purpuratus*) were collected at Point Arena, CA. and induced to shed their gametes by injection of 0.5M KCl. Fertilized eggs were washed over 20 μm nylon mesh to remove excess sperm, and cultured in 0.45 μm filtered seawater at 15° C for 30-36 hrs. at about 1500 embryos/ml. At the appropriate embryonic stage, either mesenchyme blastula (30 hrs.) or primary invagination (36 hrs.), 10 ml aliquots of the embryo suspension were removed, and embryos pelleted via hand centrifugation. The concentrated embryos were either rapidly pipetted onto Nitex (Tetko) for subsequent freeze-fixation, or washed in dissociation buffers as described below.

Rapid Freezing , freeze-substitution, and Sample Preparation

Rapid freezing and freeze-substitution for light and electron microscopy were carried out as described by Cherr et al. (1990) and Yudin et al. (1988). Propane gas (which becomes liquified at -196°C) was condensed into a copper cup (~3 ml) immersed in a dewar containing liquid nitrogen (LN_2). The liquid propane was cooled further for at least 30 min. prior to plunge freezing of embryos. Concentrated living embryos were pipetted (20 μl) onto 1-2 mm wide by 1 cm long pieces of 150 mm Nitex nylon mesh held in fine forceps. The mesh with a monolayer of concentrated embryos was plunged into the liquid propane and remained immersed for 30 sec. Care was taken not to pre-cool the embryos over the dewar prior to immersion. The samples were then rapidly transferred to LN_2 and held there until placed in methanol (described below).

For light microscopy and histochemistry, frozen embryos were placed in 100% dry (molecular sieve) methanol (with or without 5% of 2,2 dimethoxypropane; Johnson et al., 1976) at -80°C and incubated at this temperature for 3-5 days in an ultracold freezer (-80°C) . Samples were then warmed slowly (-20°C for 2hrs. and 4°C for 2hrs.) to room temperature, and infiltrated and embedded in Historesin (LKB). Thick sections (2 μm) were cut dry with glass knives on a Reichert Ultracut E. Thick sections and whole mounted embryos prepared for TEM (see below) were viewed with Hoffman modulation contrast optics on an Olympus BH2 microscope.

For TEM, frozen embryos were placed in dry methanol containing 1% tannic acid and 5% dimethoxypropane at -80°C and incubated as above. After 3-5 days, samples were thoroughly washed in dry methanol (4 times at -80°C), placed in methanol containing 1% OsO_4, and incubated at -80°C for 2 hrs. Samples were then warmed to room temperature as described above. Samples were washed with methanol at room temperature and embedded in Spurr's epoxy resin. Ultrathin and thick (0.5 μm) sections were cut using diamond knives and stained with

uranyl acetate and lead citrate or with toluidine blue, respectively. Sections were viewed with a JEOL 100CX at 60KV.

For SEM, frozen embryos (aliquots of the same embryos used for TEM) were processed as described for TEM, except critical point dried instead from dry methanol rather than embedded in resin. Samples were dry-fractured according to Morrill (1986). Complementary stubs were then coated with 20 nm of gold and viewed in a Hitachi 502 scanning electron microscope operated at 5-10 KV.

Blastocoelic Bag Preparation

For isolation of blastocoelic bags, the following solutions (Harkey and Whiteley, 1980) were employed: calcium and magnesium free artificial sea water containing 100 mM EDTA, pH 8 (CMFSW). Dissociation medium (DM): 1M glycine, 100 mM EDTA, pH 8. Blastocoelic bag isolation medium (BIM): 40% CMFSW, 40% 1M dextrose, 20% distilled water, pH 8. Percoll Stock: 84% Percoll TM (Pharmacia Fine Chemicals): 16% 5X CMFSW. Sucrose stock: 1M sucrose, 100 mM EDTA, 1M tris base, pH 8.

Early mesenchyme blastula stage embryos were dissociated into epithelial cells and blastocoelic "bags" by the following procedure developed by Harkey and Whiteley (1980). A lightly packed pellet of embryos were washed three times by hand centrifugation with 10 volumes of CMFSW, twice with 5 volumes of DM, and then resuspended in 20 volumes of BIM. All solutions were kept on ice and all washes were performed as quickly as possible. The BIM cell/bag suspension was kept on ice for 30 minutes with light mixing every 5 min. to achieve total dissociation of epithelial cells from the basal lamina. After dissociation on ice for 30 minutes, 4.0 ml of BIM cell/bag suspension was layered on top of 2.0 ml 19% Percoll stock diluted in BIM in a 13 x 100mm borosilicate tube. The preparation was centrifuged for 20 minutes at 650 g in a Sorvall HB-4 rotor with a 2.0 ml sucrose stock cushion. Concentrated blastocoels were collected from the BIM suspension/Percoll interface while epithelial cells were concentrated on the sucrose cushion. Blastocoels were attached to poly-l-lysine (0.01%) coated 10 well slides by placing one drop of CMFSW in each well followed by a drop of concentrated isolated blastocoels or a cell/bag suspension, and were allowed to settle for 30 minutes on ice. The attached basal laminar bags were then fixed in paraformaldehyde (2% diluted in BIM) for 30 minutes, transferred to CMFSW and stored at 4°C.

Lectin Labelling

Slides with blastocoelic bags attached and 2 um thick Historesin sections of freeze substituted embryos were washed twice in Tris buffered saline (TBS; 0.9% NaCl, 10 mM tris base, pH 7.5) then incubated for 10 minutes in TBS containing 5 mg/ml bovine serum albumin and 10 mM manganese and calcium (TBS blocking solution). These samples were then incubated with fluorescein conjugated Concanavalin A (FITC-Con-A, recognizing mannose and

glucose, E-Y Laboratories) at a concentration of 50 mg/ml in TBS blocking solution, for one hour at 23°C. Slides were then washed three times in TBS and mounted with 0.4% sodium azide in TBS. Control samples were treated with FITC-Con A that had been preincubated with 200mM a-methyl-mannoside. Slides were viewed by epifluorescence microscopy. Blastocoelic bags were optically sectioned using a Bio-Rad MRC 600 confocal microscope using the BHS filter pack (488nm excitation wavelength) and a 20x objective lens.

Alcian Blue Staining

Alcian Blue can differentiate between sulfated and carboxylated mucopolysaccharides at different pH's (pH 1.0 and pH 2.5 respectively; Pearse, 1968). Slides with attached blastocoels were stained for 30 minutes in 1.0% Alcian Blue 8GX (Sigma Chemical Company) in 0.1 N HCl (pH 1.0) or in 3% acetic acid (pH 2.5) followed by washing for 5 minutes with running water. Slides were then mounted in water and observed by phase contrast microscopy.

Results

Light Microscopic Views of the Blastocoelic ECM

The blastocoelic cavity appears transparent with the light microscope in both living embryos and those fixed with conventional "wet chemical" fixatives. In contrast, embryos prepared using the rapid freezing and freeze-substitution methods described above exhibited an obvious fibrous ECM within the blastocoelic cavity when viewed as whole mounts (Fig. 1). Lamellipodia/filopodia of PMC's could also be observed in these preparations. Although there was variability, the orientation of this ECM appeared to be generally along the animal-vegetal axis. Additional details of the network within the blastocoel could be observed in thick sections of resin embedded embryos (Fig. 2). Figure 2 also demonstrates that the PMC's directly contacted stained fibrils of the ECM. Little or no structure is observed within the blastocoel when conventional fixatives are employed. These preparations also suggested that the PMC's are in contact with the ECM.

In order to develop a probe which would permit visualization of the blastocoelic ECM at the light microscopic level, several different FITC conjugated lectins were screened for their ability to label the matrix. Con A was chosen as the most convenient probe since it labelled the ECM consistently and intensely relative to other lectins. FITC-Con A labelled the blastocoelic ECM and portions of epithelial cells and PMC's in Historesin sections (Figs. 3A and B). The label observed in PMC's was restricted to small spherical structures which appeared to be vesicles either within or on the PMC's.

Con A staining of intact blastocoelic bag preparations ("bags"), revealed that the blastocoel contains fibrillar-like material. This blastocoelic ECM appears to be responsible for the majority of the observed labelling with the lectin (Figs. 4A and B). The vegetal region surrounding the area of the presumptive blastopore in bags isolated from mesenchyme blastula appeared to label more intensely than other regions (Fig. 4A); this may be due to an increase in concentration of blastocoelic ECM components in this region, or due to localized increase in thickness of basal lamina constituents which also bind Con A. Confocal optical sectioning (at 5 μm intervals) of Con A labelled bags clearly demonstrates that the labelled fibrillar network extends throughout the blastocoel and is not just present on the surface of the bag (Figs. 5A-D). In fact, the only surface labelling may be at the vegetal plate, where a ring of intense labelling could be observed surrounding the presumptive blastopore.

Alcian blue stained bags at pH 1.0 equally as well as pH 2.5 (not shown), demonstrating the presence of sulfated constituents. This staining clearly showed the network-like structure of the hydrated, non-frozen blastocoelic ECM (Fig. 6). Once again, these preparations demonstrate the intensely staining ring of ECM surrounding the vegetal plate (Fig. 6).

Ultrastructural Views of the ECM

SEM of dry-fractured, freeze substituted, early gastrulae showed that the blastocoelic cavity contains an elaborate ECM (Figs. 7 and 8). PMC's were also observed within the blastocoelic ECM. The ECM fibers appeared to be oriented both slightly oblique (Fig. 7) and parallel (Fig. 8) to the animal-vegetal axis. However, the majority of embryos at these stages appeared to exhibit the parallel (animal-vegetal) orientation of the major structural elements of the matrix. The ECM was frequently detached from the blastocoelic wall in critical point dried embryos. Since the matrix completely fills the blastocoel in resin embedded preparations, we attribute the separation to differential shrinkage during critical point drying.

At higher magnifications it was apparent that the blastocoelic ECM comprises long, vertical, fenestrated sheets rather than only fibrils (Fig. 9). These sheets ranged from 0.1 to 0.5 μm in thickness and were interconnected by filaments 0.1 μm in diameter. The distance between individual sheets ranged from 1 to 3 μm. The blastocoelic ECM had connections to the surface of the blastocoelic wall; this connection was presumably to the basal lamina.

With transmission electron microscopy, the ECM appeared as a network of continuous fibrils that were variable in thickness (0.1-0.4 μm) and were interconnected by even finer fibrillar elements (Fig. 10). The distance between fibrillar elements, 1-4 μm, was similar to that measured in the SEM. The blastocoelic ECM attached at discreet points along the surface of epithelial cells, which exhibited adequate fixation with a minimal amount of ice crystal damage (Fig. 10). At higher magnifications, the details of ECM / cell surface interactions could be observed (Fig. 11). In these preparations, the basal lamina could be distinguished from the blastocoelic ECM since the basal lamina appeared as an extremely thin, electron dense coat or glycocalyx (approximately 76 nm in thickness), closely apposed to the epithelial cell plasma membrane. The blastocoelic ECM appeared to contact the basal lamina along the cell surface. Fibrillar sheets of the blastocoelic ECM attached to the basal lamina on the epithelial cell surface at 1-2 μm intervals. Between these attachment sites, the blastocoelic ECM closely apposed the basal lamina (Fig. 11). While the basal lamina and blastocoelic ECM's could be distinguished in the freeze substituted preparations, both ECM's appeared ultrastructurally similar in being composed of fine filamentous substructural elements.

When viewed at higher magnification, stereo pair SEM's showed that the blastocoelic ECM was attached to the surfaces of primary mesenchyme cells with the same periodicity as the spacing of the sheets in the blastocoel (Fig. 12). In this stereographic view, one can appreciate the three dimensionality of the ECM/cell relationships, as well as the organization of the ECM itself.

Transmission electron micrographs of the blastocoelic ECM and the PMC's are shown in Figs. 13 and 14 A,B. The matrix surrounding the PMC's consisted of parallel fibrils (sheets in

section) that were cross-linked by thinner filaments (Fig. 10,13). The fibrils were attached to the PMC's at 1-2 μm intervals; these attachments were occasionally at filopodial extensions, but were more often attached directly to the PMC surface (Figs.13 and 14 A,B). It should be noted that the PMC's did not possess a surface coat (Fig. 14 B) and that the blastocoelic ECM was in direct contact with the PMC plasma membrane rather than a recognizable extracellular coat. The blastocoelic ECM appeared fibrillar in TEM preparations, and there appeared to be alternating thick and thin regions of some fibrils (Figs. 11 and 13). This suggests that the structural elements of the matrix are not simple cylindrical structures, but sheet-like in nature.

Discussion

We have employed rapid freezing/ freeze-substitution methodologies to preserve the embryonic blastocoelic ECM and basal lamina. In addition, we also isolated blastocoelic bags and used epifluorescence, conventional and confocal microscopy in conjunction with an ECM probe to substantiate much of the data from frozen specimens.

The blastocoelic ECM's are extremely hydrated matrices and have been, at best, difficult to preserve for microscopy at both the light and electron microscopic levels. Furthermore, the distinction between the basal lamina and the blastocoelic ECM has been difficult to establish in previous studies. The elucidation of the *intact* ECM is a critical prerequisite to studies of cell/ECM interactions using molecular probes, particularly with respect to distinguishing blastocoelic ECM from basal laminar constituents.

We have shown that the blastocoelic ECM is organized into fibrillar sheets oriented parallel to the animal-vegetal axis. These sheets fill the entire blastocoelic cavity to a much greater extent than previously described. Furthermore, we have clearly differentiated the blastocoelic ECM from the basal lamina present on epithelial cell surfaces. This study has also demonstrated a distinct ring of ECM material surrounding the presumptive blastopore at the time of primary mesenchyme cell ingression.

The ECM of Frozen Embryos

Extracellular matrices contain glycosaminoglycans associated with a protein core in the form of proteoglycans. These are typically hydrated to a great degree and are difficult to preserve for microscopic examination (Heingard and Paulsson, 1984; Hascall, 1980; Talbot and DiCarlantonio, 1984; Nichols et al., 1985; Arsenault et al., 1988), particularly during dehydration of samples when they collapse due to elimination of water. While divalent cationic dyes added to the fixative (eg. ruthenium red) stabilize the ECM structure to some degree, the cross-linking of

charged molecules still causes distortion and does not prevent shrinkage during removal of intramolecular water (Luft, 1971; Spiegel et al.,1989).

The rapid freezing of living tissue, followed by freeze-substitution with an appropriate solvent/chemical mixture which replaces the ice ("substitutes") at -80° C, is known for preserving cell ultrastructure and associated ECM's (see Rehbun, 1974 and Gilkey and Staehelin, 1986 for reviews). In addition to rapidly "freezing" biological activity, this methodology has the advantage of allowing fixtives (in this study, tannic acid and OsO_4) to penetrate tissue or cells at -80° C prior to becoming active (eg. OsO_4 is only chemically active above -20° C). A major disadvantage is the formation of intracellular ice crystals upon freezing, which can cause damage to specimen ultrastructure.

In the specific case of the blastocoelic ECM, rapid freezing and freeze-substitution enabled the maintanence of the basic structure of the ECM based on views of the ECM in hydrated, non-frozen specimens. We cannot rule out the possibility that the spaces between fibrillar sheets were created artifactually as ice crystals formed in this hydrated material during freezing, thus forcing ECM material against the structural "skeleton" of the matrix and the basal lamina. However, Cherr et al. (1990) demonstrated that subtle disruptions (via limited proteolysis) in mammalian ECM's, could be resolved using the same rapid freezing/freeze substitution methods described in the current study. Thus it is possible that the "pores" or spaces observed in TEM views of the blastocoelic ECM may be filled with electron lucent material which does not stain with OsO_4, lead, or uranium. This hypothesis also may explain why the sheets observed in SEM are less obvious in the TEM. Nevertheless, the continuous, alternating thick/thin appearance of the ECM in the TEM fully supports the view of a sheet-like structure. In any given ultrathin section, the "fibrils" appear continuous; this could only occur in sectioned material that was significantly thicker than 0.1-0.4 μm (eg. a sheet-like structure), since such cylindrical structures would rapidly pass out of the plane of section.

The appearance of the sea urchin embryo ECM as an organized network of fibrillar-like elements in rapidly frozen, freeze substituted embryos is similar to freeze substituted ECM's in previous light microscopic and transmission electron microscopic studies (Abed and Crawford,1986; Summers et al., 1987; Arsenault et al., 1988; Yudin et al., 1988; Cherr et al., 1990). The appearance of the blastocoelic ECM as interconnected sheet-like structures in SEM views is very different than previous SEM studies which showed the ECM as randomly organized filamentous material which only partially filled the blastocoelic cavity (Katow and Solursh, 1979; Kawabe et al., 1981; Morrill and Santos, 1985). In addition, the use of freezing methodologies has enabled the preservation of the animal/vegetal orientation of the blastocoelic ECM, and the demonstration of the increased extent of the matrix in the cavity as compared to conventional fixation and dehydration procedures.

The animal-vegetal and parallel orientation of the blastocoelic ECM observed in this study is consistent with other studies which suggested that the sea urchin embryo blastocoel possesses parallel bundles of collagen fibrils (Crise-Benson and Benson, 1979) and that cell migration and guidance in amphibian gastrulation utilizes fibrillar ECM components oriented along the animal pole-blastopore axis (Nakatsuji, 1984; Keller and Winklbauer, 1990). Our study demonstrates that the PMC's migrate through the blastocoelic matrix at some distance from the blastocoelic wall. If the matrix collapses during fixation or dehydration, the PMC's are brought into contact with the epithelial wall. Furthermore, the frequent association of the ECM with filopodia/lamellipodia also supports the hypothesis that the PMC's may utilize the parallel blastocoelic ECM sheets as a substratum for attachment and guidance. Once again, such a system has been suggested for amphibian gastrulation (Nakatsuji, 1984). Migration of PMC's during sea urchin gastrulation also appears to involve the ECM for cell guidance (Solursh, 1986, for review). Interestingly, archenteron elongation during gastrulation occurs along the vegetal to animal axis in *S. purpuratus* embryos, and parallels the orientation of the ECM structural elements.

Previous studies on ECM's associated with the sea urchin blastocoelic cavity have suggested that the basal lamina ranges from 100-150 nm in thickness (Wolpert and Mercer, 1963; Katow and Solursh, 1979) and may or may not be distinguished from the blastocoelic matrix (DeSimone and Spiegel, 1986; Spiegel et al., 1989). In freeze substituted embryos, the structure assumed to be the basal lamina appears as a thin (~75 nm) "fuzzy" glycocalyx closely apposed to the epithelial cell plasma membrane. This epithelial cell coat could be distinguished from the overlying blastocoelic ECM which appeared "loosely" attached to it; however, both the basal lamina and the blastocoelic ECM appeared similar in substructural morphology and may represent the same material.

It has been suggested that the basal lamina disappears from the basal surface of presumptive PMC's (Solursh, 1986). This is consistent with a hypothesis that the migration of presumptive PMC's at the time of ingression depends on the disappearance of their cell coats (basal lamina), enabling direct contact between the PMC plasma membranes and the blastocoelic ECM and thus stimulating migratory behavior. In other systems it is known that ECM constituents can stimulate migratory behavior as well as cell shape changes when they interact with the plasma membrane (Hay, 1984; Turley et al., 1990). This hypothesis may be approached experimentally in sea urchin gastrulation in the future.

The ECM of the Hydrated Blastocoel

The use of isolated blastocoelic bags enables probes and stains to have access to the blastocoel and can aid in determination of its constituents (Spiegel et al., 1983). In this study, the

use of alcian blue (for sulfated constituents) and FITC-Con A (for mannose residues) with blastocoelic bag preparations substantiated the presence of an organized fibrillar network throughout the entire blastocoelic cavity. The use of optical sectioning in the confocal microscope demonstrated an absence of surface Con A labelling, except perhaps in a ring surrounding the blastopore. This ring was also observed in alcian blue preparations viewed with transmitted light and conventional microscopy. As shown in previous studies, the sulfated constituents of the blastocoel are more concentrated in the vegetal region (Sugiyama, 1972). However, to our knowledge, such a ring surrounding the presumptive blastopore has not been described previously . Whether this ring is stage-specific (transient) and forms as a result of movement of basal laminar components, or is artifactual, remains to be determined.

During isolation of the blastocoelic bags, the epithelial cells dissociate readily from the blastocoel, while PMC's (even cells that are not completely within the blastocoel) are very difficult to dissociate from the ECM. This indicates a strong adhesive association between the PMC's and the blastocoelic matrix. The TEM data from frozen embryos suggest that the blastocoelic ECM is more loosely associated with the basal lamina on the surfaces of epithelial cells than with the plasma membrane of PMC's. Thus, we suspect that the basal lamina remains with the dissociated epithelial cells and is not associated with the isolated blastocoelic bags, except possibly at the vegetal ring. A careful examination of frozen/freeze-substituted, dissociated epithelia would be useful prior to future interpretation of isolated bag studies.

In this study, we have presented methods for both light and electron microscopic investigations of the sea urchin blastocoelic ECM's. The use of rapid freezing and freeze-substitution clearly offers advantages over conventional methodologies for preserving the highly hydrated ECM. Although not demonstrated in this study, these preparatory methods are also useful for preserving antigenicity or reactivity of cellular and extracellular constituents (Murata et al., 1985; Cherr et al., 1990). Thus detailed localization of specific ECM and/or cellular antigens can be accomplished using a combination of blastocoelic bags and frozen embryos.

Figures 1-3

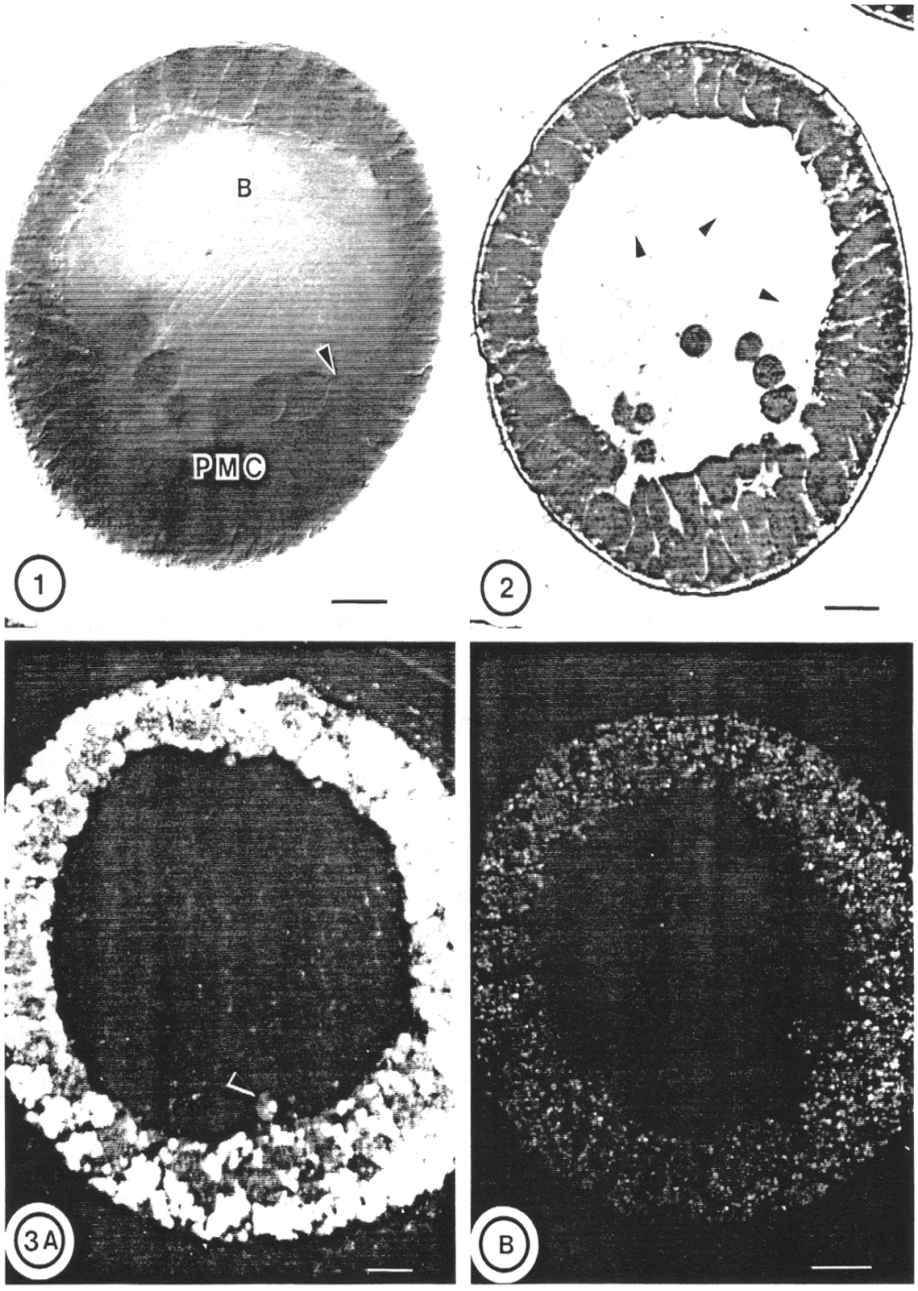

Fig. 1. Whole mounted mesenchyme blastula that had been rapidly frozen, freeze substituted and osmicated as described in Materials and Methods (see TEM processing). Note the fibrillar material in the blastocoel (B), and its orientation along the animal-vegetal axis. Lamellipodia of primary mesenchyme cells (PMC) at the vegetal region can be observed (arrow). Bar = 10 μm.

Fig. 2. Thick section (0.5 μm, Spurr's epoxy resin) of toluidine blue stained embryo prepared by rapid freezing and freeze substitution, showing the fibrillar network of the blastocoelic ECM (arrows). The PMCs are in contact with the ECM. Bar = 10 μm.

Fig. 3. **A:** Historesin section (2 μm) of mesenchyme blastula stage embryo prepared by rapid freezing and freeze substitution incubated with 50 μg/ml FITC-Con A. Note the labelling of the blastocoelic ECM, the fluorescence in the PMC in the blastocoel (arrow), and vesicles in epithelial cells. Bar = 10 μm. **B:** Control for FITC-Con A. Con A was preincubated with 200 mM a-methyl mannoside prior to incubation with the embryo. Bar = 10 μm.

Figures 4-5

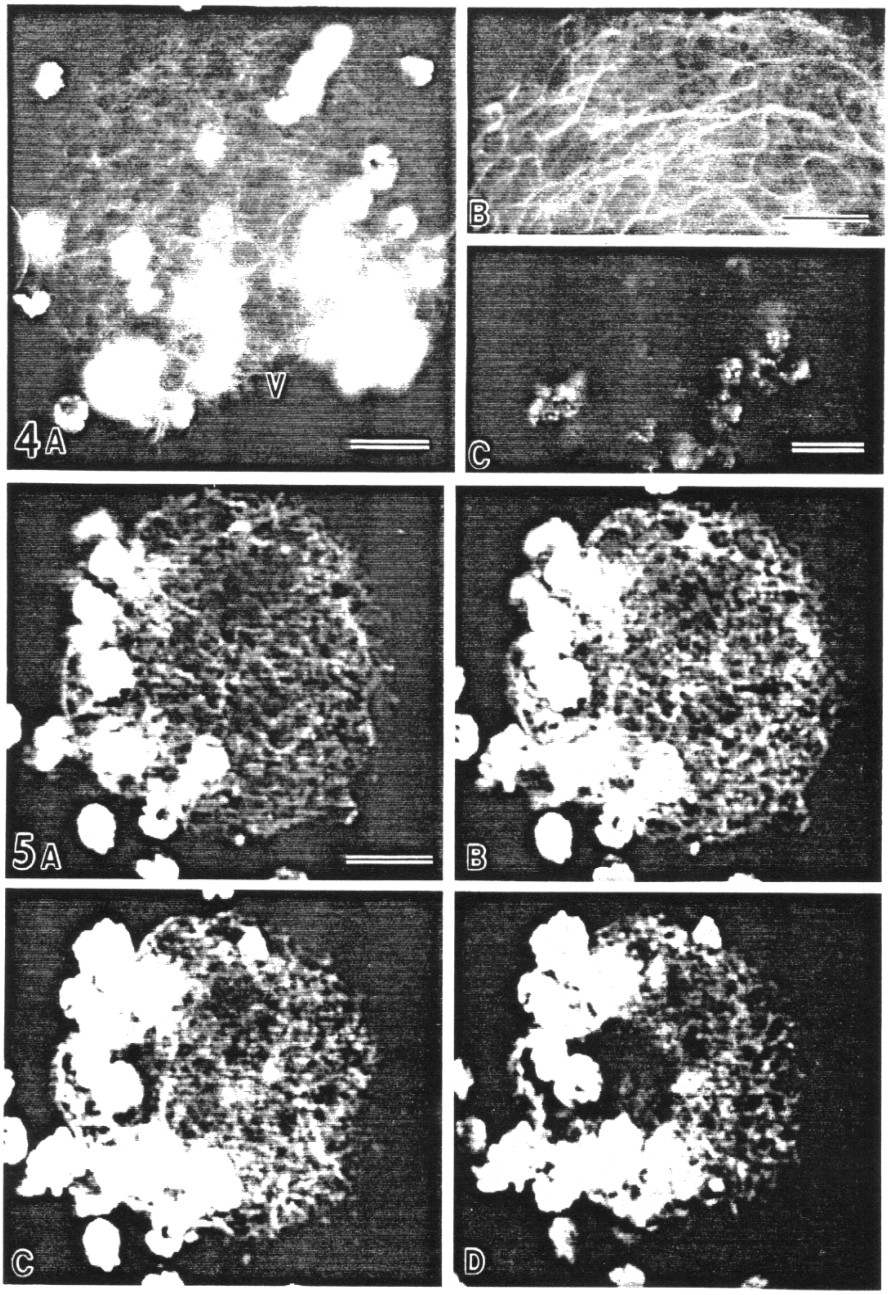

Fig. 4. **A:** TRITC-Con-A labelling of a fixed (paraformaldehyde) blastocoelic bag isolated from early mesenchyme blastula (see Materials and Methods). Fibrillar material of the blastocoelic ECM labels. The ECM in the vegetal (V) region of the bag exhibits increased labelling. Bar = 20 μm. **B:** Higher magnification of TRITC-Con A labelled blastocoelic ECM showing fibrillar network in an isolated bag. Bar = 20 μm. **C:** Control of TRITC-Con A. Con A was preincubated with 200 mM α-methyl mannoside prior to incubation with the bag. Bar = 20 μm.

Fig. 5. Four consecutive confocal optical sections at 3 μm intervals through a fixed blastocoelic bag from early mesenchyme blastula labelled with TRITC-Con A. These 12 μm were taken from the interior of the isolated bag. The presence of a fibrous ECM throughout the blastocoelic cavity is demonstrated. These bags were isolated from mesenchyme blastulae and dissociated epithelial cells can be observed in these preparations. Bar = 20 μm.

Figure 6

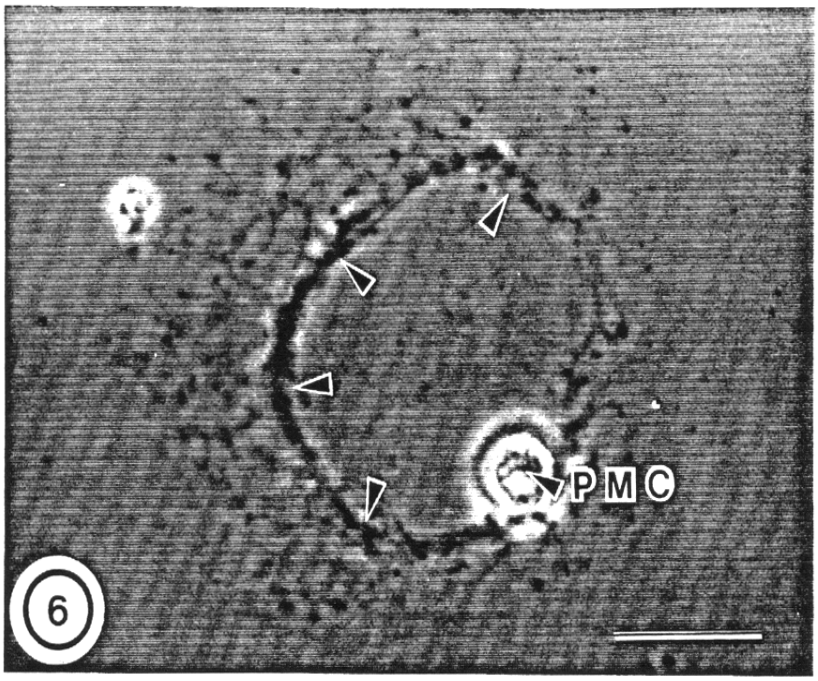

Fig. 6. A vegetal view of Alcian Blue (pH 1.0) stained blastocoelic bag from early mesenchyme blastula showing honeycomb-like net of the blastocoelic ECM. This bag is slightly distorted due to adhesion to the glass slide. Intensive staining of a ring of fibrillar material (arrows) can be observed in the vegetal region surrounding the blastopore. PMC, primary mesenchyme cell. Bar = 10 μm.

Figures 7-8

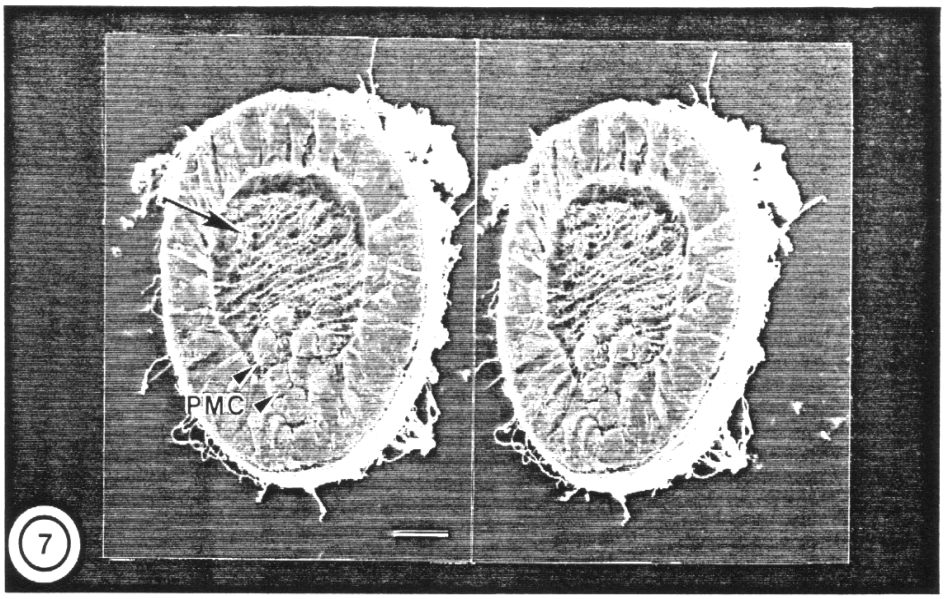

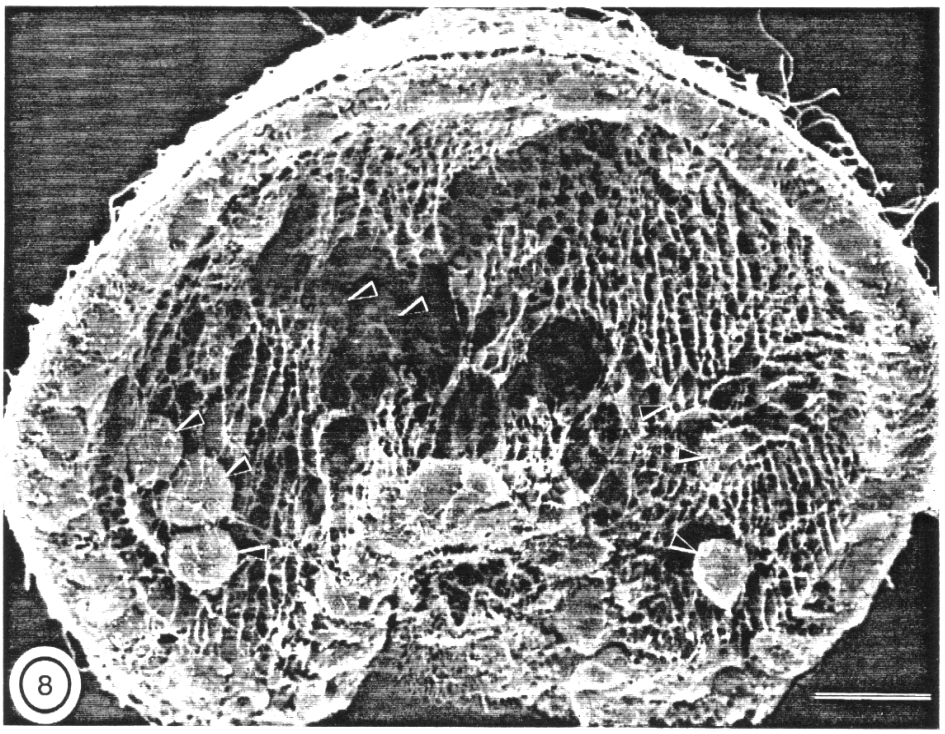

Fig. 7. SEM stereo pair of early mesenchyme blastula stage freeze substituted embryo that has been dry-fractured. The blastocoelic matrix (arrow) fills the whole blastocoelic cavity and is arranged in parallel fibrous sheets. The orientation of the ECM in this embryo is not in the animal-vegetal axis. The primary mesenchyme cells (PMC) are intimately associated with the ECM. Bar = 10 μm.

Fig. 8. SEM of fractured early gastrula stage embryo showing a ring of primary mesenchyme cells (arrows) in the blastocoelic matrix. The matrix appears to be oriented in the animal-vegetal axis and is throughout the blastocoelic cavity. Bar = 10 μm.

Figure 9

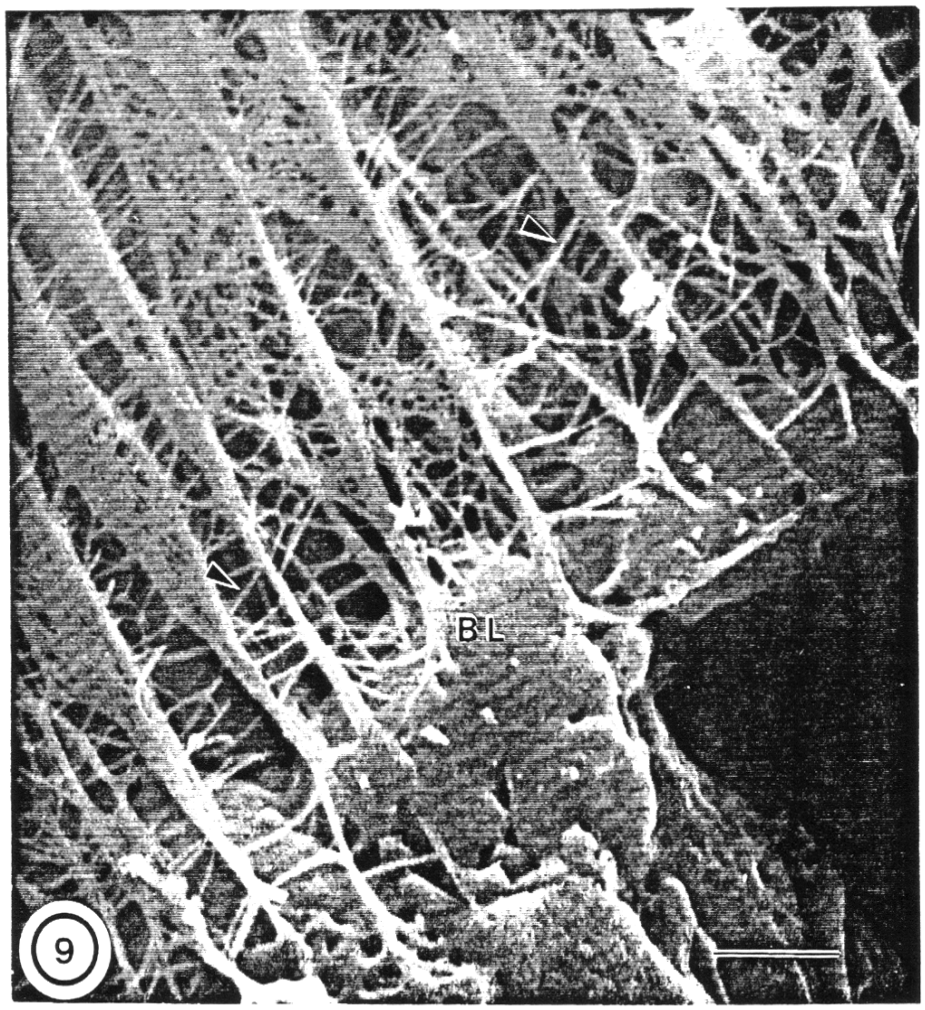

Fig. 9. High magnification SEM of the blastocoelic ECM. Note the fenestrated parallel sheets which are interconnected by thin filamentous crossbridges (arrows). The blastocoelic ECM appears to attach to the smooth perimeter surface of the blastocoelic cavity, which is presumably the basal lamina (BL). Bar = 2 μm.

Figures 10-11

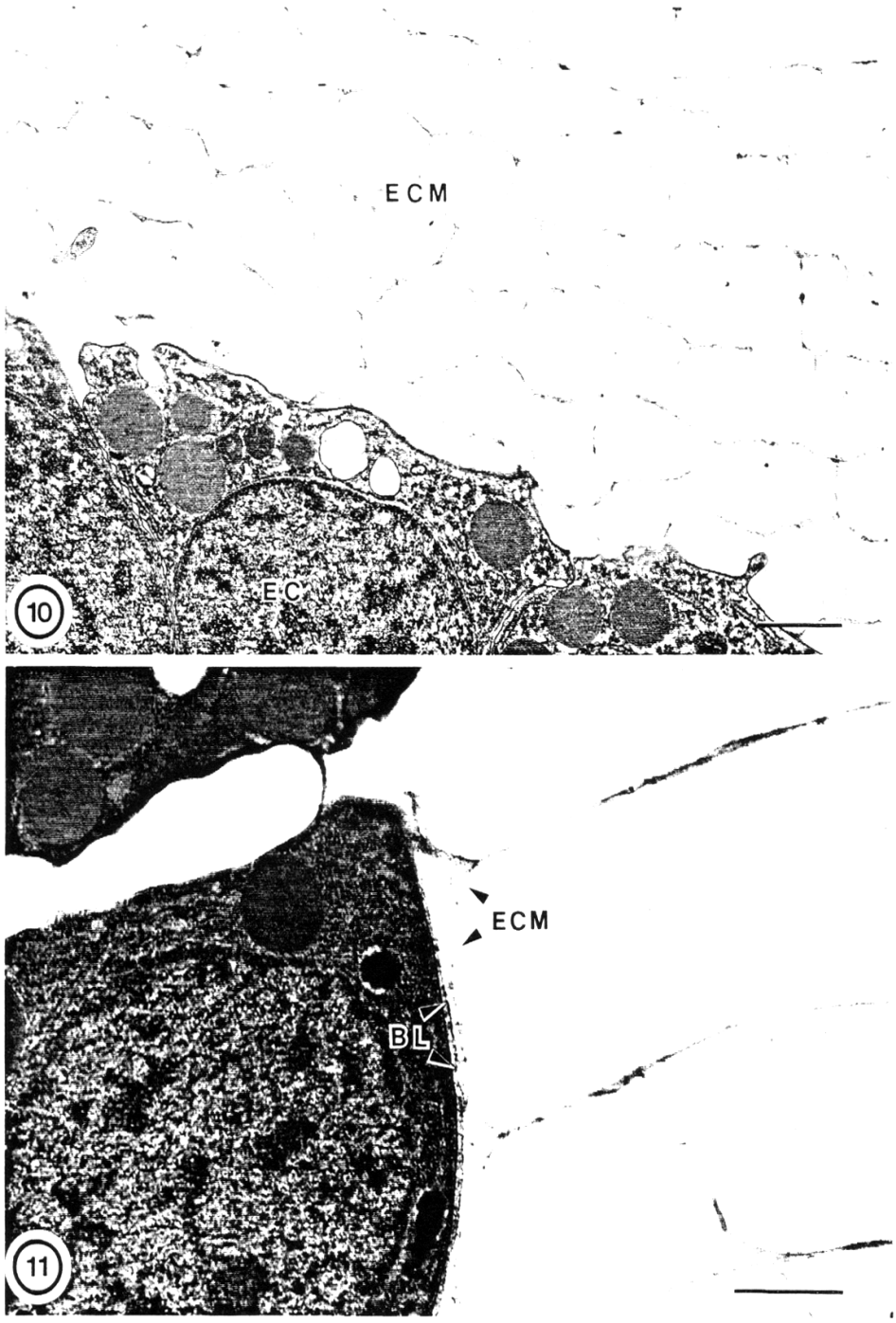

Fig. 10. TEM of a rapidly frozen and freeze substituted embryo demonstrating the perimeter of the blastocoelic cavity, the epithelial cell (EC) margin, and the blastocoelic ECM in the cavity. The ECM appears to be a network of continuous fibrils interconnected with filaments. Note the thicker and thinner regions of individual fibrils. Bar = 1 μm.

Fig. 11. Higher magnification of the epithelial cell / ECM interaction. The basal lamina (BL) can be observed as a thin cell coat closely apposed to the plasma membrane. Note the relatively loose attachment of the ECM to the basal lamina along its surface. The filamentous substructure of the ECM can be observed (near arrows). Bar = 1 μm.

Figures 12-14

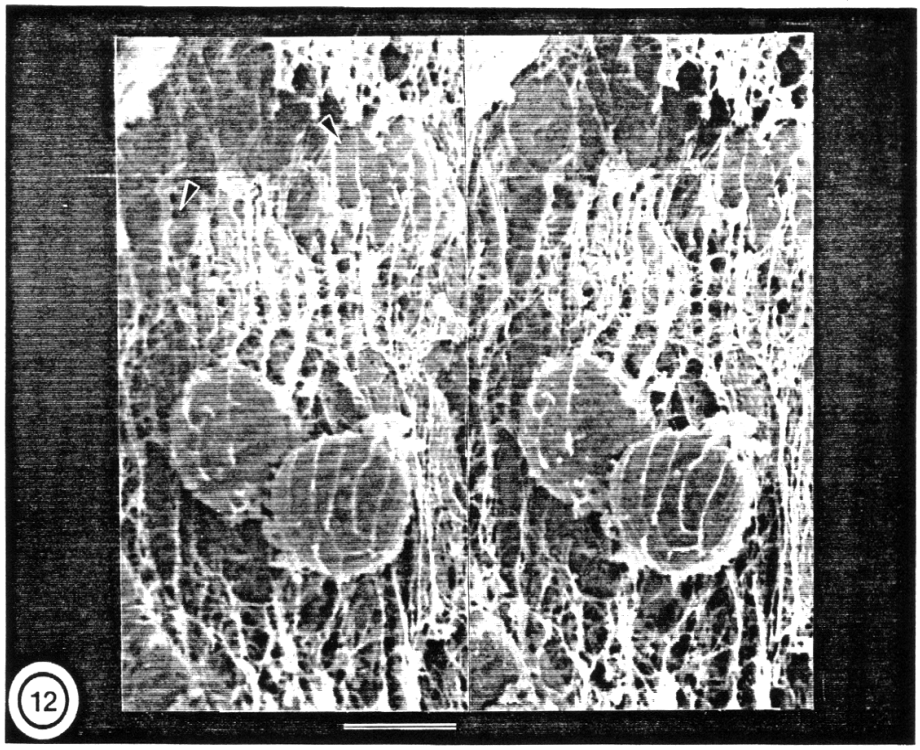

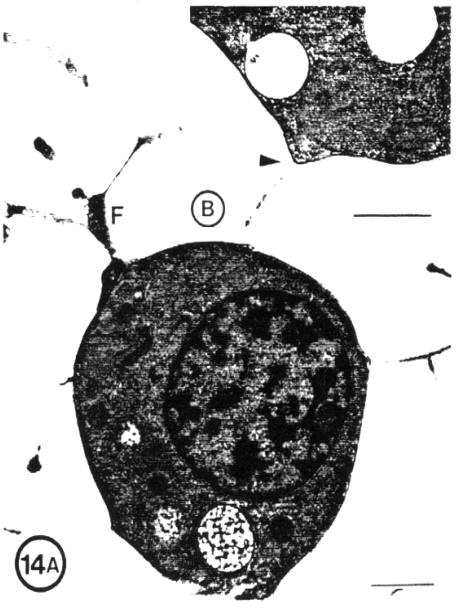

Fig. 12. SEM stereo pair of primary mesenchyme cells (arrows) in the blastocoelic matrix of a freeze substituted embryo. Note the attachment of the blastocoelic ECM to the cell surface is at the same periodicity and orientation as the matrix throughout the blastocoel (without cells). Bar = 5 μm.

Fig. 13. TEM of primary mesenchyme cells and the associated fibrillar blastocoelic ECM. The parallel orientation of the ECM and the attachment to the cells can be observed. Note the alternating thick/thin appearance of some fibrils (arrows). Bar = 5 μm.

Fig. 14. **A:** High magnification TEM of a single primary mesenchyme cell in the blastocoelic ECM. In this cell, the ECM is attached to both the cell surface and to a filopodial extension (F). A cell coat is not present on the PMCs and the ECM attaches directly to their plasma membranes. Bar = 1 μm. **B:** Higher magnification of PMC surface demonstrating the absence of a cell coat (basal lamina) and the attachment of the ECM to the plasma membrane (arrow). Bar = 0.5 μm.

Effects of PW on Sea Urchin Development

Following the elucidation of the structure of the blastocoelic matrix, studies on the effects of produced water on sea urchin embryo development were conducted. These studies were not only to define the bioeffects of produced water on embryo development, but to also search for a biomarker of both exposure and effect, with the hope of utilizing such a marker in other systems. The following is the first in a continuing effort on the bioeffects of produced water on early life stages of marine organisms, and was published in *Marine Biology* (Baldwin et al., 1992).

In California coastal waters, a main concern has been on pollution in estuaries (Luoma and Phillips, 1988; Gunter et al., 1990) and in near shore regions such as the Santa Barbara Channel where offshore oil production activities prevail (Straughan, 1976; Neff et al., 1987). Drilling activities and discharges of aqueous waste (largely geologic formation or "produced" water associated with crude oil at offshore platforms) from petroleum production are known to be sources of metal and hydrocarbon pollution (Boehm, 1987, Neff, 1987); these are derived both from drilling fluids as well as from the formation water itself (Neff, 1987). The discharge of this aqueous waste can occur both at the offshore platforms as well as in the near shore environment (Neff et al., 1987; Neff, 1987). Although normal oil and gas production activities are not likely to cause dramatic short-term impacts (Neff et al., 1987), long-term chronic effects cannot be ignored. The effects of contaminants at sensitive stages of the life cycle (ie. reproduction, embryonic development, etc.) of any species provides a key to the potential biological fate of that species in polluted environments.

Endogenous biomarkers have been used in recent years as diagnostic screening tools at the cellular and molecular levels for contaminant exposure. In addition to indicating whether a potential adverse effect has occurred, these responses may also be used to determine the causative contaminants (McCarthy and Shugart, 1990). Adverse ecological impacts on reproduction in marine organisms can often be difficult to detect; as such, contaminant-specific responses of early life stages may provide a more sensitive measure of contaminant exposure. Examples of endogenous macromolecular markers of environmental stress are the expression of "heat shock" or stress proteins (SP), and metal binding proteins such as metallothioneins (Hamer, 1986). Stress proteins have been demonstrated to be highly conserved throughout the animal kingdom (Kelley and Schlesinger, 1982). While present in low concentrations in non-stressed cells, the increased expression of SPs and metallothioneins as a result of environmental stress corresponds to both thermal and chemical exposures (Welch et al., 1989, Sanders, 1990); the appearance of these may correlate with an increased resistance of the cells to additional stress (Subjeck and Shyy, 1986; Boon-Niermeijer et al., 1986, Hamer, 1986). It has been suggested that endogenous macromolecules such as these may be excellent markers of contaminant exposure (Sanders, 1990).

In marine (and some mammalian) embryos, the major response as a result of heat and some metal exposures includes the expression of the major 70 kDa SP (Roccheri et al. 1981a, Welch et al., 1985, 1989, Roccheri et al., 1988), as well as metallothioneins (Nemer et al., 1984). Sea urchin embryos, only at specific stages of development, are known to synthesize SPs when exposed to metals or heat (Roccheri et al., 1981a; Sconzo et al. 1983, 1986; Roccheri et al., 1988). In some of these studies, only hatched embryos were capable of developing a tolerance to specific environmental stresses (Roccheri et al., 1981a), and this correlated with the ability of these embryos to synthesize SPs.

We have been investigating the effects of pollutants on embryonic stages of marine invertebrates since they undergo rapid cell growth and differentiation, and tend to be sensitive to contaminant exposure. In addition, the short-term exposure of specific developmental stages, to environmental contaminants, can have profound impacts on subsequent development and survival of the organism. As such, embryos of marine invertebrates are good model systems for investigating morphological and biochemical responses to contaminants over shorter time frames as compared with adult organisms. In this report we describe the sublethal effects of produced water (PW) on the embryonic development of the purple sea urchin, Stongylocentrotus purpuratus. These include the pattern of early development and the biochemical responses of embryos exposed to PW. In addition, we investigated the response of embryos to one of the known constituents of PW, arsenic (Neff et al. 1987).

Materials and Methods

Chemicals

All chemicals were purchased from Sigma Chemical Co. (St. Louis, Mo.) unless otherwise noted.

Embryo Culture

Adult purple sea urchins (Strongylocentrotus purpuratus) were collected from Point Arena, California, and maintained in flowing seawater at the University of California Davis Bodega Marine Laboratory, Bodega Bay, California. Gametes were collected from adults by intercoelmic injection of 0.5 M KCl. Eggs were fertilized with a dilute sperm suspension and cultured in 0.22 µm filtered sea water (FSW), pH 8.0, at 15º C as described by Strathmann (1987).

Produced Water Collection and Handling

PW samples were collected from a processing plant located in Carpenteria, California, in glass bottles (1 gallon) with teflon lined caps, and were shipped (on ice) to arrive within 24 hrs. at the marine laboratory. Samples were either used immediately for toxicity assessments, or aliquoted (10 ml) in glass vials, and frozen at -70º C. Samples were typically low in the

percentage of solids and did not require filtering prior to use in experiments. For experiments, fresh and previously frozen PW (which was typically 20 ppt salinity and pH 7.0-7.6) was salinity adjusted using a brine solution which consisted of concentrated (2x) artificial seawater (Cavanaugh 1956) and the pH was adjusted to 7.8-8.0 with 0.1 M NaOH.

Exposure to Produced Water

S. purpuratus embryos were cultured in FSW at 15º C until hatching (18 hours). The resulting ciliated blastulae (100 embryos/ml) were cultured in the presence of increasing concentrations of PW (0-20%) in FSW containing 0.01% penicillin G for an additional 54 hours. These experiments were conducted in 10.0 ml volumes in borosilicate glass scintilation vials (Fisher Scientific, Pennsylvania). At 20 h following exposure, replicate (3 to 5) subsamples were fixed with seawater-buffered glutaraldehyde (0.5%), and assessed for completion of gastrulation. The remaining replicate (3 to 5) samples for each concentration of PW were cultured until the control embryos reached the pluteus larval stage (typically 72 h posthatching). Samples were fixed as described above, when the embryos reached the normal pluteus larval morphology (the typical triangular shape), and exhibited normal spicule formation (Strathmann 1987).

Electron Microscopy

For scanning electron microscopy (SEM), embryos from control and PW treatments were fixed in 2.5% glutaraldehyde in seawater (pH 7.8) at room temperature for 2 h, and postfixed in 0.1% OsO4 in seawater for 1 h at 4º C. Samples were dehydrated in a graded ethanol series, critical-point dried, and dry fractured according to Cherr et al. (1992) using two SEM sample stubs coated with double-stick tape. The fractured embryos were coated with 25 nm of gold, and viewed in a Hitachi S-570 SEM operated at 10 kV.

Assessment of Stress Protein Expression

Purple sea urchin embryos were cultured at 15º C in 0.22 µm FSW, pH 8.0, to the early gastrula (1/4 gastrula) stage at 12 h posthatching (Strathman, 1987). Embryos were then exposed to 10-20% PW, 6.5 µM sodium arsenite, and a FSW control for 3 h at 1000 embryos / ml at both 15 and 25º C (heat shock). This concentration of sodium arsenite was chosen because it induces SP expression in cultured cells (Caltabiano et al., 1986), and was the highest concentration which did not affect the swimming behavior or morphology of the embryos over a 3 h exposure. After 2 h of exposure, 3H-leucine (ICN Biomedicals Inc., Costa Mesa, California, and NEN Research Products, Boston, Massachusetts; 20 µCi/ml final concentration) was added to each treatment for the final hour. In other experiments, embryos were exposed to PW at 25º C to differentiate the stress responses of PW and heat shock. In all experiments, embryos were pelleted by hand centrifugation, briefly washed with FSW, pelleted again, and solubilized for electrophoretic analysis in a buffer containing 1.5% sodium dodecyl sulfate (SDS) and

mercaptoethanol and stored frozen at -20º C. Total embryo protein was determined using a bicinchoninic acid (BCA) protein assay kit (Pierce, Rockford, Il.)

Electrophoresis and Autoradiography

Samples (56.5 µg protein/lane) were subjected to sodium dodecyl sulfate polyacrylamide gel electrophoresis (SDS PAGE) using 4-15% gradient gels (Bio Rad, Richmond, CA). Gels were stained with coomassie blue G-250 or R-250 and dried using a Bio Rad Laboratories Model 224 gel slab dryer. Glycoproteins were detected by periodic acid -Schiff/basic fuschin staining according to Konat et. al. (1984). Molecular weights standards were as follows: myosin (200 kDa), ß-galactosidase (116.3 kDa), rabbit muscle phosphorylase b (97.4 kDa), bovine serum albumin (66.2 kDa), hen egg white ovalbumin (45 kDa), bovine carbonic anhydrase (31 kDa), and soybean trypsin inhibitor (21.5 kDa). Autoradiography of electrophoresed proteins was carried out using Hyperfilm-3H high performance autoradiography film (Amersham, Arlington Heights, Il.) with a 96 hour exposure.

Results

Morphological Effects of Produced Water Exposure

The response of embryos exposed to fresh and frozen PW from the ciliated blastula through the pluteus stage is shown in Figure 15. There was no significant difference between the fresh and frozen PW samples in their abilities to inhibit successful pluteus development. Therefore, frozen samples were used in all subsequent experiments. The morphological effects of PW on embryo development are shown in Figures 16 and 17. Ciliated blastula were exposed to various concentrations of PW. The controls were allowed to complete gastrulation (Fig. 16A) . Produced water (3%) inhibited the completion of gastrulation (Fig. 16B). This was evidenced by the failure of the archenteron to extend to the animal pole of the blastocoel. In addition, extracellular material was observed on the surface of these embryos; however, swimming behavior appeared qualitatively normal. At higher concentrations of PW (5% through 15%), archenteron formation was greatly inhibited (Fig. 15C). Depending on the concentration of PW, the archenteron ranged from a slightly shortened structure (5% PW) to simply a mass of cells in the vegetal pole of the blastocoel (7% and 10%). The morphological responses described above were observed for three different PW samples received at the laboratory.

In the absence of PW, embryos reached the pluteus stage within 72 hours post-hatching (Fig. 17A). In the presence of PW (3%), embryos exhibited a loss of the characteristic angular shape of the pluteus stage (Fig. 17B). These embryos also possessed enlarged gut compartmentation, however, they still appeared to exhibit normal spicule development. At higher PW concentrations (7% and 10%), there was a complete loss of the typical pluteus shape, and spicule formation was inhibited (Fig. 17C). These embryos however, exhibited normal

directed swimming behavior. The effects of PW on gastrulation and pluteus formation are shown in Figure 18. In general, there was a more graded response at the gastrula stage than the pluteus stage. Furthermore, the small number of abnormal gastrula stage embryos in 3 % PW, developed into normal pluteus larvae, suggesting that a developmental delay occurred (Fig. 18).

The complete formation of the archenteron in control embryos could be observed in dry-cleaved embryos prepared for SEM (Fig. 19A). Primary mesenchyme cells migrating through the extracellular matrix could be observed in these embryos. In embryos cultured in the presence of PW, inhibition of gastrulation occurred (Figs. 19B). As observed at the light and electron microscopic levels (see Fig. 16C and 19B), PW (7%) exposed embryos exhibited archenterons that were reduced to cell masses at the vegetal pole of the blastocoelic cavity. In addition, these embryos possessed unusually large quantities of extracellular matrix within the blastocoelic cavities (Fig. 19B). Cellular protrusions could be observed to extend from the tip of the archenteron to the roof of the blastocoel (Fig. 19B); these protrusions were presumably from secondary mesenchyme cells.

Macromolecular Indicators of Produced Water and Arsenic Exposure

Early gastrula stage embryos exposed to PW, sodium arsenite, or heat (25 º C) for 3 hours did not exhibit morphological abnormalities as assessed at the light microscopic level. In some experiments, one dimensional SDS-PAGE stained for protein showed that embryos exposed to PW (10-15%) for 3 hrs. expressed a high molecular weight protein. This protein was present in very low concentrations in control embryos (Figs. 20A, C). This protein, which had an apparent molecular weight of 250-255 kDa (253 kDa average), could not be observed in 7.5% or 10% gels due to the poor resolution in this molecular weight range. As such, 4-15% gradient gels were used for all experiments.

Autoradiography of control and PW exposed embryo proteins are shown in figures 20B and 20D. The 253 kDa glycoprotein, identified in coomassie blue stained gels of PW exposed embryos, was synthesized during the PW exposure as evidenced by 3H-leucine incorporation (Fig. 20D); this protein was not apparent in control embryos (Fig. 20B). Further characterization revealed that the 253 kDa band was glycosylated as demonstrated using periodic acid -Schiff/basic fuschin staining (Fig. 21).

Heat shock (25º C) of embryos induced a 73 kDa protein (Fig. 22B) which was not observed in control (15º C) embryos (Fig. 22A). Exposure of embryos to PW (15%) induced the expression of the 253 kDa glycoprotein, but not the 73 kDa protein (Fig. 22C). Heat shock did not induce the expression of the 253 kDa glycoprotein. When embryos were exposed to PW and heat shock (25º C) simultaneously for 3 hrs, both the 73 kDa protein and the 253 kDa glycoprotein were expressed (Fig. 22D). Exposure of embryos for 3 hr.to sodium arsenite (6.5 µM), a constituent of PW (Neff et al. 1987), also induced the 253 kDa glycoprotein(Fig. 23A,

B). Neither PW nor sodium arsenite at the concentrations used, induced the expression of the 73 kDa protein, or other proteins previously described in other systems.

Discussion

Morphological Effects of Produced Water on Embryos

Ciliated blastulae that were exposed through gastrulation to PW (3%) exhibited an apparent delay in their ability to form a complete archenteron. While embryos exposed to higher concentrations of PW (5-10 %), formed archenterons that ranged from short structures to simple masses of cells at the vegetal region of the blastocoelic cavity; this demonstrated that PW was a potent inhibitor of normal cell behavior during gastrulation. Embryos challenged with higher concentrations of PW exhibited unusually long protrusions from secondary mesenchyme cells which extended toward the animal pole. These embryos possessed blastocoels containing large quantities of extracellular matrix (ECM). These data suggest that PW can perturb the cellular processes required for normal gastrulation. They also suggest that PW may induce an abnormal synthesis of ECM material in the *S. purpuratus* blastocoelic cavity, which in turn perturbs normal mesenchyme cell functions. However, we cannot rule out direct PW effects on intracellular processes in the mesenchyme cells. Since the cellular origin of the blastocoelic ECM is unclear, the nature of embryonic cells directly affected by PW remains to be investigated.

The ECM is thought to be largely responsible for mediating the normal processes of gastrulation in the sea urchin embryo (Solursh, 1986, Wessel and McClay, 1987; Burke and Tamboline, 1990). The blastocoelic ECM is a highly hydrated matrix of proteoglycan and glycosaminoglycan molecules (Wessel et. al., 1984). It has been suggested that these components of the ECM act as receptors or "guides" to migrating cells within the blastocoel (Hay, 1984). It has also been shown that perturbations to the blastoceolic ECM will inhibit the normal cell migrations and morphological changes accompanying the processes of gastrulation (Burke and Tambolin, 1990). Alterations (increases or decreases) to one or more of the components of the ECM as a result of PW exposure may be responsible for the abnormal gastrulation observed in this study. At low concentrations of PW, the effect on the ECM and the cellular processes it regulates may be subtle enough to only delay embryonic development. At higher PW concentrations, an alteration or inhibition of normal development may arise due to direct effects on the microenvironment (blastocoelic cavity) surrounding cells within the embryo . PW did not appear to affect the directional swimming behavior of the embryos, which is largely dependent on ciliary movement.

Embryos that were exposed to PW from ciliated blastula through the pluteus stage also exhibited abnormal development. At low concentrations of PW (3%), embryos did not exhibit

the normal angular shape of control pluteus stage embryos and appeared only to be delayed in development. Based on the different responses of the gastrulation and pluteus endpoints at low concentrations, some abnormal gastrulae at 3-5% PW (see Fig. 18) apparently went on to develop into normal pluteii. As a result, the gastrula endpoint was the most sensitive, but this sensitivity was apparently due to a delay in development. At higher concentrations of PW however, embryos exhibited abnormal pluteus morphology, and spicule formation was almost completely inhibited. The angular shape of the normal pluteus stage embryo is largely dependent on the differentiation of the primary mesenchyme cells, which is an ECM-dependent process (Burke and Tamboline, 1990), to form the skeletal rods or spicules of the embryo. In sea urchins, the ECM has been shown to be critical in the differentiation of the primary mesenchyme cells into normal spicules (proper shape and orientations) within the developing embryo (Harkey and Whiteley, 1980). PW appears to perturb normal ECM composition and structure which, in turn, may alter normal spicule formation.

Biochemical Response of Embryos to Produced Water and Arsenic

We have identified a biochemical response of sea urchin embryos to PW, the synthesis of a high molecular weight, approximately 253 kDa, glycoprotein. This is a molecular weight estimate averaged over numerous experiments in which the bands ranged from 250-255 kDa. Three different samples of PW elicited the same response. Since this band is well above the highest molecular weight standard (200 kDa), all molecular weight determinations can only be estimations. To our knowledge, expression of this glycoprotein has not been described in the literature for any organism as a stress response, and is not associated with the classic heat shock response (reviewed by Subjeck and Shyy, 1986; Welch et al., 1985, 1989; Sanders, 1990). In our experiments, the 253 kDa glycoprotein expressed in PW exposed embryos was often not observed in coomassie stained gels, but was generally detected by autoradiography. The concentrations of PW that induced the expression of the 253 kDa glycoprotein, in embryos exposed for 3 hours, did not elicit any morphological effects at the light microscopic level. Preliminary experiments suggest that lower PW concentrations (3%) were capable of eliciting a similar response (data not shown). As such, it is likely that much lower concentrations of PW (and most likely longer exposures) will induce 253 kDa expression to varying degrees, but these parameters have not been investigated at the present time.

Our experiments demonstrate that the expression of the 73 kDa protein and the 253 kDa glycoprotein in *S. pupuratus* embryos is independent of each other. Interestingly, heat shock is known to suppress overall protein synthesis in sea urchin embryos (Roccheri et al., 1981a); however, in the presence of PW, heat shocked embryos were still capable of synthesizing the 253 kDa glycoprotein, suggesting that this may be an important macromolecule in the development of sea urchin embryos under stress.

While SPs up to the 90-100 kDa range have been observed in heat shocked mammalian embryos (Kim et al., 1987), higher molecular weight proteins have not been observed. It should be noted that we did not observe the 253 kDa glycoprotein in heat shocked embryos, supporting the notion that this protein is in fact a specific response of the embryos to PW and arsenic. Other studies which have utilized sea urchin embryos in stress response experiments have not observed the expression of high molecular weight (>200 kDa) proteins. This could be in part due to their use of 7.5-10% non-gradient gels, which have poor resolution in the >200 kDa range. However, our data suggest that the expression of the 253 kDa glycoprotein in our experiments is not associated with the heat shock response, and may be specific to PW exposure of embryos.

Sodium arsenite, a constituent of PW (Neff et al., 1987, our unpublished data) also induced the expression of the 253 kDa glycoprotein. In some experiments, low levels of the 73 kDa protein could be observed in sodium arsenite exposed embryos (not shown), but was not a consistent or obvious response at the concentrations (6.5 μM) or exposure times used in this study. Sodium arsenite has been shown to induce the expression of the 70 kDa SP in mammalian (Caltabiano et al., 1986), avian (Schlesinger et al., 1989) and Drosophila (Debec et al., 1990) cell lines. In addition, arsenite also induces the synthesis of proteins in the 32-34 kDa range in some systems (Caltabiano et al., 1986; Taketani et al., 1989). The time course and intensity of the response of some cells to arsenite can be very different from that observed as a result of heat shock (Debec et al., 1990). This could explain our inability to detect the above responses in sea urchin embryos, which were exposed to arsenite for 3 hours. Alternatively, our autoradiographic methodology may not have been sensitive enough to detect the synthesis of other proteins; as such, in this study, we may only be detecting expression of the major proteins expressed as a result of arsenite (or PW) exposure.

Previous studies of the stress responses of sea urchin embryos have shown that the 70-73 kDa is the major SPs expressed as a result of heat shock and zinc exposures (Roccheri et al., 1981a, Roccheri et al., 1988). The expression of the 70 kDa SP in sea urchin embryos has been shown to be developmentally stage-specific, and it is localized to the soluble cytoplasm of the ectodermal cells (Roccheri et al., 1981b). Prior to hatching, embryos do not express SPs, and are susceptible to heat shock. Following hatching, embryos typically are capable of expressing SPs, and this correlates with an increased resistance to subsequent heat shock (Roccheri et al., 1981a,b; Sconzo et al., 1983, 1986). Zinc ions have been shown to induce the same SPs (70 and 72.5 kDa) as observed in heat shocked embryos (Roccheri et al., 1988), suggesting a similar activating mechanism. However, zinc does not impart thermotolerance and thus may have different effects in the embryos. Metals have been shown to induce the synthesis of metallothioneins in sea urchin embryos (Nemer et al., 1984). These are low molecular weight proteins which are induced by zinc, cadmium, copper, etc. (Viarengo et al., 1980; Lerch, 1980;

Hamer, 1986). It has been suggested that the appearance of SPs and metallothioneins in thermally and chemically stressed organisms correlates with an increased resistance to the exposure, or to subsequent exposures (Hamer, 1986; Sanders, 1990). To our knowledge, this has not been investigated with respect to SPs and chemical stressors in previous sea urchin embryo experiments, nor ours. Now that the biochemical response of *Strongylocentrotus purpuratus* embryos to PW exposure has been defined, appropriate experiments can be undertaken in our laboratory.

As described in the preceding subsection, we observed that, during gastrulation, PW exposed embryos synthesized large quantities of ECM compared to control embryos. The ECM of *Strongylocentrotus purpuratus* embryos has been shown to contain high molecular weight (>200 kDa) sulfated proteoglycans (Lane and Solursh, 1988, 1991). These components, which are typically observed in isolated ECM preparations, are glycosylated (mannose residues based on Con A binding; Lane and Solursh, 1988, 1991), and their appearance on SDS-PAGE is similar to the 253 kDa glycoprotein observed in the present study. It is attractive to suggest that the 253 kDa glycoprotein we observed in PW and sodium arsenite exposed embryos was apparent due to an increased synthesis in ECM. The effects of abnormal blastocoelic ECM on gastrulation may be difficult to detect in embryos challenged with PW due to the short (3 h) exposures used in this study. However, it would be possible to investigate the nature of this abnormal ECM using recent advances in ECM preservation (Cherr et al., 1992). The 253 kDa component is present in control embryos at very low levels, and this would also support this hypothesis. Thus, the increased expression of the 253 kDa component in PW exposed embryos may correlate with the morphological abnormalities observed in the present study. Since ECMs are critical in cell-cell interactions during development (Hay, 1984), a stimulation in synthesis of specific ECM components as a result of toxicant exposure would potentially be detrimental to normal cellular functions. This hypothesis as to mechanisms of PW perturbations remains to be tested in sea urchin embryos, as well as in other systems.

It should be noted that PW is a complex aqueous waste (reviewed by Neff, 1987) which contains petroleum hydrocarbons, phenolics, metals, and numerous unidentified constituents, any or all of which could potentially elicit the morphological and biochemical responses described in the present study. However, preliminary data suggest that fractions containing metals are responsible for mollusc embryo toxicity (Higashi et al., 1992), while those containing petroleum hydrocarbons are not. This is consistent with the observed effects of arsenic in this study; however, additional morphological and biochemical studies using *Strongylocentrotus purpuratus* embryos and the isolated PW constituents would be critical in further elucidating the specific PW constituents responsible.

Sanders (1990) has suggested that SPs can be used as specific biomarkers for environmental monitoring. An ideal situation would be to identify biomarkers for different stressors within the same organism. The research presented here demonstrates that this can be done for at least heat shock and PW. The maximal usefulness of a particular biomarker in the environment would be to distinguish a specific stressor(s) from the multiple stresses an organism typically experiences (Sanders, 1990). The ability of other organisms to express the 253 kDa glycoprotein needs to be documented before one can judge the usefulness of this biomarker beyond the sea urchin embryo system. Once demonstrated in adult sea urchins and in other organisms, the 253 kDa glycoprotein expressed as a result of PW (and sodium arsenite) exposure may be well suited for subsequent use in environmental monitoring in sites impacted by petroleum wastes.

Figure 15

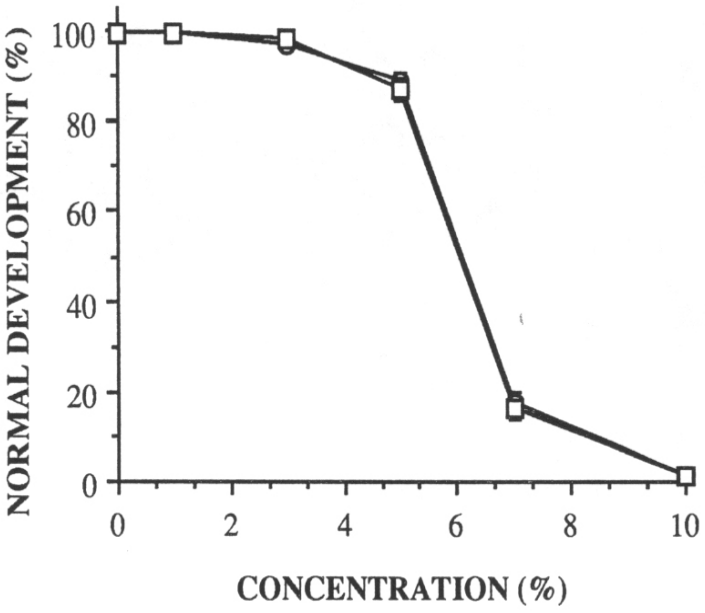

Strongylocentrotus purpuratus embryos exposed to fresh (○) and frozen (❑) samples of produced water from the time of hatch (ciliated blastula) through pluteus stage. There was no significant difference between the two samples. Error bars represent standard deviations of replicate samples.

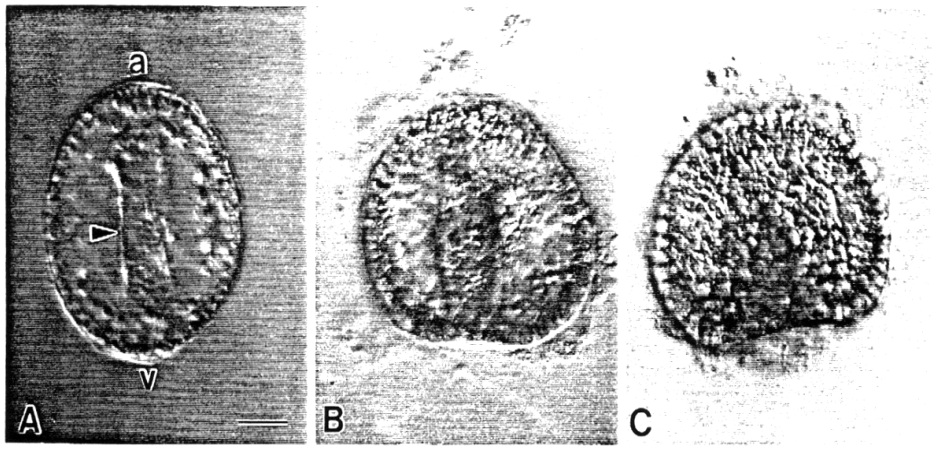

Fig. 16 *Strongylocentrotus purpuratus*. Embryos exposed to different concentrations of produced water (PW) from time of hatch (ciliated blastula) through complete gastrulation. (A) Embryos in seawater (control) exhibiting a complete archenteron (arrowhead) extending from vegetal pole (v) to animal pole (a). (B) Embryo exposed to 3% PW, showing inhibition of formation of a complete archenteron. (C) Embryo exposed to 7% PW; note that archenteron formation is greatly inhibited, such that it appears as a mass of cells at the vegetal pole. (Scale bar = 30 μm)

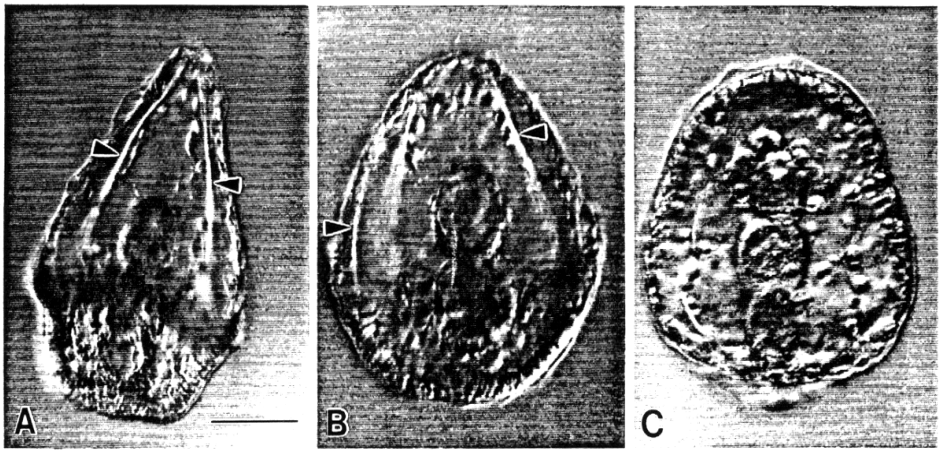

Fig. 17 *Strongylocentrotus purpuratus*. Embryos (ciliated blastulae) exposed to different concentrations of PW through pluteus stage. (A) Control embryos exhibiting angular shape and spicules (arrowheads) characteristic of pluteus stage. (B) Embryo exposed to 3% PW exhibiting moderate loss of distinct angular shape, but exhibiting normal spicule formation (arrowheads). (C) At concentration of 7% PW, embryos have completely lost typical pluteus shape and spicule formation is almost completely inhibited; note enlarged compartments of gut. (Scale bar = 10 μm)

Figure 18

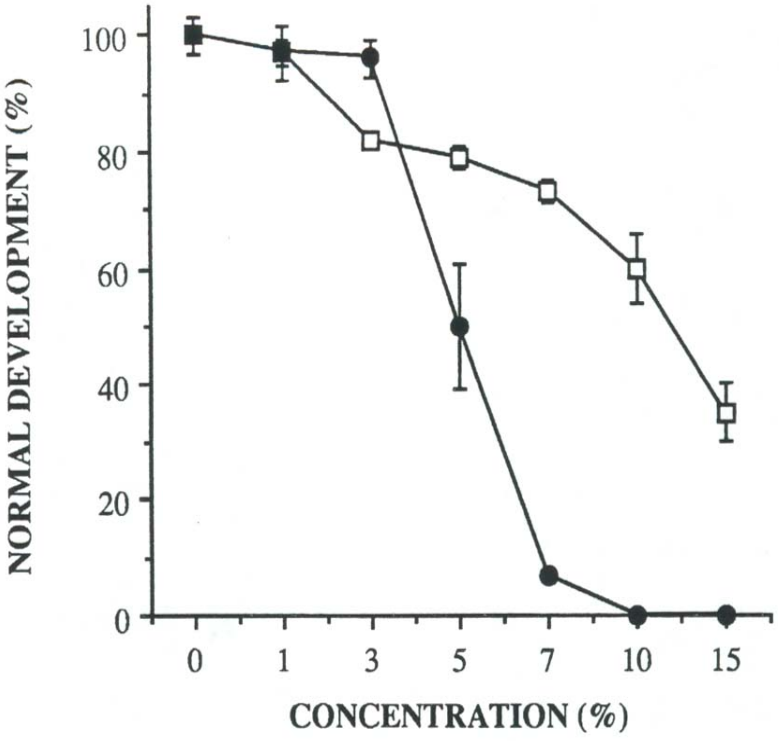

Strongylocentrotus purpuratus embryos (ciliate blastulae) exposed to different concentrations of PW through gastrulation (●) and through pluteus stage (❐). Effects of PW are apparent at lower concentrations at gastrula stage, however, more dramatic effects were observed at later pluteus stage. Error bars represent standard deviations of replicate samples.

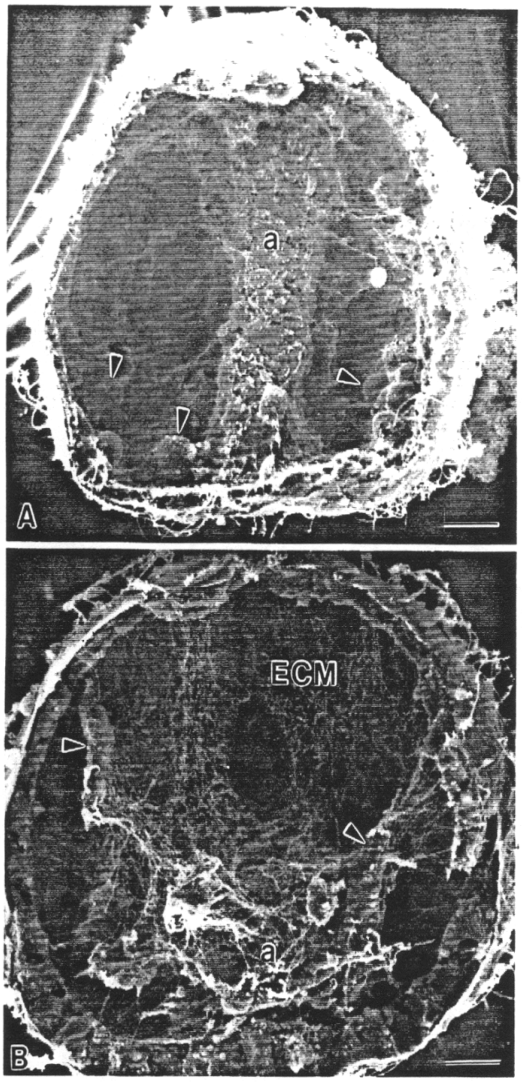

Fig. 19 *Strongylocentrotus purpuratus*. Scanning electron micrographs of gastrula-stage embryos exposed to different concentrations of PW. (A) Seawater control embryo exhibiting complete archenteron (a) and migrating primary mesenchyme cells (arrowheads). (B) Embryo exposed to 7% PW exhibiting greatly reduced formation of archenteron, with cellular protrusion (secondary mesenchyme cells) extending toward roof of blastocoelic cavity (arrowheads); these embryos also possessed large quantities of extracellular matrix (ECM). (Scale bars = 10 μm)

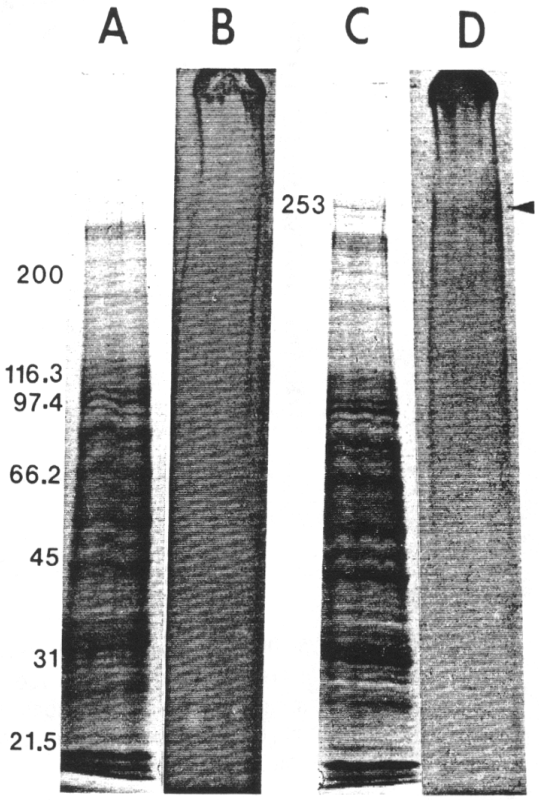

Fig. 20 *Strongylocentrotus purpuratus*. SDS-PAGE (4 to 15% gel) and autoradiograms of early gastrula-stage embryos exposed to PW (15%) for 3 h. A: seawater control embryos stained with Coomassie Blue. B: autoradiogram of seawater control embryos. C: Coomassie Blue-stained gel of 15% PW-exposed embryos; note appearance of a band at 253 kDa. D: autoradiogram of 15% PW-exposed embryos showing a protein at 253 kDa (arrowhead). Molecular weight standards used were: myosin (200 kDa), β-galactosidase (116.3 kDa), rabbit muscle phosphorylase b (97.4 kDa), bovine serum albumin (66.2 kDa), hen egg-white ovalbumin (45 kDa), bovine carbonic anhydrase (31 kDa), and soybean trypsin inhibitor (21.5 kDa)

Figures 21-23

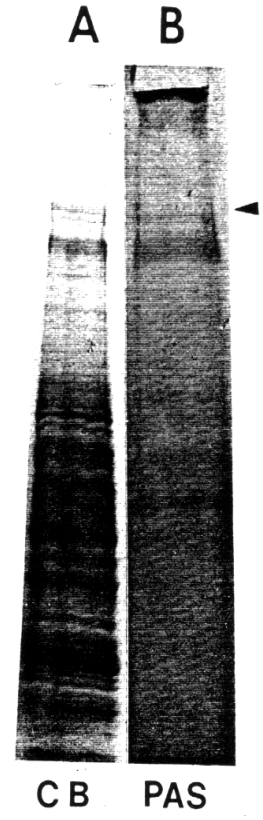

Fig. 21 *Strongylocentrotus purpuratus*. A: Expression of a 253 kDa protein in embryos exposed to 15% PW (gels stained with Coomassie Blue, CB). B: positive staining of the 253 kDa protein (arrowhead) for carbohydrate is demonstrated by periodic acid-Schiff/basic fuschin (PAS)

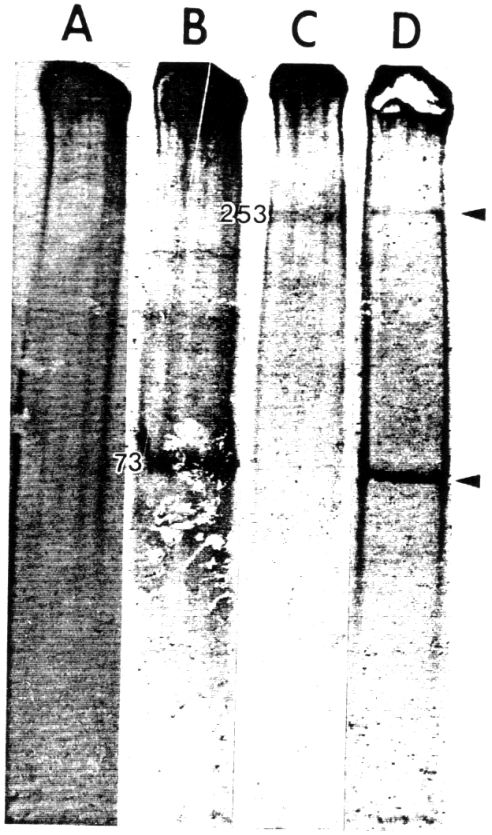

Fig. 22 *Strongylocentrotus purpuratus*. Autoradiograms of embryos exposed to PW and heat shock for 3 h, with addition of ^{3}H leucine (20 µCi/ml) for last hour. A: seawater control. B: 25 °C heat shock induces expression of 73 kDa protein. C: PW (15%) induces expression of 253 kDa protein, but no 73 kDa protein. D: simultaneous exposure of embryos to 15% PW and 25 °C heat shock induces expression of both the 73 kDa and 253 kDa protein (arrowheads)

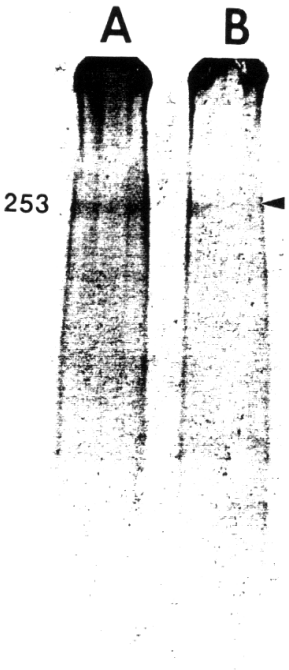

Fig. 23 *Strongylocentrotus purpuratus*. Autoradiogram of embryos exposed to PW and sodium arsenite for 3 h, with addition of ^{3}H leucine (20 µCi/ml) for last hour. A: 15% PW induces expression of 253 kDa protein; B: 6.5 µ*M* sodium arsenite also induces expression of 253 kDa protein (arrowhead)

STUDIES WITH KELP GAMETOPHYTES

We have been investigating the effects of PW on gametophytic development in the giant kelp, *Macrocystis pyrifera*. Preliminary experiments suggested that PW had only slight effects on germination and germ tube growth, two developmental events previously used as indicators of toxicant effects in this system (Anderson and Hunt, 1988). Further investigations suggested that nuclear events, however, were impacted by PW. These events, which include basic processes of the cell cycle, had never been elucidated. As such, the time course of these cell cycle events, as well as the subcellular components involved had to be investigated prior to studies of toxicant perturbation.

Kelp gametophytes have recently been utilized for assessing the toxicity of effluents as well as ambient water (Anderson and Hunt, 1988; Anderson et al., 1990). Distinct phases of development occur in *Macrocystis* gametophytes, and thus we investigated the temporal and mechanistic separation of these events such that the results and approaches could be directly applied to studies with produced water and its toxic constituents. The goal of such an approach was to establish impacts an a commercially and ecologically important species, and to establish *Macrocystis* gametophytes as a toxicological tool for discerning bioeffects from different toxicants in a complex medium. The latter has been realized as a continued research on the present SCEI-funded project has resulted in the submission of a manuscript on the differential effects of produced water and its metal constituents (Garman et al., submitted to *Aquatic Toxicology*).

Cytoskeletal elements regulate a wide variety of cellular processes in plant development and function . For example, cytoplasmic microtubules and microfilaments have been shown to govern several aspects of cell growth, cell polarity, and cell cycle events in higher plants (see Lloyd 1982). The movement of the nucleus to the future division site is an important feature of cell patterning since this influences the polarity of the dividing cells. This limited nuclear migration, prior to cell division, appears to be controlled by mechanisms which involve microtubules (Gunning and Wick 1985, Doonan et al.1985). As a result, this event is influenced by microtubule disrupting agents (Hensel 1984, 1985, Katsuta and Shibaoka 1988, Meindl 1983). Specifically, participation of microtubules in nuclear movement has been demonstrated with respect to the orientation of microtubule arrays around the nucleus (Doonan et al. 1985, Nakai and Ushiyama 1978, Oakley and Morris 1980; Ott, 1992). Like microtubules, actin microfilaments have also been shown to regulate a variety of subcellular processes during plant development. These include pollen grain germination and tube growth, as well as movement of organelles and cytoplasmic inclusions within developing pollen tubes (Franke et al. 1972, Mascarenhas and Lafountain 1972, reviewed by Steer and Steer 1989). Actin microfilaments

have been shown to also govern nuclear movement in angiosperm pollen tubes and it appears that the translocation of vegetative nuclei along the pollen tube following germination depends on their association with actin filament bundles (Heslop-Harrison and Heslop-Harrison 1989).

While cell shape changes and organelle movement occur during development and growth in lower plants, the role of cytoskeletal elements in the regulation of these developmental events has received relatively less attention than in higher plants. Dynamically changing microtubule arrays have been shown to be associated with mitotic and post-mitotic events in the green algae (LaClaire 1987, Shihira-Ishikawa 1987). Kropf et al. (1990) showed that cytoplasmic microtubules are primarily responsible for events such as tip growth, mitosis and cell division during early embryonic development in sporophytes of the brown alga *Pelvetia*. Other events such as axis formation and germination (rhizoid growth of the zygote) in this species do not appear to involve microtubules. While these studies provide some information on early sporophyte development in the brown algae, to our knowledge, the cellular mechanisms of other phases of development (eg. germination and germ tube elongation) have not been investigated.

To address the involvement of cytoskeletal elements during early gametophytic development in the marine brown alga *Macrocystis pyrifera* ("giant kelp"), we have examined the effects of cytoskeletal (microtubules and actin microfilaments) disrupting agents on specific cellular events associated with differentiation of the zoospore into a gametophyte. Development in *M. pyrifera* gametophytes, like in other laminariales, involves a number of distinct events. Gametophyte development is initiated by the release of haploid zoospores (following meiosis) from sporangia in adult sporophytes; this is followed by germination and subsequent differentiation of the zoospores into male or female gametophytes (vegetative phase). These dioecious gametophytes produce gametes; following successful fertilization, the diploid zygotes develop and differentiate into sporophytes (sexual phase). These sporophytes eventually develop into mature plants (Charters and Neushul 1979, North 1971). Although the cellular events associated with the sexual phase of development have been described in many algal species (Goff and Coleman 1984, Motomura 1990, 1991), information regarding the vegetative phase of development is limited. Cole (1968) has examined some aspects of the vegetative phase of development in *M. integrifolia* and this study included some notes on the division of the zoospore nucleus during germination. While data were not presented, her study also suggested that a daughter nucleus and most of the cytoplasm translocated along the germ tube during early gametophyte development. The cellular details and the mechanisms of regulation of these events were not investigated.

In this study, we present evidence that the early developmental events (germination, germ tube growth, nuclear translocation) in *M. pyrifera* gametophytes are temporally distinct and appear to be governed by descrete cytoskeletal elements. To our knowledge, this is the first

demonstration of the role of cytoskeletal elements in cellular events during gametophytic development in a brown alga. A portion of this work has been reported in preliminary form (Pillai et al. 1990).

Materials and Methods

Zoospore Release and Culture

Mature sporophylls were collected from the bases of *Macrocystis pyrifera* sporophytes at Santa Barbara and Bodega Bay, California. Induction of zoospore release was performed according to Anderson and Hunt (1988). Briefly, reproductive sporophylls were air dried for 1 hr at room temperature. They were then extensively washed in running seawater, blotted to dryness, and placed in "culture medium" (CM; 0.45 micron filtered sea water containing 0.01% penicillin G, pH 7.9) in the dark at 15º C. Sporophylls were monitored periodically for zoospore release, which usually occurred in 45-60 minutes (Anderson and Hunt, 1988). Sporophylls were removed once a high density of motile zoospores were present in CM as determined by darkfield microscopy (100x magnification). Debris present in the CM was allowed to settle for 15-20 minutes. Zoospores were cultured (7.5 x 10^4 cells/ml) in 5 ml Lab-Tek chamber slides (Nunc Inc. Napperville, Ill.) at 15º C under continuous white fluorescent light adjusted to give 100 $\mu E/m^2/s$ (Deysher and Dean 1984, Luning and Neushul 1978). Alternatively, zoospores were cultured on circular (22 mm) glass coverslips in 10 ml class B borosilicate glass vials (Fisher Scientific, Pittsburg, PA) under the same conditions.

Morphological Studies of Early Gametophytic Development

For light microscopic studies of early development, samples of zoospore cultures at different stages of development were fixed with seawater containing 1% paraformaldehyde and observed with an Olympus BH-2 light microscope (Olympus Corporation, Lake Success, New York) equipped with Hoffman modulation optics (Modulation Optics, Greenvale, New York). Specimens were photographed with Kodak T_{MAX}-100 professional film and a 100X oil immersion objective. To determine the time course of germination and germ tube elongation, samples of zoospore cultures at different stages of development were fixed as described above. Successful germination was determined when the germ tube was equal to or longer than the diameter of the zoospore. For measurement of the germ tube lengths, following completion of elongation, at least 10 cells from samples, in triplicates, at each time point were randomly selected and the length of germ tubes measured using an occular radicle which had been calibrated using a stage micrometer. Division and movement of nucleus (nuclear translocation) during gametophytic development were determined by probing the cells with the vital DNA stain Hoechst 33342 (Sigma Chemical Company, St. Louis, MO). Samples at different time points were fixed as described above, briefly rinsed with seawater, treated with Hoechst 33342 (1 µg/ml

final concentration) for 5 minutes and observed with an Olympus BH-2 light microscope equipped with epifluorescence and ultraviolet filters. Specimens were photographed with either Kodak T_{MAX}-100 or T_{MAX}-400 professional film and Hoffman modulation objectives (40X and 100X) using an exposure of 20s.

Electron Microscopy

For transmission electron microscopy (TEM), zoospores were cultured through different stages of development in 5 ml microbeakers (Electron Microscopy Sciences, Ft. Washington, PA) at a concentration of 7.5 X 10^5 cells/ml. At different time points, cells were fixed with 2.5% glutaraldehyde in 0.15 M sodium cacodylate (pH 7.6), containing 6% sucrose for 2 hrs at room temperature. The cells were then removed from the bottom of the beaker by gently scraping with a teflon spatula and sedimented by gentle centrifugation in conical tubes. Samples were then post-fixed with 1% osmium tetroxide in cacodylate buffer for 30 minutes, dehydrated in a graded acetone series, and embedded in Spurr's epoxy resin. Thin sections were cut with a Reichert Ultracut E ultramicrotome (Reichert-Jung, A-1171 Wein, Austria), stained with aqueous uranyl acetate and lead citrate and, examined with either an Hitachi HU-11 A (Hitachi Ltd., Tokyo, Japan) or Zeiss 902 (Carl Zeiss, D-7082 Oberkochen, West Germany) electron microscope.

Effects of Cytoskeletal Disrupting Agents on Early Development

The effects of colchicine, amiprophos-methyl (APM), and cytochalasin D (CD) on early gametophytic development were investigated by adding the drugs to the cultures at different times following release of the zoospores. Zoospores (7.5 X 10^4 cells/ml) were introduced to Lab-Tech culture slides in 5 ml volumes and allowed to settle for 3 hrs at 15º C. The cultures were then briefly rinsed with CM in order to remove the unsettled cells and added 5 ml of fresh CM. The drugs were added to the culutres either at 3 hrs (to study the effects on germination or germ tube elongation) or 20 hrs (to study the effects on nuclear translocation) post-release of the zoospores. Cytochalasin D was also added to the cultures while germ tube elongation was proceeding (11 hrs post-release) in order to examine its effect on further germ tube growth. In addition, to further examine the effect of CD on nuclear translocation, the drug was added to the cultures at 16 hrs post-release, well before the initiation of nuclear events. Colchicine (Sigma Chemical Company, St. Louis, MO) was dissolved in distilled water, and APM (a gift from Mobay Corp., Kansas City, MO) and CD (Sigma Chemical Company, St. Louis, MO) were diluted from stock solutions in dimethyl sulfoxide (DMSO). Cytochalasin D was used up to a final concentration of 400 µM (diluted appropriate times from a stock solution of 80 mM), APM up to 5 µM (diluted appropriate times from a stock solution of 1 mM), and colchicine up to 360 µM (diluted appropriate times from a stock solution of 75 mM). Cells were cultured until the control samples (containing 0.5% DMSO in seawater) completed germination and nuclear translocation. Samples were then fixed with seawater containing 1% paraformaldehyde and

examined as described below. To examine the effect of drugs on germination, at least 100 cells at random from each treatment were counted for percent germination as described above. To assess the effect of drugs on germ tube elongation, at least 10 cells from each replicate of each treatment were measured for its germ tube lengths. For this, only germinated zoospores, determined as described above, were measured. Effects on nuclear translocation was assessed by probing the cells with Hoechst 33342 as previously described. At least 100 cells at random from each replicate of each treatment were examined and percent cells that underwent nuclear translocation was determined. Specimens were photographed with Kodak T_{MAX} professional film and Hoffman modulation objectives (40x), using an exposure of 20 s. The concentrations of the drugs which resulted in effects which were significantly different than controls were determined for each experiment using analysis of variance (ANOVA) followed by Dunnett's multiple comparison test.

Results

Morphology and Time Course of Gametophytic Development

The motile zoospores of *Macrocystis pyrifera* are approximately 3-4 μm in diameter and are biflagellated (Fig.24 A). After their release from the sporophyll, the zoospores adhere to a substratum, lose their flagella, and initiate germination. Morphologically, the initiation of germination involved germ tube protrusion from the zoospore cell wall as a "nipple-like" projection (Fig. 24 B). The germ tube continued to grow (Figs. 24 C, D) until it reached a maximum length of approximately 15 μm. There appeared to be coincident cytoplasmic streaming and organelle translocation along the elongating germ tube (arrows in Figs. 24 C, D, E). Once the tube attained its maximum length, the growing end of the tube began to differentiate into a 3-4 μm diameter bulbous structure (Figs. 24 E, F). Under our present culture conditions, germination was initiated at 5-8 hours post-release of the zoospores. At this time, majority of the cells (typically > 80%) possessed germ tubes that were equal to or longer than the diameter of the zoospore (4-5 μm; Fig. 25). Germ tube elongation was typically completed by 18-20 hrs. of culture and attained germ tube lengths of approximately 13-15 μm (Fig. 25).

The vital DNA stain, Hoechst 33342 was used to investigate the nuclear division and positioning within the cell during different stages of germination and germ tube elongation. The zoospore possessed a single nucleus (Fig. 26 A). The nucleus remained similar in appearance with respect to the degree of condensation and position throughout germination and germ tube elongation (Figs. 26 B, C). Following completion of germ tube elongation, there was typically a 2-4 hrs delay until the nucleus initiated division. The dividing nucleus did not appear to undergo chromosomal condensation as observed in Hoechst 33342 stained cells. During division, the nucleus was observed to undergo a constriction (Fig. 26 D) resulting in an apparent fission-like

division (Fig. 26 E). Until complete separation of the daughter nucleus was achieved, small amounts of nuclear material were often observed to provide continuity between the two nuclei (Fig. 3D). Following division, the two daughter nuclei were readily observed (Fig. 26 E), and subsequently, the distal daughter nuclei immediately began translocation along the germ tube. This nucleus was typically elongate, with the leading end appearing to taper towards the distal end of the germ tube (Fig. 26 F). Towards the end of translocation (Figs. 26 G, H), the nucleus resumed it's original spherical appearance. Once initiated, completion of nuclear division and translocation occurred within 1 hour.

Following completion of nuclear translocation, the first gametophytic cross wall was observed (arrow in Fig. 27 A). This typically occurred within a few hours of completion of nuclear translocation. Subsequent to cross wall formation, the daughter nucleus remaining in the original zoospore body, underwent re-positioning (Fig. 27 B). This resulted in the nucleus assuming a position in the germ tube near the cross wall, with the zoospore body lacking nuclear material. Germ tube elongation and nuclear translocation were found to be temporally distinct events (Fig. 28). In all cases, nuclear translocation did not initiate until germ tube elongation was completed and maximum germ tube length was attained.

Ultrastructure of Zoospores and Gametophytes

At the ultrastructural level, the zoospore possessed a thick cell wall, a centrally located nucleus, chloroplasts, Golgi bodies, storage bodies, mitochondria, and many small vacuoles (Fig. 29 A). The nucleus was surrounded by a distinct nuclear envelope. The cell wall possessed moderately electron dense material; this may represent the adhesive coat of the zoospore. A distinct cell wall was present throughout gametophytic development. As described earlier, once nuclear translocation was completed, one daughter nucleus was often observed at the distal end of the germ tube while the other daughter nucleus remained in the central portion of the original zoospore body (Fig. 29 B). These gametophytes possessed distinct cross walls, and a complete complement of organelles as described above for the zoospores.

Effects of Cytochalasin D on Gametophytic Development

A zoospore was considered to have successfully germinated if the cell possessed a germ tube that was equal to or longer than the diameter of the zoospore (3-4 μm). In the present study, CD significantly ($p \leq 0.01$) inhibited completion of germination at concentrations of 100 μM and above (Fig. 30). The cells that failed to complete germination in the presence of CD, possessed small "nipple-like" projections of 1-2 μm long (rather than the minimum 3-4 μm), and therefore were considered "un-germinated"; however, this small projection indicated that germination had initiated. The nuclear division and/ or nuclear translocation did not begin until well after germination and germ tube elongation were completed, an event that normally took 18-20 hrs under our present culture conditions (see Fig. 28). As such, for investigating the effects of

cytochalasin D and other cytoskeletal disrupting agents on the nuclear events, we added the agents to the culture at 20 hrs post-culture. When CD, up to final concentrations of 400 μM, was added at 20 hrs of culture, neither nuclear division nor translocation was inhibited (Fig.30). In both controls (seawater ± 0.5% DMSO) and treatments (400 μM CD) more than 80% of the cells underwent nuclear division and translocation. Hoechst 33342 staining revealed that such cells possessed two nuclei, each located at the proximal and distal ends of the gametophytes (see Fig. 35 A). Those cells which did undergo complete germination in the presence of CD (typically < 30 %), at the concentrations used, possessed germ tubes that were not significantly shorter than from the control (sea water ± 0.5% DMSO) samples (Fig. 31). Prolonged culture of the zoospores in the presence of 100-200 μM CD for an additional 6 hrs did not show any significant effect on germination and germ tube elongation.

Cytochalasin D, when added during germ tube elongation, significantly inhibited further growth of the tubes. At the time CD (400 μM) was added to the cultures (11 hrs post-release of the zoospores), the majority of the cells possessed germ tubes that were 6.2 ± 0.2 μm in length (mean ± SD). Continued culture of these cells, in the presence of CD, resulted in germ tubes that were 9.12 ± 0.53 μm in length (mean ± SD); this was significantly shorter than that observed in the control groups which were 13.51 ± 0.27 μm in length (mean ± SD; n= 3, $p< 0.01$). In contrast, the addition of CD at 16 hrs post-release of the zoospores (well before the initiation of nuclear events), did not have any effect on the nuclear translocation. Both treated (400 μM CD) and control (sea water ± 0.5% DMSO) groups showed similar rates of nuclear translocation: 85.6 ± 1.6 % (mean ± SD) in the treated groups and 84.3 ± 1.7 % (mean ± SD) in the control groups.

Effects of Microtubule Disrupting Agents on Gametophytic Development

Cells cultured in the presence of colchicine (up to 360 μM) underwent normal rates of germination (Fig. 32). Morphological examination, at the light microscopic level, revealed that cells that germinated in the presence of colchicine had undergone tip differentiation as well as organelle (except nuclei) translocation along the germ tube. Those cells which did not germinate in the presence of 360 μM colchicine (typically < 15%), did not possess nipple-like projections (as seen in the presence of CD) and appeared similar to recently released zoospores except that they lacked the paired flagella (not shown). In contrast, nuclear division and translocation were significantly ($P\leq 0.01$) inhibited by colchicine at concentrations above 50 μM (Fig. 32), even though other cellular organelles were translocated along the germ tube. Such cells possessed a single nucleus located in the original zoospore body (see Fig. 35 B).

In addition to colchicine, we used the anti-microtubule agent APM (Kiermayer and Fedtke 1977, Morejohn and Fosket 1986) to investigate its effect on early gametophytic development. Similar to colchicine effect, germination was unaffected by APM at concentrations

of 1-5 μM (Fig. 33); however, these cells failed to undergo tip differentiation. At concentrations of 1 μM and above, APM significantly inhibited nuclear division and translocation (Fig. 33). APM treated cells appeared similar to those treated with colchicine with respect to nuclear positioning; cells possessed a single nucleus in the zoospore body (see Fig. 35 C). Neither controls (seawater ± 0.5% DMSO) affected any of the above developmental events (see Fig. 35 D). Prolonged culture in the presence of colchicine (50-100 μM) or APM (1μM) for an additional 6 hrs did not have any effect on the nuclear events (ie. the nuclear events were not simply delayed in the presence of the drugs). The gametophytes cultured in the presence of colchicine or APM possessed germ tubes of normal lengths that ranged from 13 to 16 μm (Fig. 34).

Discussion

The early stages of gametophytic development in *M. pyrifera* include zoospore germination, germ tube elongation, nuclear division and nuclear translocation. Some of these events are similar to those described previously for *M. integrifolia* (Cole 1968) as well as for other laminariales in general (Levyns, 1933; Papenfuss, 1942; Gerhardini and North, 1972). The present study has demonstrated that the above cellular events associated with the gametophytic development, which occur prior to differentiation into male or female gametophytes, are temporally and mechanistically distinct. Nuclear events did not begin until a complete germ tube was formed demonstrating that these events are temporally distinct from events associated with initiation of germination and germ tube elongation.

In the present study, zoospores initiated germination within 5-8 hrs after their release from the sporophyll blades and produced approximately 12-15 μm long germ tubes by 18-20 hrs. This was considered the process of "germination" in this study. The normal events associated with germ tube elongation in *M. pyrifera* gametophytes appear to be remarkably similar to events which occur during pollen tube growth in higher plants (Allen and Allen 1978, Cresti et al. 1977, Mascarenhas and Lafountain 1972, Nothnagel et al. 1981, Heslop-Harrison and Heslop-Harrison 1991). Cytochalasin D, a well known inhibitor of actin microfilament based cellular processes in both higher plants and algae (Perdue and Parthasarathy 1985, Kropf et al. 1990, Heslop-Harrison and Heslop-Harrison 1991), effectively inhibited germ tube elongation, but not initiation of germination as evidenced by the presence of small projections on the zoospore body. When CD was added to the cultures during germ tube elongation, rather than prior to initiation, cells did not attain germ tubes of normal lengths. In these treated cells, it is not surprising that germ tube elongation continued for a period of time following addition of CD due to the presence of a formidable cell wall and the relatively slow growth of the germ tube. These data suggest that actin microfilaments are intimately involved in germ tube elongation. In addition,

microtubule disrupting agents, colchicine (Wilson and Meza 1973) and APM (Morejohn and Fosket 1986), did not affect germination and germ tube elongation, thus supporting the hypothesis that actin microfilaments alone are responsible for these events. However, in the presence of CD (added at 3 hrs post-zoospore release), a low percentage of cells went on to form germ tubes of normal lengths. This could be due to the possibility of CD not being taken by these cells. It is well known that actin microfilaments play an important role in cell motility and morphogenesis in plants (Nagai and Rebhun 1966, Kersey et al. 1976, Williamson, 1986; see also Hepler and Palevitz 1974 for a review). For example, several studies involving administration of cytochalasins have clearly demonstrated that actin microfilaments regulate pollen tube growth and the associated cytoplasmic streaming and organelle translocation (Franke et al. 1972, Mascarenhas and Lafountain 1972, Perdue and Parthasarathy 1985, Picton and Steer 1982, Steer and Steer 1989, Heslop-Harrison and Heslop-Harrison 1991). Although biochemical evidence is lacking, it has been suggested that cytochalasins may block apical growth in pollen tubes by capping the growing ends of the actin microfilaments within the tube (Cooper 1987). It would be of interest to explore the role of actin microfilaments during *M. pyrifera* gametophyte development further by elucidating its dynamics at distinct stages of germination and germ tube elongation.

The nuclear events (nuclear division and nuclear translocation) that occur during gametophytic development has been clearly demonstrated using the vital DNA stain Hoechst 33342. Subsequent to division of the zoospore nucleus, one of the daughter nuclei is translocated to the distal end of the germ tube as has been previously reported in *M. integrifolia* (Cole 1968). This nuclear translocation occurs over a significant distance (12-15 μm) and is unlike the limited nuclear movement and positioning that occurs prior to cell division in higher plants (Meindl 1983, Gunning and Wick 1985, Doonan et al.1985), but similar to the movement of vegetative nucleus observed in pollen tubes (Venema and Koopmans 1961, Heslop-Harrison and Heslop-Harrison 1989) and in coenocytic green algae (Ott, 1992). Nuclear division and translocation in *M. pyrifera* did not begin until a complete germ tube was formed and other cytoplasmic organelles were observed at the distal end of the tube, demonstrating that nuclear events are temporally distinct from events associated with germination and germ tube elongation. In addition, nuclear division and translocation preceded the gametophytic cross wall formation; in fact cross wall formation often occurred several hours after nuclear translocation was completed. Whether this relatively long time lag between nuclear translocation and formation of the gametophytic cross wall is specific to *M. pyrifera* within the algae is not clear at the present time.

Colchicine and APM, two microtubule disrupting agents (Wilson and Meza 1973, Kiermayer and Fedtke 1977, Morejohn and Fosket 1986), inhibited nuclear division and subsequent translocation of the daughter nucleus suggesting that these are microtubule mediated

developmental processes. In the coenocytic alga, *Voucheria longicaulis*, nuclear translocation has been shown to be mediated by microtubular system (Ott, 1992). In this, each nucleus with in the vegetative cell, moves as an independent unit attached to a bundle of microtubules. In several other plant species however, the involvement of both actin filaments and microtubules have been shown to govern nuclear events. For example, in cultured tobacco cells (Katsuta and Shibaoka, 1988) and crest root statocytes (Hensel 1985), actin microfilaments govern nuclear migration and positioning while microtubules are primarily responsible for the pre-mitotic nuclear events in the protonema of *Adiantum* tip cells (Mineyuki and Furuya 1986). While germination and germ tube elongation in *M. pyrifera* are similar to pollen grain germination and tube growth with respect to its regulation by actin microfilaments, the mechanism of nuclear movement differ dramatically between these two systems. In the latter, movement of the vegetative nucleus has been clearly shown to be dependent on its local association with the actin cytoskeleton (Tiwari and Polito 1988, Heslop-Harrison et al. 1988, Heslop-Harrison and Heslop-Harrison 1989). The role of microtubules in nuclear translocation in *M. pyrifera* was further supported by our preliminary experiments (data not shown) in which a percentage of gametophytes possessing divided (but non-translocated) nuclei were pulsed with APM. In this case, nuclear translocation was inhibited in the cells exhibiting divided nuclei. In these experiments, subsequent division of nuclei in other cells during the APM exposure period was blocked. This suggests that both nuclear division and translocation are mediated by microtubules, but additional studies are necessary. Furthermore, when CD was employed at 16 hrs (i.e. 4-6 hrs prior to initiation of nuclear division), or at 20 hrs (just prior to nuclear division) post-zoospore release, neither nuclear division nor translocation was affected. While we cannot rule out the possibility that some actin microfilaments involved in nuclear events are resistant to disruption by CD, the data strongly suggest that microfilaments are not directly responsible for nuclear division and translocation. At present, it is unclear if the mechanisms of translocation of the second daughter nucleus from the original zoospore body, following cross wall formation, is similar to the one described above.

In summary, this investigation has described the cellular events of early development in *M. pyrifera* gametophytes. While several aspects of zoospore germination and germ tube elongation are similar to pollen tube growth in higher plants, the mechanisms of regulation of these cellular processes seem to differ in these systems. Our study indicates that germination and germ tube elongation in *M. pyrifera* involve actin microfilaments, rather than microtubules. The nuclear division, which occurs following germ tube elongation, immediately precedes the translocation of a daughter nucleus to the distal end of the tube. Based on our pharmacological studies, it appears that the nuclear division and translocation are dependent on microtubules, rather than actin microfilaments. Changes in the dynamics and distribution of these cytoskeletal

elements within the cell during different phases of gametophytic development deserve further research attention and are currently under investigation in our laboratory.

Figure 24

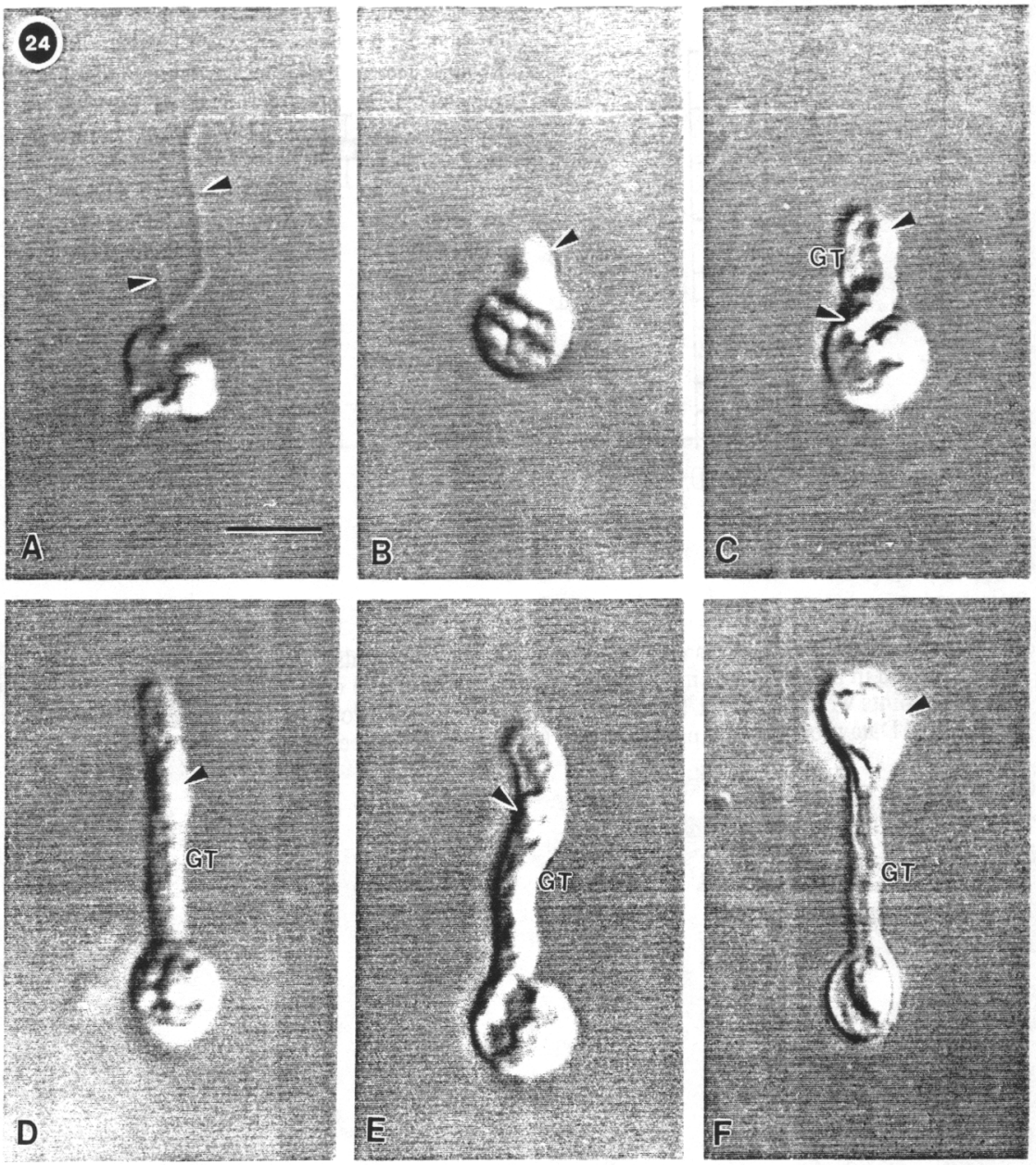

Fig. 24 Light micrographs (photographed with Hoffman modulation optics) of gametophytes from *M. pyrifera* at different stages of development. **A** A recently released zoospore; ▶ paired flagella; **B** zoospore that has initiated germination (6 h post-release), the germ tube bulges out from the zoospore as a "nipple-like" projection (▶); **C** a mid germ tube (*GT*) stage (12 h post-release) cell, cytoplasmic organelles (▶) begin to translocate along the growing germ tube; **D** at 18 h post-release, the cell has attained the maximum germ tube length; ▶ organelle(s) being translocated along the germ tube; **E** germ tube that has just initiated tip differentiation, 24 h post-release, ▶ cytoplasmic organelles; **F** a completely germinated cell (30 h) with its tip differentiated into a bulbous structure (▶). Bar: 5.0 μm

Figure 25

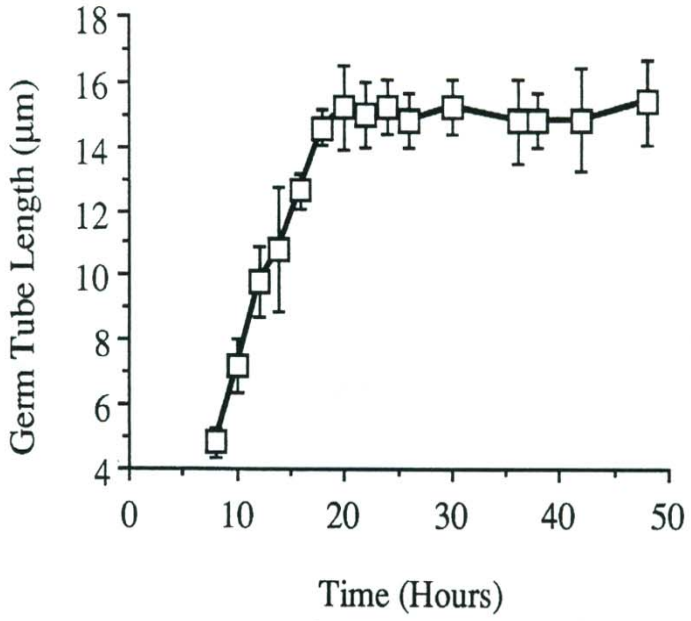

Graph illustrating the germ tube length at different time points of culture. Cells were cultured as described in materials and methods and the germ tube length of at least 10 cells at the specified time points were measured. Zero time indicates the time of zoospore release from sporophyll blades. Data presented are pooled means (±S.D.) from 3 experiments.

Figure 26

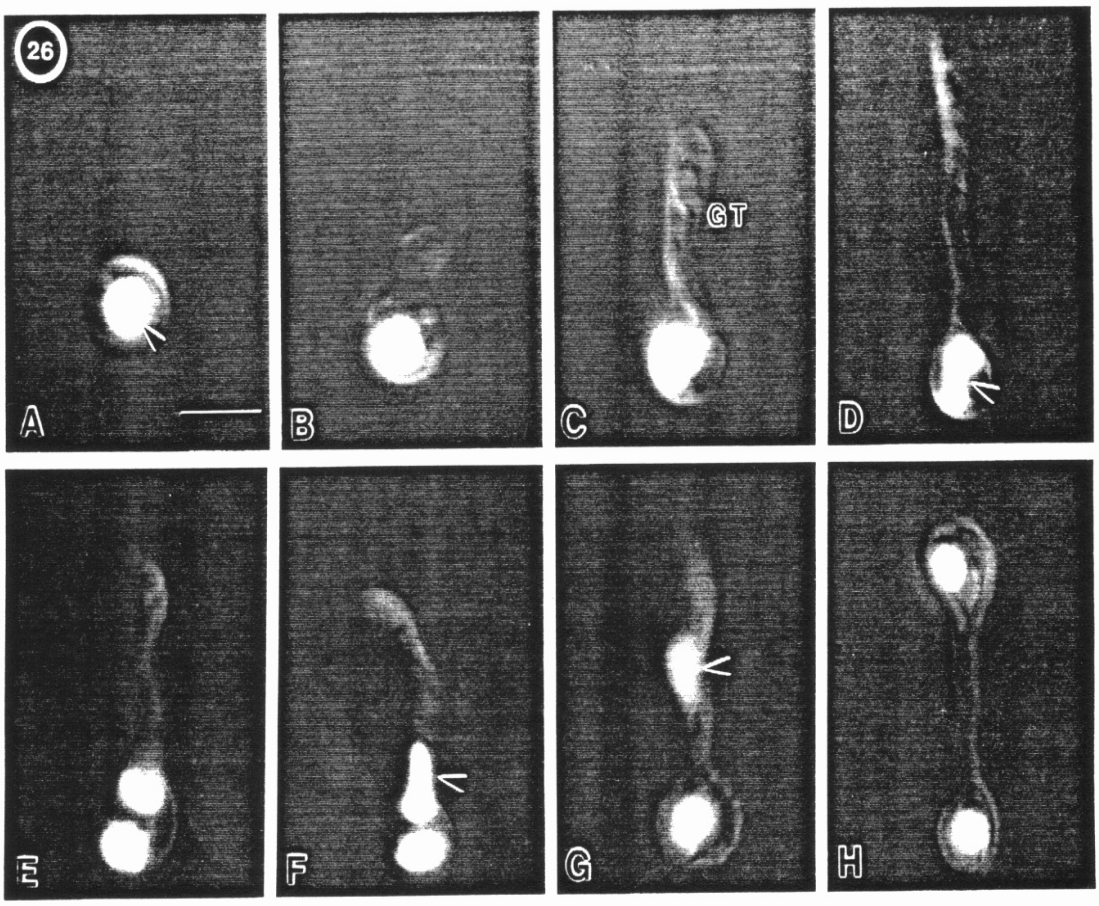

Fluorescence micrographs of zoospores from *M. pyrifera* showing the sequence of nuclear events at different stages of gametophytic development. Cells were fixed at different stages of development and probed with the vital DNA stain Hoechst 33342 as described in Materials and methods to visualize the nuclear material. **A** A recently released zoospore with a single nucleus (▶); **B** a zoospore that has initiated germ tube elongation (6 h post-release) with a basally located nucleus; **C** a cell at 18 h post-release with the nucleus still located in the original zoospore region; *GT* germ tube; **D** a germinated cell (24 h post-release) with the nucleus undergoing a "fission-like" division (▶); **E** after nuclear division, two distinct daughter nuclei are readily observed in the zoospore region; **F** after division, one daughter nucleus (▶) initiated translocation along the germ tube; **G** a cell with one nucleus having translocated half-way along the germ tube (▶); **H** a cell at 30h post-release with the daughter nucleus having translocated to the distal end of the germ tube. Bar: 5.0 μm

Figures 27-28

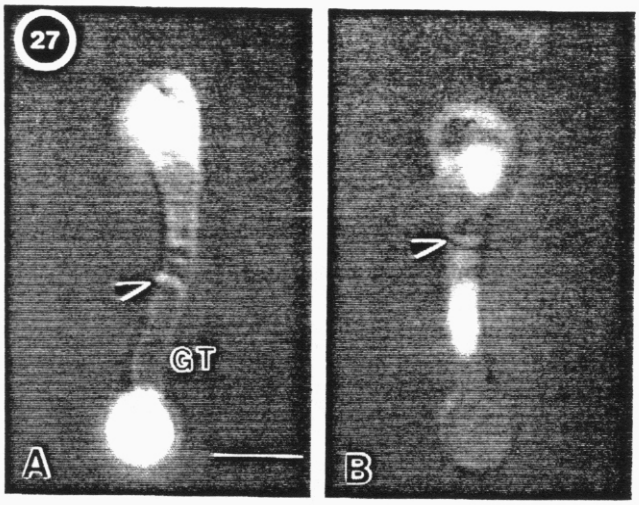

Combination modulation optics and fluorescence (Hoechst 33342) micrographs of **A** germinated zoospores after the completion of nuclear translocation and formation of the gamethophytic cross wall (►) and **B** germinated zoospore 48 h after zoospore release, demonstrating the re-positioning of the second daughter nucleus within the germ tube. Note the gametophytic cross wall (►); *GT* germ tube. Bar: 5.0 µm

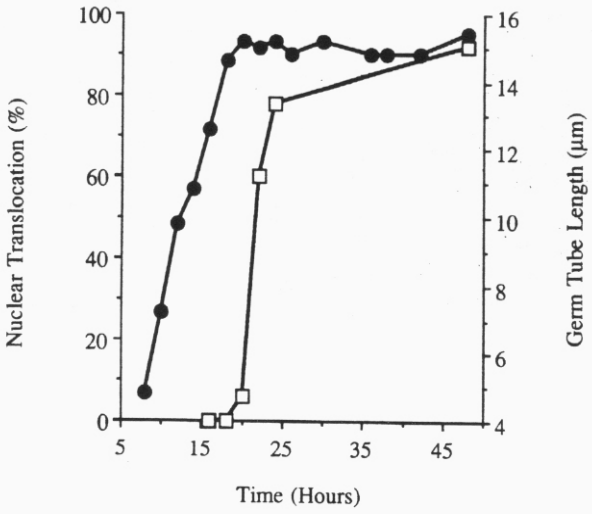

Fig. 28 Relationship between germ tube length (●) and the occurrence of nuclear translocation (□) at different time points. Notice that the nuclear translocation did not initiate until several hours (3–5) after the maximum germ tube length was obtained (18–20 h post-release). The germ tube length shown represents the mean germ tube lengths of at least 10 cells from samples at each time point. The nuclear translocation was scored in at least 100 cells from samples at each time point. Data is from one experiment but the temporal separation of germ tube elongation and nuclear translocation is representative of that observed in many experiments

Figure 29

Transmission electron micrographs of *M. pyrifera* zoospore (**A**) and completely germinated zoospore after the initial gametophytic cell wall has formed (**B**). Note the presence of a cross wall (arrow) and two distinct nuclei (N) in the gametophyte. CH- chloroplast; CW- cell wall; G- golgi bodies; GT- germ tube; M- mitochondrion; N- nucleus; SB- storage bodies; V- vacuoles . Bar = 1.0 µm.

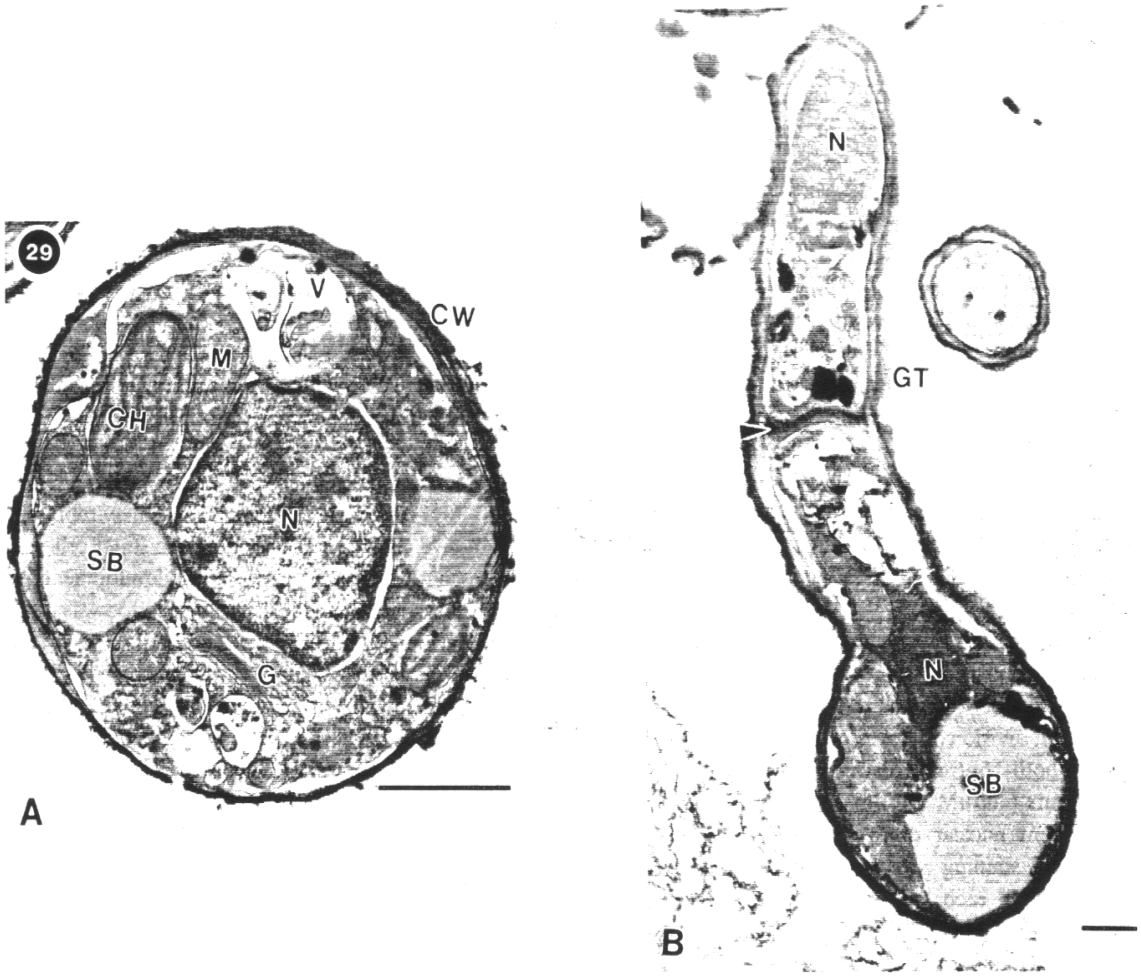

Figures 30-31

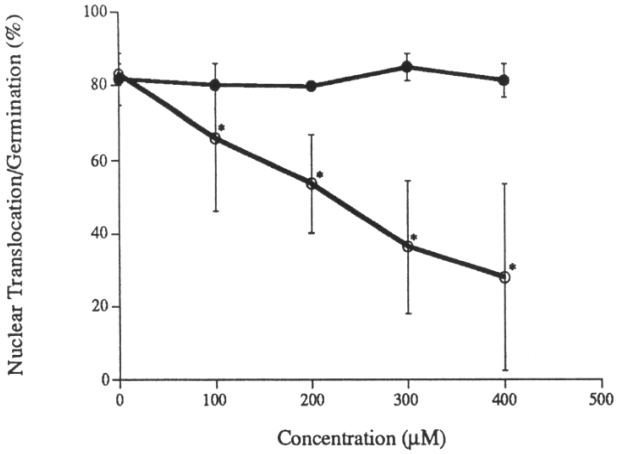

30: Graph showing the effects of cytochalasin D on germination (○) and nuclear translocation (●). The drug was added to the culture either at 3 hrs (to study its effect on germination) or at 20 hrs post-release (to study its effects on nuclear translocation). A cell was considered to be germinated if it possessed a germ tube that was equal to or longer than the diameter of the zoospore. Data presented are pooled means (±S.D.) of 4 experiments. Asterisks denote concentrations significantly different from control ($p \leq 0.01$).

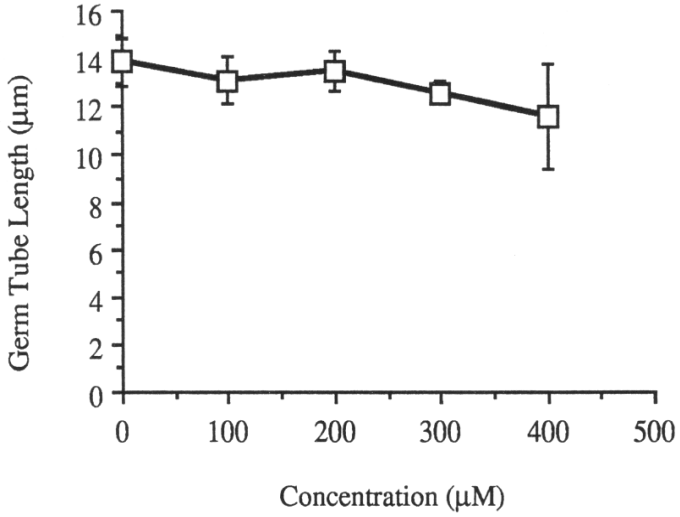

31: Effect of cytochalasin D on germ tube elongation (germ tube length) during gametophytic development. Notice that these data represent the germ tube lengths of those cells which did undergo germination and germ tube elongation (typically < 30%) in the presence of the drug. There was no significant difference in the germ tube lengths at the different concentrations of cytochalasin D as compared to sea water (0.5% DMSO) controls.

Figures 32-33

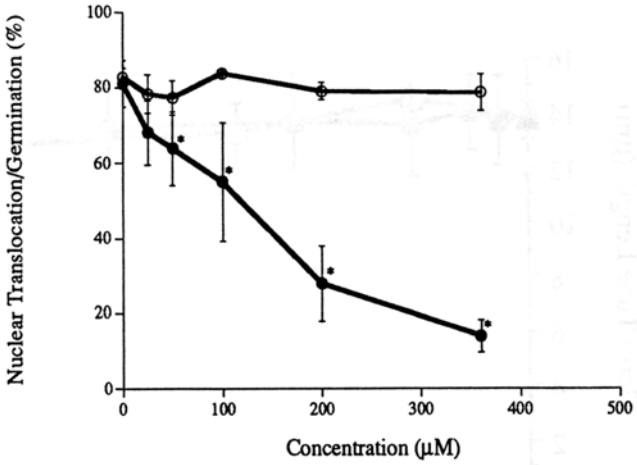

32: Effects of colchicine on germination (○) and nuclear translocation (●). The drug was added either at 3 hrs (germination) or 20 hrs (nuclear translocation) post-release of the zoospores. Data presented are pooled means (± S.D.) of 3 experiments. Asterisks denote significant difference from the control ($p \leq 0.01$).

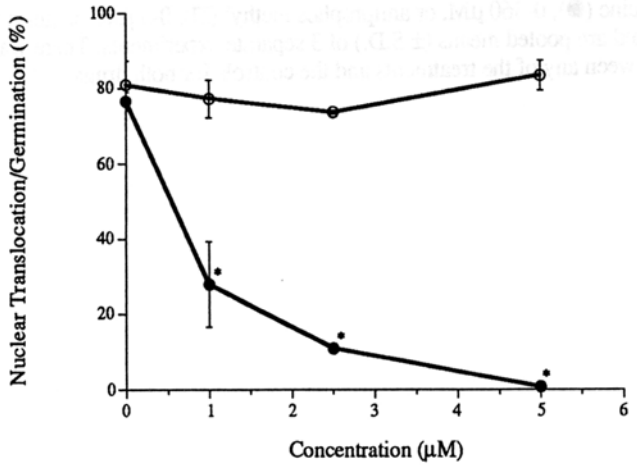

33: Effects of amiprophos methyl on germination (○) and nuclear translocation (●). The drug was added to the culture at 3 hrs (germination) or 20 hrs (nuclear translocation) post-release of the zoospores. Data are pooled means (± SD) of 3 experiments. Asterisks represent significant difference from the control ($p \leq 0.01$).

Figure 34

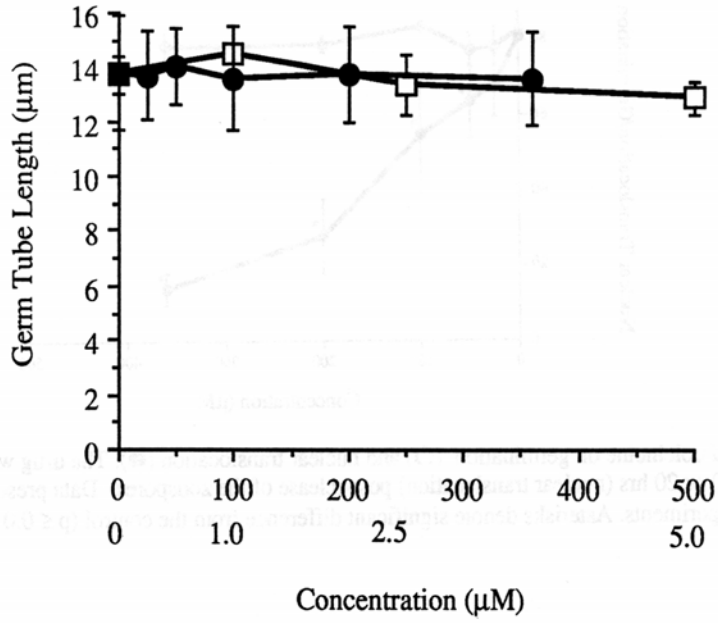

34: Effects of colchicine (●), 0-360 µM, or amiprophos methyl (❐), 0-5 µM, on germ tube elongation (germ tube length). Data presented are pooled means (± S.D.) of 3 separate experiments. There was no significant difference in germ tube lengths between any of the treatments and the controls for both drugs.

Figure 35

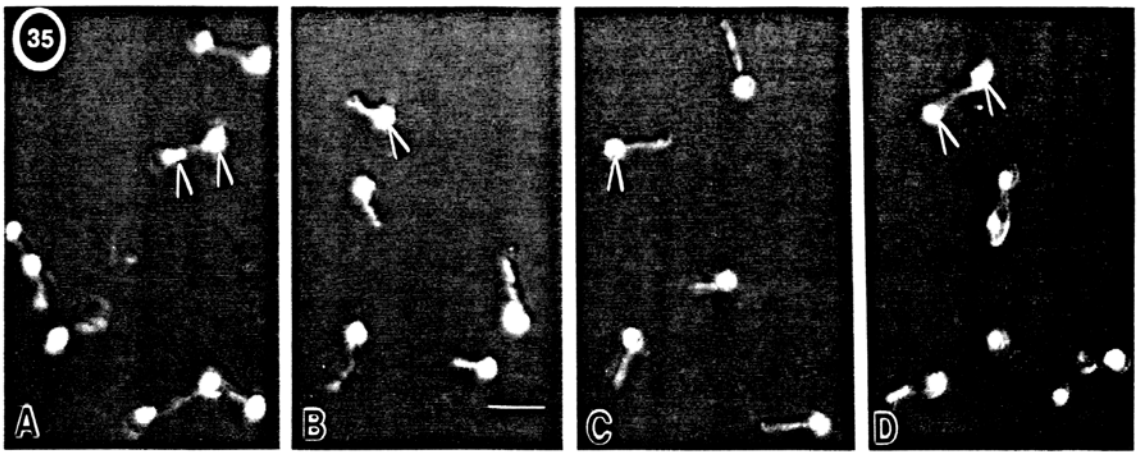

Fig. 35 Fluorescent micrographs of Hoechst 33342 labelled cells showing the effects of 300 µM cytochalasin D (**A**), 200 µM colchicine (**B**), 2.5 µM amiprophos methyl (**C**), or the control solution, seawater ± 0.5% DMSO (**D**) on nuclear translocation during gamethophytic development. The respective drugs were added to the culture at 20 h post-release. ▶ Position of the nuclei within the germ tubes under different experimental conditions. Bar: 15.0 µm

STUDIES WITH MUSSELS EMBRYOS

The following data are preliminary in nature, and much of this work is on-going as part of the current project "Chronic Toxicological Effects of Produced Water on Reproduction and Development in Marine Organisms", G.N. Cherr and T. W-M. Fan, Principal Investigators. The emphasis on mussels was due primarily to their use in field outplants at the PW discharge (Osenberg et al., 1992), and their use in the identification of toxic constituents of PW (Higashi et al., 1992).

Materials and Methods

Field Outplants

California mussels of approximately 4 cm maximum length were collected near Montana del Oro State Park, County. The mussels were transported back to Bodega Marine Laboratory where they were placed in a tank of flowing seawater. Approximately 250 mussels were measured, marked with numbered bee tags, and placed in mesh oyster culture bags. To minimize the clumping of mussels, ten mussels were placed in each of three bag subunits, separated from other subunits by constriction of the bag with cable ties.

Three bags of thirty mussels were assembled for each field site and shipped to Santa Barbara. After one week holding time in flowing seawater tanks in Santa Barbara, mussels were outplanted by SCUBA divers at sites associated with a produced water discharge near Carpinteria. Three bags were attached to two buoy arrays approximately 1m above the sediment at sites 1m, 5m, 10m, 100m, and 1000m from outfall in discharge plume. A second set of bags were hung from the buoy arrays at mid depth (approx. 4.6 m above bottom) to compare water column effects to effects influenced by sediment processes.

Bags were outplanted in early June, 1990, a time when sampled mussels were found to be in the indeterminate or early developing stages of gametogenesis. Mussels remained in the field for nearly five months during which time they continued gametogenesis. Monthly water samples were taken from each site for determination of non-filterable, combustible residue to obtain an estimate of organic matter available as food for mussels. On two occasions in early and mid October trial bag subunits were cut from one of the three bags at the 1m and 1000m from outfall near-sediment sites (Hereafter, near-sediment sites will be referred to with the label "Low", while water column sites will be referred to with the label "Mid", ie, 1m from the outfall near-sediment = 1m Low, while 1m water column = 1m Mid). Trial bag subunits were shipped to the Bodega Marine Laboratory where they were placed in individual containers of concentrated culture of *Isochrysis galbana* to stimulate spawning. Mussels from 1m Low site spawned readily on both occasions while mussels from the 1000m Low site did not spawn but appeared ripe upon

examination of gonads in mid October. In order to maximize the chances of getting mussels from all sites to spawn, assays were scheduled for late October/early November.

Laboratory Studies and Assessments

Mussels which underwent gametogenesis at various sites near the PW discharge were brought to the laboratory and induced to spawn as described above and by Cherr et al. (1990). Following quantitation of the sperm and eggs from each animal, sperm was pooled from 3 males in equal quantities, and the sperm/egg ratios resulting in optimal (>95% or the maximal attained) fertilization were determined for each female which spawned according to Cherr et al. (1990). Aliquots of eggs were also fixed for subsequent determination of chromosome morphologies. For assessment of embryo sensitivity to PW, females from different outplant sites were fertilized with the same sperm from Bodega Head control males, and the zygotes exposed to increasing PW concentrations.

For toxicity testing, pooled aliquots of eggs from 3 females from each site were fertilized, washed and exposed to increasing concentrations of PW as described by Higashi et al. (1992). For assessing shell calcification, embryos were cultured in control filtered seawater (FSW) or PW for 96 hrs. (15º C), fixed, and viewed using polarization microscopy according to Cherr et al. (1990).

Assessment of Stress Protein Expression

Mytilus californianus embryos fom either control sites (Bodega Bay, CA) or PW discharge sites (1m and 10m) were cultured at 15º C in 0.22 µm FSW, pH 8.0, to the gastrula stage at 19 h postfertilization. All eggs were fertilized with pooled sperm from Bodega Head males. Embryos were then exposed to either 10% PW or ASW control for 3 h at 1000 embryos / ml at 15º C. After 2 h of exposure, ^{3}H-leucine (ICN Biomedicals Inc., Costa Mesa, California, and NEN Research Products, Boston, Massachusetts; 20 µCi/ml final concentration) was added to each treatment for the final hour. In all experiments, embryos were pelleted by hand centrifugation, briefly washed with FSW, pelleted again, and solubilized for electrophoretic analysis in a buffer containing 1.5% sodium dodecyl sulfate (SDS) and mercaptoethanol and stored frozen at -20º C.

Electrophoresis and Autoradiography

Samples were subjected to sodium dodecyl sulfate polyacrylamide gel electrophoresis (SDS PAGE) using 4-15% gradient gels (Bio Rad, Richmond, CA). Gels were stained with coomassie blue G-250 or R-250 and dried using a Bio Rad Laboratories Model 224 gel slab dryer. Molecular weights standards were as follows: myosin (200 kDa), ß-galactosidase (116.3 kDa), rabbit muscle phosphorylase b (97.4 kDa), bovine serum albumin (66.2 kDa), hen egg white ovalbumin (45 kDa), bovine carbonic anhydrase (31 kDa), and soybean trypsin inhibitor (21.5 kDa). Autoradiography of electrophoresed proteins was carried out using Hyperfilm-3H

high performance autoradiography film (Amersham, Arlington Heights, Il.) with a 96 hour exposure.

Results and Discussion

As described by Higashi et al. (1992), we have found that PW inhibits normal embryonic development in mussels (Fig. 36), and, at lower concentrations, also appears to inhibit veliger larval shell calcification (Fig. 37). Although inhibition of shell calcification has been reported in veligers exposed to other toxicants (Cherr et al., 1990), these effects are likely due to delays in development. In the case of PW, we incubated the larvae to 96 hrs., which is 48 hrs. past complete formation of the larval shell. As such, it would appear that PW interferes with normal shell calcification, perhaps due to the presence of barium (Fan et al., unpublished observations). This was further substantiated by observations that the shells of adult mussels near the discharge were extremely fragile and were broken simply due to handling (Garman, unpublished observation).

Fertilization data in control seawater for females and males from the various outplant sites are shown in Table 1. For 1990-91, there was an indication that increased sperm concentration was necessary to achieve maximal fertilization in gametes from the various sites. However, there was not a linear relationship between location to the discharge and gamete quality since fertilization in the 1000m animals was as low as fertilization in the 10m animals. Nevertheless, all sites were different than Bodega Bay control animals handled in a similar manner. For 1991-92, no effects on the discharge site animals as compared to Bodega Head controls were observed (Table 1).

Data from these same studies show that abnormal oogenesis can occur in some females at sites near the PW discharge. Of the females that spawned at each site, a percentage of eggs from most of the females exhibited an unusual chromosome morphology (Table 2). This morphology involves the scattering of chromosomes throughout the cytoplasm, instead of the normal organized metaphase alignment (Cherr et al., 1990). For example, in 1990-91, five out of twelve females outplanted within five meters of the discharge, showed chromosomal abnormalities in greater than 22% of their eggs, and in one female, up to 53% of the eggs were abnormal. In eggs from mussels at control sites (eg. Bodega Head), chromosomes were typically in metaphase I, and were polarized towards the egg cortex. The abnormal chromosome arrangements in eggs from discharge site females included situations where all of the condensed chromosomes were scattered throughout the egg, or the chromosomal arrangement did not follow a typical metaphase pattern; this correlated with the inability of these eggs to be fertilized (data not shown). It is likely that the perturbation in oogenesis resulting in lack of fertilizability is related to the abnormal chromosome orientation in oocytes. Since microtubules play a pivotal role in

maintaining chromosomes at the metaphase plate and during cell division, the abnormal chromosomal arrangement in eggs from PW exposed individuals could be due to an abnormal orientaion of microtubules, which is currently under investigation. Furthermore, it has been demonstrated that divalent cations, specifically, Sr and Ba, were capable of inhibiting normal oocyte development (Kindle *et al.*, 1990). Thus, it is possible that these two divalent cations, which are present in both PW and water samples collected at the discharge site (Higashi *et al.*, 1992), may be in part responsible for the perturbed oogenesis in PW-exposed mussels, and this hypothesis is also currently being tested.

Embryos from adults outplanted (1990-91) at 1 m from the PW discharge are less sensitive to PW exposure in the laboratory than those from adults outplanted at the 100 m site or than Bodega Head reference animals (Fig. 38). However, the animals from the 1000m site also showed some sensitivity decrease as compared with Bodega Head reference females; this correlates with the presence of abnormal chromosome morphologies in these animals, and substantiates the notion that the 1000m site may not be free from impact at the level of gametogenesis. This decrease in sensitivity appears to be maternal in origin, since sperm used in these experiments were all from control animals. No changes in sensitivity of embryos, to PW, from adults outplanted in 1991-92 was observed (not shown). This lack of effect was once again consistent with the lack of effect on fertilization rates and chromosome morphologies during this time period.

One of the mechanisms by which cells can develop tolerance to thermal and chemical stress may be the expression of "stress proteins". These can also be used as convenient biomarkers of exposure, and may relate to specific dysfunctions as a result of stress. We have found that sea urchin embryos exposed to PW for 3 hrs., express a high molecular weight glycoprotein rather than the heat shock proteins previously described as a result of thermal stress (Baldwin et al., 1992). Experiments using PW-exposed mussel embryos indicate that they also express a protein which is higher in molecular weight (195 kDa) than typical heat shock proteins, but is significantly lower in molecular weight than the sea urchin protein (250 kDa) (Figs. 39). This protein was not expressed in seawater control exposures.

We also conducted protein expression experiments on embryos from adults at the 1m, 10m, and 1000m discharge sites in whch gastrula stage embryos were simply cultured in seawater in the presence of the labeled amino acid. In these experiments we were determining if the differential expression of the 195 kDa component in the absence of PW, was related to the environmental history of the adult. The embryos from adults outplanted at both the 1m and 10m sites showed expression of the 195 kDa protein, and this was particularly apparent in the 10 m embryos (Figs. 40). The embryos from adults outplanted at 1000m from the discharge appeared similar as Bodega Head control embryos (compare Figs. 39 and 40) in that they did not express

the 195 kDa component. This may relate to previous observations in the literature suggesting that offspring from adults living in polluted environments develop tolerance to the pollution through expression of stress proteins (Sanders, 1990). Even more intriguing is the indication that a specific message (mRNA) for the 195 kDa protein is in the oocytes of PW exposed females, and it is expressed during development, regardless of subsequent PW exposure. This could be a genetic basis for differences in organisms which are from polluted environments.

Figures 36-37

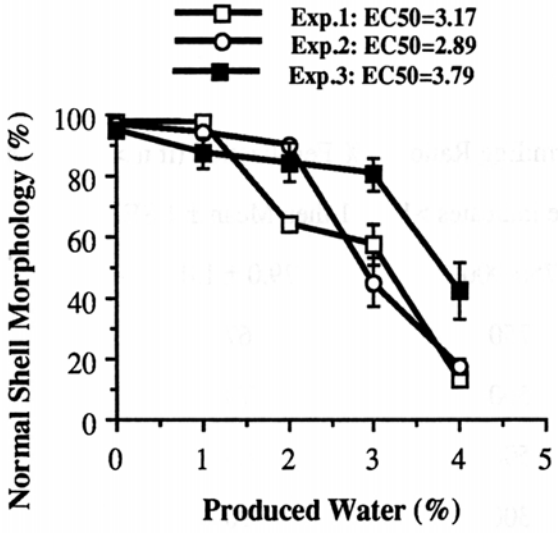

36: Effects of produced water on larval shell morphology during mussel embryo development. These assessments were conducted at 96 hrs. of culture and were based on standard morphological criteria as described in Cherr et al. (1990). Data are from three experiments.

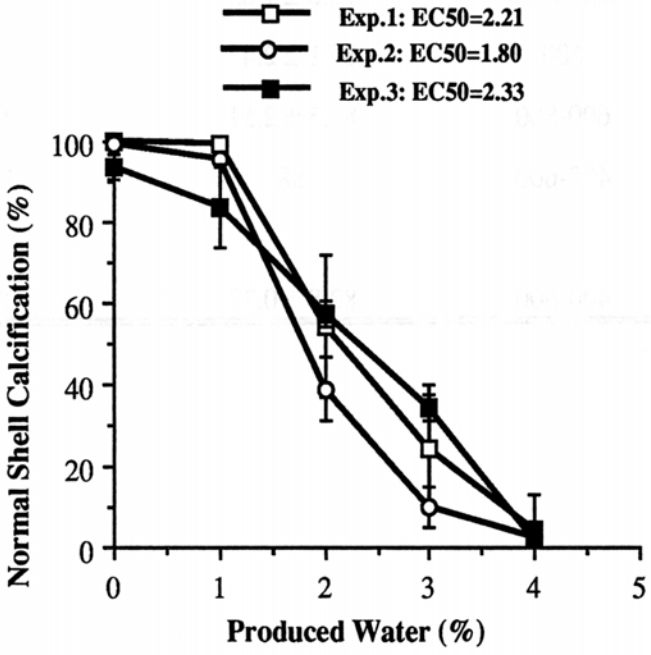

37: Effects of produced water on larval shell calcification during mussel embryo development. These are the corresponding embryos from Fig. 36, in which the shells were viewed using polarization microscopy. These more in-depth assessments clearly show that produced water affects normal shell calcification at lower concentrations than those which affect shell morphology. The data are from three experiments and the experiment number corresponds to those in Fig. 36.

Table 1 : Sperm to egg ratios used and % fertilization for 90-91 and 91-92 field mussel experiments.

Site	Sperm:Egg Ratio (range indicates >1	% Fertilization (if n > 1 then Mean ± 1 SE	# of Males
90-91			
1 m	750-900	79.0 ± 1.0	2
10 m	750	67	3 (pooled)
100 m	500	79	3 (pooled)
1000 m	500	65	3 (pooled)
B. Bay	300	90	3 (pooled)
91-92			
1 m	400-600	82.2 ± 2.93	3
10 m	600-1000	70.0 ± 7.65	3
100 m	600	84.1 ± 2.43	3
1000 m	600-800	87.5 ± 2.51	2
Upstream (1000 m)	400-600	88	1
B. Bay	400-600	82.8 ± 0.73	3

Table 2: Occurence of abnormal chromosomes in eggs from field mussels. 1990-1991 and 1991-1992.

Site	Total # Females That Spawned	# Individuals with Abnormal Chromosomes	Range of % Abnormal Chromosomes
90-91			
1 Low	4	3	14-53
1 Mid	4	3	7-23
5 Low	1	0	0
5 Mid	3	3	28-36
10 Low	3	3	3-17
100 Low	1	1	13
1000 Low	3	3	6-38
B. Bay	2	0	0
91-92			
1 L	14	3	8-13
1 L (M. del Oro from 90-91)	6	3	9-20
10 L	4	1	3
100 L	9	3	3-5
1000 L	2	1	6
Upstream (1000 m)	3	1	7
B. Bay	4	0	0

Figure 38

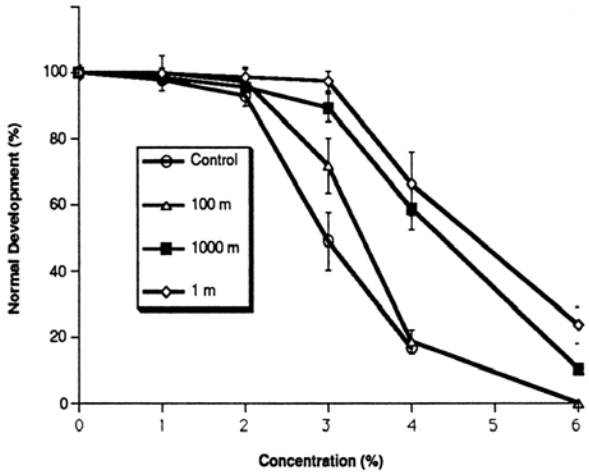

Response of embryos, to produced water, from adults outplanted at 1m, 100m, and 1000m from the produced water discharge. Control embryos are from Bodega Head mussels handled in a similar manner. The sperm used to fertilize eggs from females at each site were from pooled batches from control males. Note the decreased sensitivity of the embryos from the 1m females as compared to the other sites. The 1000m site embryos also appeared to exhibit some effect.

Figure 39

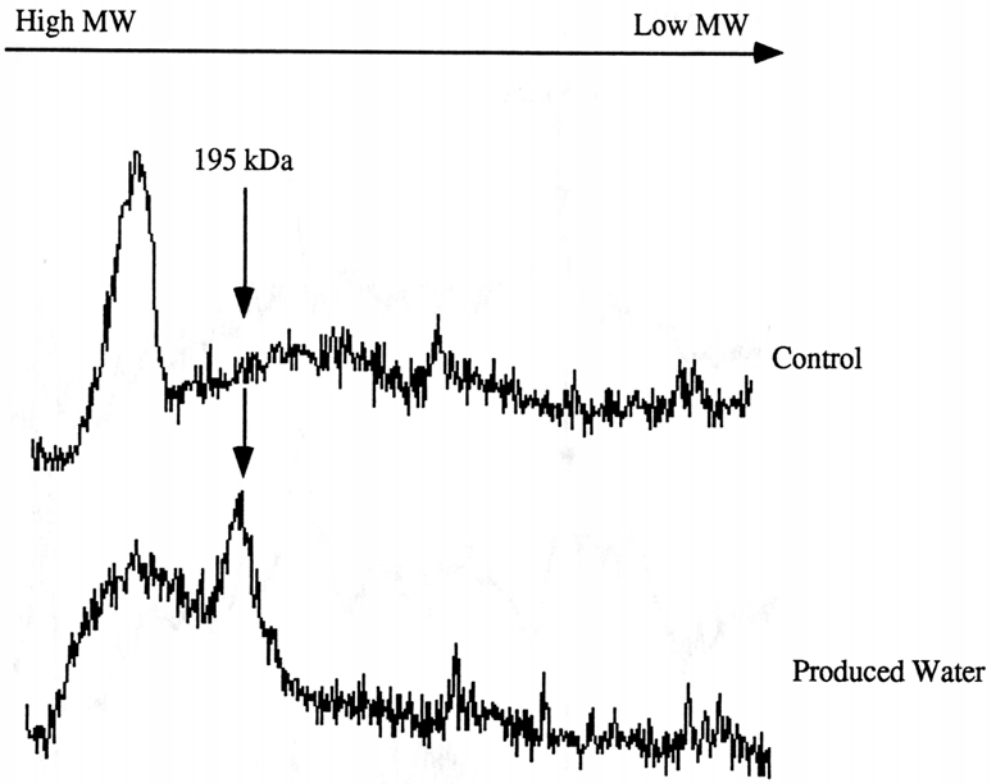

Scans of autoradiograms from 4-15% gradient gels of gastrula stage mussel embryos exposed to either control seawater or produced water (10%) and coincubated with ^{3}H leucine. Note the presence of a 195 kDa protein in the produced water exposed embryos. The higher molecular weight protein present in controls is decreased in produced water exposures. Embryos used for these experiments were from adults collected at Bodega Head and are considered "control" animals.

Figure 40

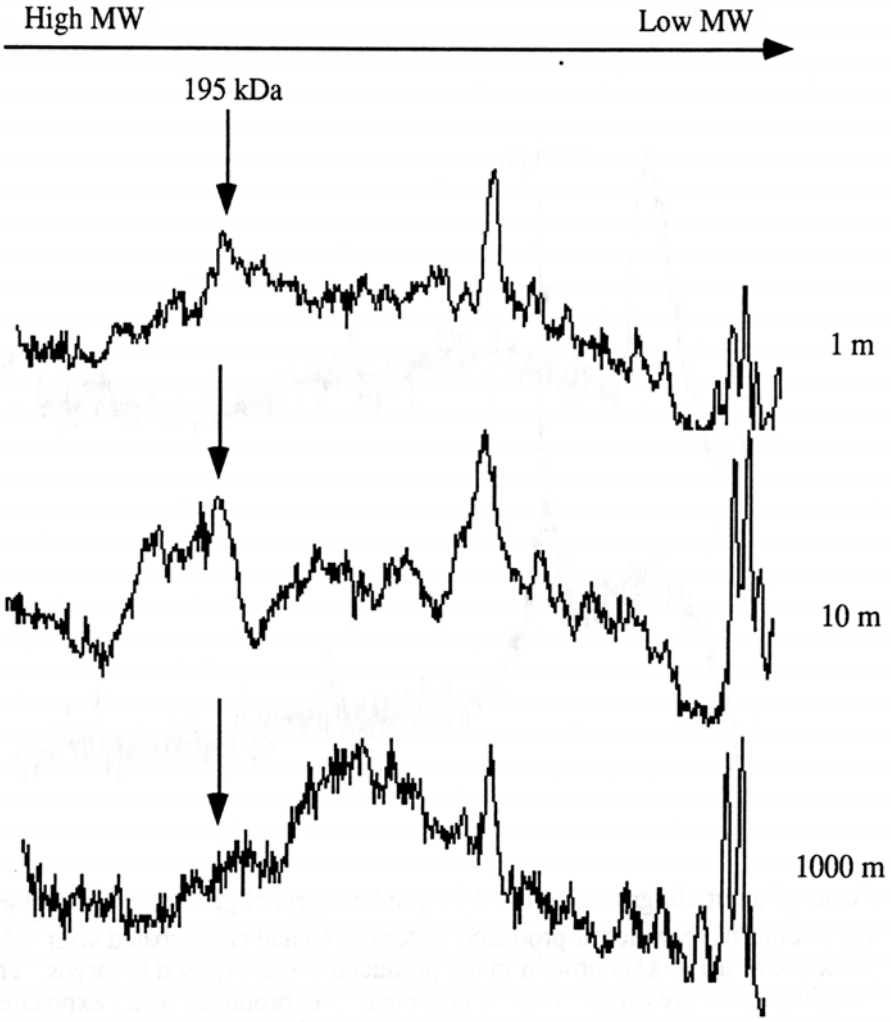

Scans of autoradiograms from 4-15% gradient gels of gastrula stage mussel embryos from adults outplanted at 1m, 10m, and 1000m from the produced water discharge. Note that the 195 kDa protein is expressed at 1m and 10m, but not at 1000m, suggesting its presence is due to exposure of oocytes to PW. Sperm used for these experiments were from the same control (Bodega Head) males.

SECTION II

EFFECTS OF PRODUCED WATER ON ADULT ORGANISMS

To complement the research on early life stages described in the previous section, we have investigated the impact of PW on reproduction and health of adult organisms indigenous to the California coast. To assess reproductive success and organismal health, we have developed a noninvasive approach utilizing nuclear magnetic resonance (NMR) spectroscopy and imaging. This technology has originally been developed for biomedical research and are now routinely used in clinical dignostics. In this report, We demonstrated the utility of such approach for diagnosing the functioning of indigenous organisms. The principal advantages of the NMR approach are 1) long-term metabolic changes can be monitored on the same individual without interferences from intrinsic organismal differences; 2) metabolic information central to our understanding of organismal functioning and yet difficult to acquire with invasive approach can be obtained; 3) detailed structure information on important functional indicators are readily obtained. These advantages were illustrated in four separate studies on three marine invertebrates, *Mytilus edulis* (blue mussel), *M. californianus* (Calinfornia mussel), and *Syciona ingentis* (ridgeback prawn). Three of the studies emphasized on the development of NMR methodologies while the fourth applied the methodologies to investigating the chronic effect of PW on mussel reproduction.

METHOD DEVELOPMENT

Emergence and Recovery Response of Phosphate Metabolites and Intracellular pH in Intact Mytilus edulis as Examined In Situ by In Vivo ^{31}P NMR (*Biochim. Biophys. Acta* 1092:39-47)

We employed surface probe-localized ^{31}P NMR spectroscopy to examine in situ the impact of short-term emergence (hypoxia) and resubmergence on phosphate metabolites and intracellular pH (pHi) in intact mussels. The use of intact organisms ensured that all intrinsic responses remained active while monitoring of individuals minimized uncertainties resulting from stochastic behavior and other individual differences. The use of a photoetched, balanced-match foil probe combined with ^{1}H NMR images allowed ^{31}P NMR spectra to be acquired from the posterior adductor muscle with good signal-to-noise. Upon emergence, all mussels exhibited an increase in [Pi], a decline in [phosphoarginine] and pHi, and very little changes in [ATP] with time. The complementary behavior of [phosphoarginine] and [Pi] indicated a precursor-product relationship involved in the maintenance of [ATP] but the similarity between [phosphoarginine] and pHi time courses cannot be so readily explained. Irregularity in the time courses of some

parameters could have reflected stochastic gaping activity. Resubmergence responses exhibited a reversal of the emergence responses, except that the pHi eventually became supraalkaline with irregular fluctuations. This might be related to the "oxygen debt" phenomenon and increased oxidative phosphorylation.

Introduction

Intertidal bivalve molluscs are routinely subjected to periods of tidal emergence (exposure to air) that can lead to continued aerobic respiration at the risk of dessication/predation, or hypoxia due to closure of valves, or some mixture of the two extremes (McMahon, 1988). As a result, emergence can be more complex than hypoxia per se. In the case of the mid-littoral blue mussel, Mytilus edulis, emergence is dominated by general closure of valves coupled with occasional valve opening (gaping) (Wijsman, 1975; Booth et al., 1984; Coleman, 1973) and reduction in metabolic activity (evidenced by slowing of the heart rate) (Coleman and Trueman, 1971). Also evident are metabolic hypoxic symptoms, which include tissue acidosis (Wijsman, 1975; Walsh et al, 1984) and accumulation of multiple fermentation end products such as succinate, alanine, and volatile fatty acids (de Zwaan, 1977). These symptoms are common to obligate aerobes such as mammals (Garlick et al., 1979; Gadian et al., 1982) and most terrestrial plants (Davies et al., 1974; Fan et al., 1988), except that mammalian tissues are dominated by lactate fermentation and exhibit a greater extent of acidosis for a comparable duration of hypoxia (de Zwaan et al., 1976). The multiple fermentation pathways of molluscs are expected to provide more efficient energy production and better maintain the redox balance under low pO2 conditions than the lactate pathway alone (de Zwaan et al., 1976). They should also contribute to the smaller extent of acidosis observed in *M. edulis* (de Zwaan et al., 1976). Due to these complexities associated with emergence, intertidal mussels represent an outstanding system for examining the cyclic transition between aerobic and hypoxic metabolism, particularly regarding energy metabolism and intracellular pH (pHi) regulation.

Several aspects of hypoxic metabolism in *M. edulis* have been investigated; among those that dealt with emergence, a few have examined changes in either pHi (Walsh et al., 1984) or concentrations of "energy" phosphates (Wijsman, 1976), including a study on recovery alone from medium to long-term emergence (Zurburg et al., 1982). However, detailed time course changes in both pHi and energy metabolites, especially under the more commonly encountered short-term (< 24 h) emergence, remain undetermined. This information may be particularly important for understanding the complication of stochastic behavior such as gaping in relation to hypoxic response. Gaping is thought to allow some O_2 uptake through aerial exchange in emerged mussels (Coleman, 1973), and to also serves to vent accumulated CO_2 (Booth et al., 1984). How such exchange simultaneously affects pHi and energy metabolite status of the

emerged mussel is not clear. Finally, little information is available on the temporal relationship between energy metabolism and pHi during recovery from air exposure (Ellington, 1983). The metabolic regulation governing this relationship warrants special attention in light of the phenomenon of "oxygen debt", or increased oxygen consumption, by mussels during early recovery period (Zurburg et al., 1982, Bayne, 1971; de Vooys and de Zwaan, 1978).

Previous determination of energy metabolites of emerged *M. edulis* employed chemical or enzymatic analyses of tissue extracts (Wijsman, 1976; Zurburg et al., 1982) while pHi was determined by the DMO[1] method (Walsh et al., 1984). None of these studies examined in detail the changes involving a full cycle of emergence and recovery. The extract analyses were likely to be sensitive to extraction artifacts (Meyer et al., 1986) and concentration variation among individual animals (Wijsman, 1976; Fan et al., unpublished results], both of which could obliterate small changes in the time course. The measurement of pHi with fine time points is not feasible by the DMO method, precluding the observation of short-term changes. The valve gaping also adds to the noise and its irregular occurrence can hamper detailed biochemical and pHi monitoring by these techniques that rely on either in vitro analyses or *in vivo* methods that require long intervals between measurements. A previous *in vivo* ^{31}P NMR study of submerged hypoxia (not emergence) in *M. edulis* circumvented some of these problems (Ellington, 1983). However, since excised tissue was used in this study, the approach could not observe the effect of valve gaping, the extracellular bicarbonate buffer system, and other in situ processes on energy metabolism while introducing uncertainties from excision damage. Thus, it is clear that in situ biochemical and pHi analyses on individual whole organisms, with finer time points over a cycle of emergence and recovery, need to be implemented in order to characterize the complex metabolic response of mussels to the intertidal environment.

Here we report changes of energy-related phosphate metabolites and pHi in the posterior adductor muscle (PAM[1]) of six intact, subtidally acclimated *M. edulis* during 15 h of air exposure using surface probe localized ^{31}P NMR. The sessile nature of mussels eliminated the necessity of using anesthetics or restraints and live individuals were readily maintained under superfusion without changes in their energy phosphates and pHi for at least 24 h. Three of the mussels were also exposed to 8 h of emergence followed by resubmergence in seawater in order to follow their responses to a cycle of emergence and resubmergence and to investigate the impact of "O_2 debt" on

---

[1]Abbreviations: DMO, 5,5-dimethyloxazolidine-2,4--dione; MDP, methylene diphosphonate; PAM, posterior adductor muscle; PArg, phosphoarginine; PCA, perchloric acid; PCr, phosphocreatine; pHi, intracellular pH; Pi, inorganic phosphate; S/N, signal-to-noise ratio; [ ], bracket enclosure denotes concentration.

phosphate metabolites and pHi. The focus of this study was on the PAM for its central functioning in the survival of mussels during emergence, for high levels of phosphorous

metabolites, and for location near the shell surface (suitable for localization with a surface probe). A previous group had difficulty obtaining acceptable NMR spectra from a whole mollusc (Thompson and Lee, 1985), possibly due to the interference from the shell itself or air enclosed within it. The surface probe (Fan and Higashi, 1989) approach employed in this study circumvented this problem and localized ^{31}P NMR spectra of the mussel PAM with acceptable signal-to-noise ratio (S/N^1) was 1attained despite the shell and high salt content. This allowed acquisition of detailed time course changes of pHi and phosphate metabolites during emergence and subsequent recovery. In addition, verification of signal localization on the PAM and the absence of air cavities in intact mussels were supported by two-dimensional ^1H magnetic resonance images.

Materials and Methods

Organisms and Emergence Procedure

All procedures involving seawater used filtered natural seawater collected near Bodega Bay, California. The water was in all cases optically clear, free of silt, temperature at collection ranged from 12–15 °C, and salinity ranged from 33–34 ‰. Mytilus edulis ranging in size from 80-100 mm shell length were collected from subtidal areas near Bodega Bay, California. The animals were kept submerged in seawater aquariums at 14 °C and fed weekly with cultures of the microalgae, Isochrysis galbana (Tahitian strain).

The "emergence-recovery" experimental protocol used on three animals employed a general-purpose aquatic NMR chamber described previously (Higashi et al., 1989), with a styrofoam block inclusion sculpted in the shape of the mussels to assist in animal positioning and to reduce dead volume in the chamber. Animals were removed from their holding aquarium, positioned in the chamber, and the chamber was positioned over the surface probe (see next section for positioning procedure). For the baseline NMR measurements, seawater flow through the aquarium was 100 mL/min from a reservoir kept constant at 14 °C. To ensure temperature stability at 14°C, we additionally arranged an air blower attached to an automobile heat exchanger cooled with a refrigerated circulating bath to provide 10 °C air (measured at the blower outlet) flowing through the NMR bore; this arrangement was necessary as sample temperature control was not available on the horizontal wide-bore NMR instrument used. To begin the emergence phase, the water was pumped out of the sample chamber in < 30 s as the air flow served to maintain the chamber interior at 13–14 °C. To begin the recovery phase, seawater flow was restored at 100 mL/min from the reservoir. Valves were verified to be open or closed by direct visualization of the mussel through the optically clear chamber wall.

Experiments involving emergence alone from water were performed on six animals, including the same three used for emergence-recovery. The procedure consisted of simply lifting the organism out of the seawater in two to five seconds, depositing it in a polyethylene bag left

open for atmospheric exchange, and positioning it over the surface probe in the NMR instrument (see next section for positioning procedure). Animals were kept at 13–14 °C for the duration of the experiment by the air flow arrangement described above. The same animals were later monitored by NMR with seawater drained from the shell; this was accomplished in the same fashion as the normal emergence except that a plastic pipe was placed between the valves prior to lifting the animal out of the water; this prevented the valves from closing and allowed us to drain the seawater out through the pipe.

NMR Measurements

The *in vivo* ^{31}P NMR measurements were carried out using a two-turn 3.5 cm planar surface probe. The coil was etched from a photosensitized printed-circuit board using a coil template drawn on a computer-aided-design program (Fan and Higashi, 1989). The probe was constructed with a balanced-match circuit to optimize sensitivity on the highly conductive mussel sample. Positioning of the PAM of *M. edulis* over the probe was assisted with ^{1}H images and known anatomy of the mussel (the procedure is described in more detail in the Results section). Both the *in vivo* ^{31}P NMR spectra and ^{1}H images were obtained using a General Electric ™ CSI-2T 200 mm horizontal bore imaging/spectroscopy system.

For acquiring ^{1}H NMR images, we constructed a three-inch diameter "birdcage" design probe (Hayes et al., 1985) operating at 85.6 MHz and a multislice spin-echo pulse program available from the CSI systemwas used. The pulse parameters for emerged mussels included an echo time of 20 (transverse plane) and 120 ms (coronal plane), an interpulse delay of 1 s (transverse plane) and 1.5 s (coronal plane), 512 data points x 256 phase-encode steps, 2 mm slice thickness, 2-5 mm slice separation, and 4 transients per slice; for deliberately drained mussels, the pulse parameters were the same except for an echo time of 26 ms, an interpulse delay of 1.5 s, and 2 mm slice separation. For the *in vivo* ^{31}P NMR time course study, the spectrometer was operated at 34.6 MHz and each time point represented averages of 1024 or 2048 transients acquired with 15 μs pulse width, ± 2000 Hz sweep width, 1.128 s interpulse delay, and 1024 data points. For the perchloric acid (PCA[1]) extracts (pH 7.66) of mussel organs (the PAM and the rest), ^{31}P NMR spectra were obtained on an Nicolet NT-360 instrument operating at 145.7 MHz for ^{31}P nucleus, using a 10 mm probe, a 67° pulse width (10 μs), ± 4000 Hz sweep width, 4096 data points, 2 s interpulse delay, and 1024 transients. The ^{31}P NMR resonances from the extract were referenced to that of an external standard, methylene diphosphonate (MDP[1]) at 0 ppm chemical shift (Fan et al., 1988), whereas the *in vivo* ^{31}P NMR resonances were normalized to the internal PArg peak at –19.6 ppm chemical shift.

To determine pHi, chemical shift differences between PArg and Pi were compared with a calibration curve constructed with a standard composed of Pi, PArg, and ATP at 15 pH values. The precision of the pH measurements was determined experimentally with the standard at pH

7.50 in a glass vial that approximates the diameter of the PAM. Ten spectra were acquired with the same surface probe, spectral parameters, and S/N as the *in vivo* experiments. The result of these ten pH determinations was 7.47 ± 0.04.

In vitro analyses

Two mussels (*M. edulis*) with shell lengths of 92.0 and 85.6 mm were dissected to separate the PAM (1.77 g and 1.62 g, respectively) from the rest of the tissues, and both portions freeze-clamped in liquid nitrogen. All dissection operations were completed within 60 s. PCA extractions were performed according to a previous procedure (Higashi et al., 1989) that was modified from Gutmann and Wahlefeld (Gutmann and Wahlefeld, 1974). The final extracts were lyophilized at pH 3.5 and stored at –70 °C for future analysis.

All chemicals were obtained from Fisher Scientific (Pittsburgh, PA), except for $PArg^1$, PCr^1, and ATP standards which were obtained from Sigma Chemical (St. Louis, MO).

Results

^{31}P NMR Spectroscopy and ^1H NMR Imaging of Mussel PAM

The acquisition of localized ^{31}P NMR spectra of the PAM of live mussels requires accurate positioning of the surface probe relative to this organ, which was a nontrivial task because PAM is concealed between the two valves and its exact location varies somewhat among individuals. To solve this problem, we obtained ^1H NMR images of intact mussel to guide our ^{31}P NMR probe positioning before each experiment. An image which revealed the location of the PAM is shown in a coronal slice image (Figure 41a), where the muscular bundles of PAM were evident. This relationship was previously verified in several mussels by ^1H NMR imaging followed by dissection. A transverse slice image through the PAM (not shown), when it coincided with the center of the surface probe, verified that the coil was correctly positioned under the PAM. Additional evidence for localization on the PAM was inferred from a similarity between the *in vivo* ^{31}P NMR spectrum (Figure 42a) and the spectrum of the PCA extract of excised PAM (Figure 42c). The higher inorganic phosphate (Pi^1) peak intensity (representing $[Pi]^1$) in the extract relative to the *in vivo* spectrum may be caused by muscle contraction just prior to dissection, hydrolysis of PArg and other labile phosphates, or a mobilization of bound Pi during extraction (Meyer et al., 1986).

In addition to the two emergence treatments described below with water fully retained in the shell, we later conducted a third set of emergence experiments on the same individuals with water drained from the shell. The absence or presence of air cavities inside the mussel shells in all cases were examined using a multislice ^1H NMR imaging technique, well-known to generate images in which air is distinguished from water and tissue. With either standard (30 s) or rapid (< 1 s) emergence procedures, all normally emerged mussels gave images indicating full water

retention (e.g. Figure 41b) while with water deliberately drained from the shell, large air cavities were present in the images (Figure 41c). Thus, the survey found that emergence did not readily result in the formation of air cavities in *M. edulis*, which if present could significantly affect the amount of O_2 available to the mussel during emergence.

Using our chamber system originally designed for studies of abalones (Higashi et al., 1989) individual *M. edulis* could be maintained in the horizontal-bore magnet without spectral change in their PAM for at least 24 hr under aerated submerged conditions. The spectral appearance of all submerged (normoxic) mussels used in this study were qualitatively similar, but with a variation among individuals in terms of the S/N of the spectra (data not presented). The different S/N was probably largely due to natural variation in the amount of metabolites present; this was supported by a more extensive survey of mussels collected from several locations in California (Fan et al., unpublished data).

As shown in Figure 42a, a typical spectrum of the PAM under aerobic conditions exhibited peaks corresponding to Pi, PArg, and nucleotide (assumed here to be adenosine) phosphate compounds. These assignments were based on the chemical shifts in both *in vivo* and in vitro (Figure 42c) ^{31}P NMR spectra as well as guides from the literature (Ellington, 1983; Burt et al., 1976); hence the peaks labeled α, β, and γ were attributed to αADP+αATP, βATP, and γATP+βADP, respectively. The high [PArg]: [Pi] and [PArg]: [ATP] ratios are characteristic of other resting muscles from several invertebrate taxa (Ellington, 1983; Higashi et al., 1989; Burt et al., 1976; Graham et al., 1986; Dubyak and Scarpa, 1983). For pH measurements using Pi, we recognize that other factors – such as large changes in ionic character or non-protic acid-base equilibria – could lead to changes in the chemical shift of Pi. Here we follow the literature convention that assumes chemical shift changes are largely due to changes in pHi.

Emergence Time Courses

To obtain time course changes in phosphate metabolites, peak heights normalized to that of MDP standard were measured, which minimized errors resulting from any instrumental instability and gave similar results as peak area measurements, within experimental error.

A total of six mussels were subjected to emergence treatment for up to 15 hr. In addition, three of the mussels were monitored under the experimental sequence of submergence (normoxic background), 8 h of emergence (hypoxic treatment), and resubmergence (normoxic recovery); we shall refer this experimental protocol as "emergence-recovery". There were no mortalities attributable to NMR experimentation described in this paper. As previously described, all normally emerged mussels were verified in each experiment to be free of air cavities by ^{1}H NMR imaging. In addition, valve closure was observed to occur upon each emergence. Although gaping could have occurred during the experiments, we were not able to verify this behavior

well-known to occur in *M. edulis* due to its irregularity and for lack of a continuous monitoring device (e.g. video camera) that would function properly in the vicinity of the magnet.

All PAM of mussels examined exhibited an increase in [Pi], decrease in [PArg], and only very small change in b-adenosine phosphate peak intensities in response to emergence (cf. Figures 42a and b). As for pHi, individual variation was observed where 4 out of 6 cases showed significant acidification (varied from 0.21 to 0.56 pH units) while pHi change was negligible for the other two (data not shown). Acid shift of pHi was observed previously on hypoxic (not emerged) excised *M. edulis* PAM (Ellington, 1983). To illustrate the emergence effects including the early changes, example time courses obtained from an emergence-recovery experiment are shown in Figure 43a–c (150-640 min). Emergence caused a sixfold increase in [Pi] and a comparable decrease in [PArg] over an 8 h period; the kinetics of the two time courses were exponential and basically mirrored each other (Figure 43a). Also the response of [Pi] and [PArg] beyond the first hour of air exposure became slightly irregular. Irregular responses of a larger relative amplitude were apparent over the entire time courses of g, a, and b-adenosine phosphate peaks (Figure 43c). Nevertheless, the three adenosine phosphate peaks changed similarly in intensity and timing, which suggests that changes in free [ATP] instead of [ADP] were responsible. Besides the irregular response, adenosine phosphate peaks started to show a slight decrease in intensity beyond 8 h of emergence (Figure 43c). This subtle change was observed in 4 individuals although 2 others did not exhibit any noticeable change (data not shown).

While [PArg] was decreasing, the pHi response, as illustrated in Figure 43b, showed a decline in this case, from 7.47 to 6.91 at the end of 8 h of emergence. The response curves of pHi and [PArg] also appeared to be closely related. Furthermore, as with [Pi] and [PArg], a small irregularity in the pHi response was noted (Figure 43b) during emergence. This phenomenon was always associated with individuals where significant acidification of pHi occurred, whereas a smoother response curve was observed whenever pHi did not change appreciably (data not shown). Smaller amplitude irregular response was also evident in aerated submerged mussels. Finally, pHi did not drop below 6.9 at any point for any normally emerged mussel in this study, although pHi of deliberately drained mussels described earlier reached as low as 6.7 (data not shown).

Recovery Time Courses

Resubmergence caused the mussels to open their valves within 5 min and a reversal of the emergence response for [Pi] and [PArg] was observed, where both eventually returned to the background level after 10 h of recovery, as illustrated in Figure 43a (640-1330 min). The recovery response curves for the two metabolites were mirror images of emergence. The

adenosine phosphate peak intensities continued their irregular pattern but otherwise did not show appreciable change during 11 h of recovery, as shown in Figure 43c.

For pHi, the response became more irregular, especially 5 h after resubmergence, and eventually exhibited a supraalkalinization (Figure 43b). The extent of supraalkalinization varied with individuals but in every case pHi went from about 7.4 to beyond 7.6. In fact, in two out of three cases (e.g. Figure 43b), pHi reached higher than 7.9 which is the approximate limit of measurement of physiological pHi using this method (Busa et al., 1982).

Discussion

Many intertidal bivalves can switch between aerobic and anaerobic metabolism in response to tidal changes (McMahon, 1988), and several biochemical adjustments are made to accommodate this transition. Multiple fermentation reactions are utilized to compensate energy production (de Zwaan et al., 1976) and to maintain redox balance. Another principal function of these reactions is to alleviate intracellular acidosis by removing excess H^+, a type of "metabolic" – or dynamic – pH buffering. pH regulation can also be effected by involving existing protic (Brønsted-Lowry) buffers or synthesis of these static buffers. All the above means of pH regulation fall under the Usanovich definition of general (not just protic or static) acid-base equilibria (Huheey, 1972; Gehlen, 1954). An example of Usanovich buffering in mussels involves an extrapallial fluid bicarbonate system which is thought to operate through solvation of the carbonate stores such as the shell Booth et al., 1984; Lindinger et al., 1984). This, of course, requires that the intracellular protons undergo a net extrusion into the medium, which is difficult to demonstrate rigorously (Lindinger et al., 1984).

In addition to the biochemical adjustments described above, emerged mussels can acquire some O2 through occasional gaping (Coleman, 1973) and possibly through the formation of air cavities; the latter mechanism has not been addressed previously. All these mechanisms – as well as others not yet fathomed – delineate emergence from submergence hypoxia and may contribute to sustaining emerged mussels for a much longer period than ischemic mammalian tissues.

Since energy metabolism and pHi regulation are the main driving forces for physiological compensation under hypoxia, the examination of these two aspects together would be revealing. *In vivo* ^{31}P NMR provides a unique tool for such a purpose because it allows in situ repeated measurements of energy metabolites and pHi on the same individual mussel. Thus, uncertainties arising from individual variation are minimized and more subtle metabolic fluctuations can be observed.

Employing the *in vivo* ^{31}P NMR method, this study demonstrated that the PAM of emerged *M. edulis* exhibited a qualitatively similar ^{31}P NMR spectral response regarding energy

phosphates (PArg and ATP), Pi, and pHi as compared to other hypoxic vertebrate and invertebrate muscles (Houlet et al., 1974; Barrow et al., 1980). This response is consistent with the current understanding that [ATP] is replenished in hypoxic PAM from PArg and anaerobic glycolysis, the latter of which also gives rise to excess H^+ production and lowering of pHi. It should be noted that although the surface-probe NMR technique is generally not suitable for precise quantitation, the comparable spectral changes between PArg and Pi (Figure 43a) support this notion that a significant portion of [ATP] being maintained through phosphoryl transfer from PArg

$$PArg^- + MgADP^- + H^+ \rightleftarrows Arg^+ + MgATP^{2-} \quad \text{(Equation 1)}$$

(Eqn.1). It is also interesting that the rate of changes in the emerged mussel PAM (e.g. a half-life of 4-6 hr for [PArg]) was slower than in hypoxic mammalian muscles; similar observation was made by Barrow et al. (Barrow et al., 1980) on the hypoxic excised muscle of an estuarine mollusc. In *M. edulis*, this slower change presumably reflects a combination of lower energy demand through reduction in valve movement and heart rate (Coleman and Trueman, 1971), maintenance of residual aerobic metabolism through occasional gaping (Coleman, 1973), and diversion of means of energy production to multiple glycolytic fermentation (de Zwaan and Wijsman, 1976). The possibility that O^2 is available via air cavities formed inside the shell upon emergence was eliminated in the present study since none of the emerged *M. edulis* exhibited air pockets in their ^1H NMR images (Figure 41b). However, this mechanism may well be operative in a related species, *M. californianus* (Bayne et al., 1976), where large air pockets were frequently observed upon emergence (data not shown).

Although the emergence and recovery responses of [PArg], [Pi], and [ATP] is consistent with a straightforward precursor–product relationship, that of pHi represents a more complex situation involving several types of Usanovich buffering. During emergence, through mass action the excess H+ produced from glycolysis would favor the breakdown of PArg catalyzed by arginine phosphokinase (Eqn. 1), which may in part account for the apparently coupled response of [PArg] and pHi (Figure 43b). A similar conclusion was reached in an earlier study of a superfused acid-treated molluscan cardiac muscle (Ellington, 1985). Secondly, the more acidic pHi would have a similar effect on H^+–consuming fermentation reactions operating in hypoxic PAM. All the above reactions help to "metabolically" buffer pHi and may contribute to its maintenance at or above 6.9. Thirdly, buffering from the extrapallial bicarbonate system (Booth et al., 1984; Lindinger et al., 1984) could also be operative in the emerged mussels of this study. This is supported by the more acidic pHi (6.7) exhibited by the deliberately drained mussels

which can be expected to have a reduced capacity of bicarbonate buffering due to formation of large air pockets (Figure 41c).

The finding that the pHi became supraalkaline during recovery period (Figure 43b) warrants discussion. Although pH changes (within calibration limits) can be measured with better than 0.05 unit precision by ^{31}P NMR (Gadian, 1982), as was the case in this study (see Materials and Methods), the limit of Pi calibration for pH is around 7.9 (Busa et al., 1982). Thus, the full extent of supraalkalinization is difficult to determine when pHi rose above this value. Nevertheless, pHi of the PAM always became at least 0.2 unit more alkaline during recovery than preemergence periods. This change may be associated with the "oxygen debt" phenomenon reported in the literature (Bayne, 1971; de Vooys and de Zwaan, 1978). The extra O_2 uptake is indicative of an increased capacity of oxidative phosphorylation which can result from increased metabolic demands such as oxidation of accumulated fermentation end products (de Zwaan, 1977; Widdows et al., 1979). The higher rate of ATP synthesis can then directly contribute to alkalinization of pHi, although it is not clear whether this is a main factor. Also unclear is the origin of the large swings in pHi that repeatedly accompanied supraalkalinization. At the current time, the only explanation we can offer is that these swings may be related to occasional valve closure in aerated water (Wijsman, 1975). The same behavior may also underlie the irregular pHi drifts in submerged normoxic mussels observed in this study.

The present finding that ATP on the average remained constant differed from the drop in ATP observed by others (Wijsman, 1976; Zurburg et al., 1982; Zs-Nagy and Ermini, 1972; Shapiro, 1981) in hypoxic *Mytilus* sp. This difference may be attributed to several factors including the shorter duration of hypoxia in this study, different species, or different means of inducing hypoxia. Our choice of inducing hypoxia by emergence and the short duration of treatments were intended to probe hypoxic responses of mussels under commonly encountered habitat conditions. In the case of emergence, all normal physiological compensations are expected to occur whereas some factors, including the effect of gaping, are missing if hypoxia is induced via submergence with N2 aeration. For instance, it is possible that the irregular responses of energy-related compounds and pHi observed for emerged *M. edulis* in this study are related to the irregular gaping behavior reported for this species (Wijsman, 1975; Booth et al., 1984; Coleman, 1973; Walsh et al, 1984). Irregular gaping during emergence can lead to the observed responses by causing fluctuations in O_2 uptake and thus variations in the level of residual oxidative phosphorylation.

In summary, we utilized the technique of surface probe-localized *in vivo* ^{31}P NMR to examine in situ the impact of a cycle of emergence and recovery on energy metabolism and pHi in the PAM of intact subtidally-acclimated marine mussels. The short-term emergence-recovery conditions reflected a common tidal cycle regime experienced by these organisms in their natural

habitat. The intrinsic metabolite variation, the well-documented individuality of response of mussels to emergence, and the need for coordinated time course measurements of pHi and energy metabolites all formed the basis for the use of *in vivo* NMR. In addition, ^{1}H NMR imaging proved useful for examining a previously unaddressed complicacy involving air cavity formation in emerged *M. edulis*. Our findings on the time courses of [PArg], [ATP], [Pi], and pHi obtained with ^{31}P NMR revealed some of the complex interplay between multiple fermentation pathways, energy production, pHi regulation, and possible gaping activity during emergence and subsequent recovery.

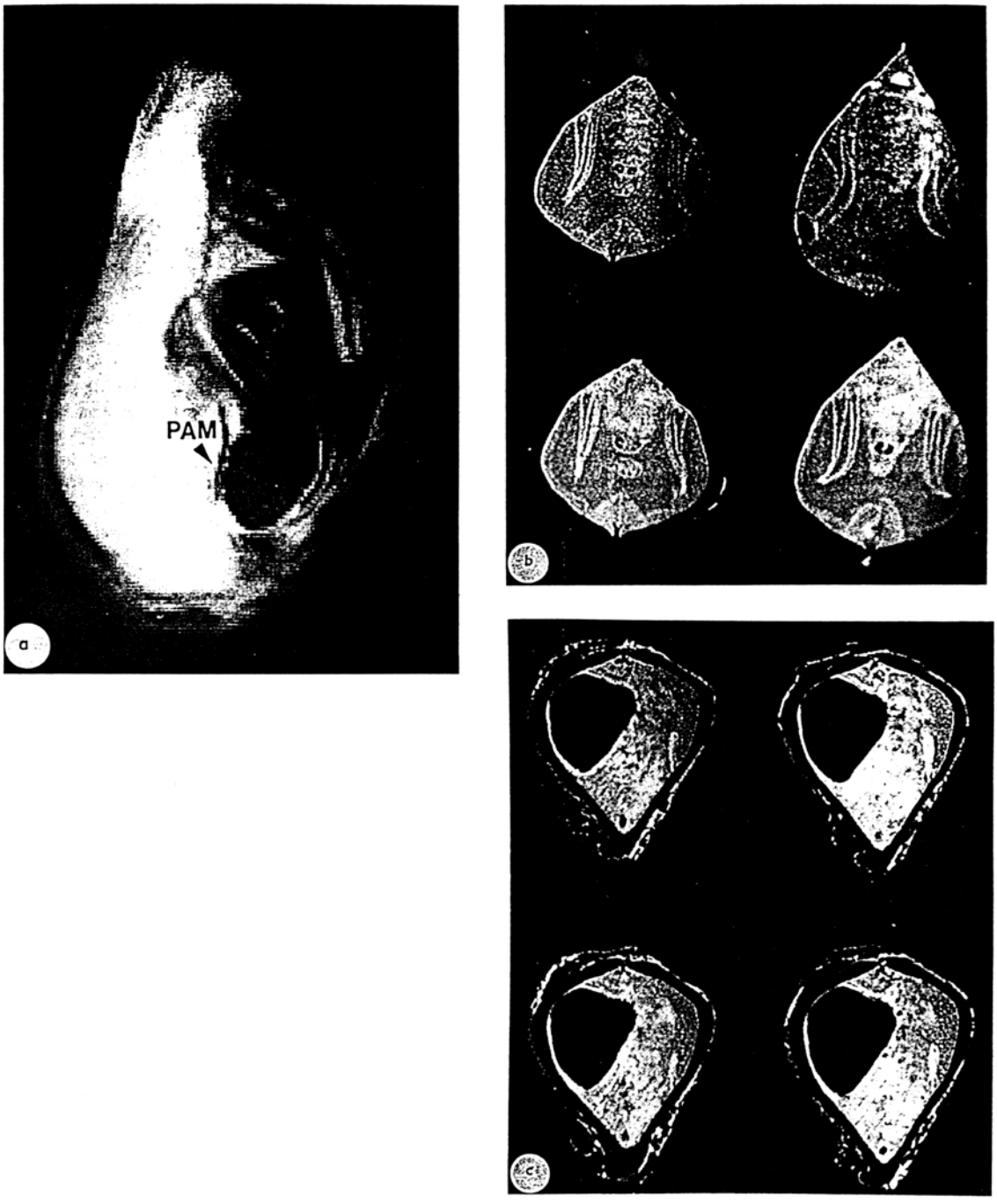

Figure 41. ^{1}H NMR images of emerged and deliberately drained mussels.

A multislice (8 slice) spin echo pulse sequence as described in the Materials and Methods was used to acquire consecutive transverse (16) and coronal (8) images of the mussel, each 2 mm thick and 2 mm apart. An example coronal image that depicted the location of the PAM (indicated by arrow) is shown in Figure 1a. Serial transverse images (clockwise from top left) corresponding to the main body of an emerged mussel is illustrated in 1b, where no air cavities are visible. For deliberately drained mussel, a large dark space, indicative of an air cavity, is evident in 4

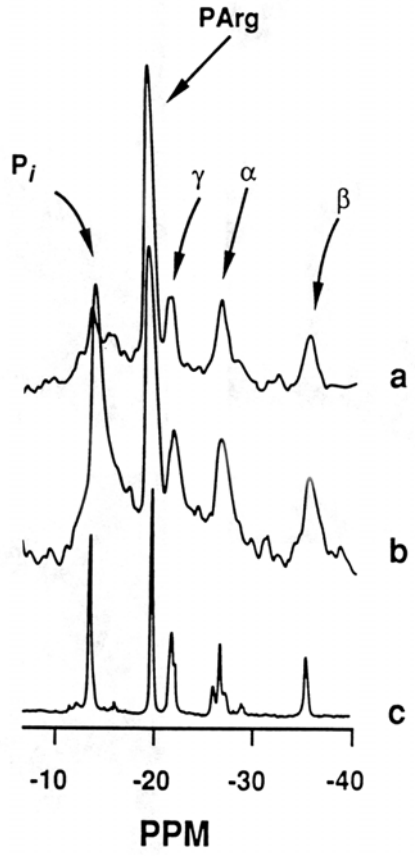

Figure 42. *In situ* and *in vitro* ^{31}P NMR spectra of the PAM of mussels.

The experimental conditions under which these spectra were obtained are stated in the Materials and Methods. The *in vivo* spectra (a, submerged; b, emerged for 8 hr) were processed with a line broadening of 15 Hz while the PCA extract (pH 7.66) spectrum (c) was processed with 10 Hz of line broadening.

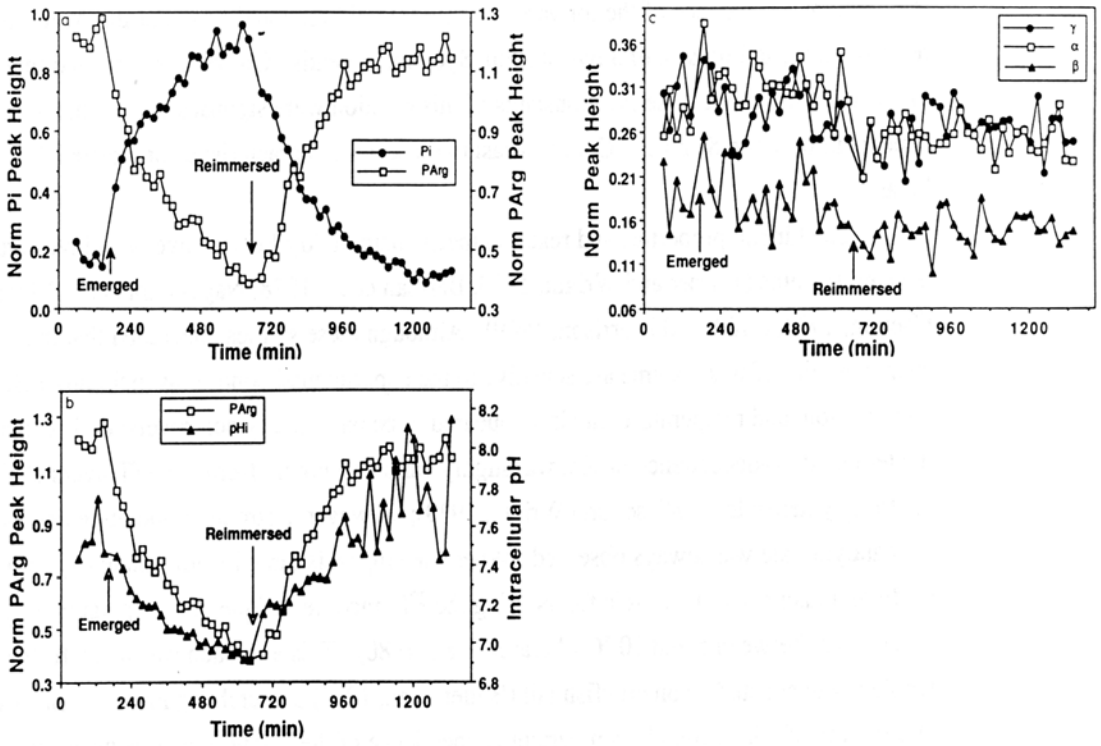

Figure 43. *In situ* time courses of phosphate metabolites and intracellular pH of a mussel during emergence and recovery.

"Norm peak height" represents peak height normalized to that of the MDP standard. Time course changes in Pi (filled circles) and PArg (open squares), pHi (filled triangles) and PArg, and γ (filled circles), α (open squares), and β (filled triangles) adenosine phosphates are shown in 43a, 43b, and 43c, respectively.

Temperature Dependence of Arginine Kinase Reaction in the Tail Muscle of Live Sycionia ingentis as Measured In Vivo by ^{31}P NMR Driven Saturation Transfer (*Biochem. Biophys. Acta*, 1135:44-49)

We have employed the driven ^{31}P NMR saturation transfer method to measure *in vivo* the temperature dependence of the forward and reverse unidirectional fluxes of the Arginine kinase reaction in the tail muscle of a live shrimp, Sycionia ingentis. Our results indicated that neither the forward nor the reverse rate constants of this reaction were significantly temperature-dependent between 8 and 16 °C, in contrast to the kinetic characteristics of isolated Arginine kinases.

The kinetic properties and reaction mechanism of Arg kinase have been investigated in isolated systems (Wieser and Wright, 1979; Barman et al., 1978; Nageswara et al., 1976; Cheung, 1973; Smith and Morrison, 1969). Although these studies concluded that the kinetic characteristics of this enzyme are sensitive to the experimental conditions including pH, ionic composition, and temperature, the last appeared to be particularly controversial. For example, the temperature-dependence of Km was highly variable ranging from none (Travers et al., 1978) to strongly dependent (Wieser and Wright, 1979); however, a strong temperature dependence of the catalytic rate was always observed. When the emphasis turned from isolated systems to a study on intact barnacle muscle fibers using the ^{32}P tracer technique, no temperature dependence was evident between 5 and 20 °C (Alvarez et al., 1980). This approach was taken further to whole organism studies on crayfish tail (Butler et al., 1985) and crab leg muscles (Briggs et al., 1985), both of which found a temperature dependence of the reaction rates as measured by *in vivo* ^{31}P NMR saturation transfer method.

Clearly, enzymic reactions depend on *in vivo* reaction conditions, bringing up an important issue regarding the relevance of in vitro biochemistry to *in vivo* enzyme activities and metabolic regulation. For example, it has been common practice to interpret environmental adaptive mechanisms of organisms based on characteristics obtained from in vitro enzyme studies (Wieser and Wright, 1979). However, as the exact conditions appropriate to the cellular milieu are not known, we must consider that the actual enzymic fluxes *in vivo* can differ from those extrapolated from in vitro measurements. It is therefore imperative that actual *in vivo* rates be measured prior to interpretation about enzyme regulation in whole organisms. Conversely, the *in vivo* rate data may provide useful hints as to the actual reaction conditions in organisms.

For the ridgeback prawn (*Sycionia ingentis*), the temperature dependence of the Arg kinase reaction is of special significance to its reproduction. These organisms can ascend from depths of greater than 200 m to the surface for spawning and return to the depths, during which they may experience a temperature change of at least 8 to 16 °C within a short period. How Arg

kinase in this shrimp adapts to such a temperature shift in both directions while maintaining sufficient ATP to sustain swimming and predator avoidance activity is unclear. In this report, we adopted a driven ^{31}P NMR saturation transfer method to measure *in vivo* both forward and reverse pseudo-first order unidirectional rates of the Arg kinase reaction in the tail muscle of live Sycionia at 8 and 16 °C. As this shrimp is naturally docile and linear in aquaria, no anesthesia or organism modification was necessary for insertion and maintenance in standard NMR tubes.

The most common means of measuring unidirectional fluxes *in vivo* by NMR is to use the steady-state saturation transfer method (Gadian, 1982), though transient methods have also been described (Butler et al., 1985; Malloy et al., 1985). The steady-state method is best-suited for a pure two-site exchange process and is easy to implement on most spectrometers, while the transient method is time-consuming and requires careful analysis of the biexponential time course. However, if the exchange network consists of three or more chemical species, data analysis for either method becomes complicated, causing derived rate constants to be significantly in error. Consequently, several ways of circumventing this problem have been described, including multi-site irradiation to reduce the problem to two-site exchange (Ugurbil, 1985) and measurement of the initial rate of recovery from an inversion pulse (Malloy et al., 1985; Brindle, 1988). The former method requires knowing in advance all the exchange pathways and having the capability to saturate all but two resonances in the spectrum. The reliability of the latter method is critically dependent on the accuracy of the inversion pulse.

Instead of these, we have adopted the driven saturation transfer experiment analogous to that used for measuring nuclear Overhauser effects in macromolecules (Wagner and Wüthrich, 1979), which has been shown to give the most accurate kinetics for two-site exchange systems (Malloy et al., 1985). Instead of defining the entire saturation transfer time course, we have measured the initial slope of the magnetization transfer. If sensitivity permits, the initial slope method is not affected by the presence of additional exchange processes. This is similar to measuring the initial slope in the inversion transfer experiment (Malloy et al., 1985). We have chosen the saturation method over the inversion method as it is more difficult to invert a resonance than to saturate it, particularly when it is broad (as in the case of *in vivo* resonances). This difficulty is illustrated by one report (Butler et al., 1985) where inversions of only 70% were typically obtained. When inversion is incomplete, additional corrections need to be made (Malloy et al., 1985). Also, the magnetization transfer time course deviates from linearity less rapidly for the saturation than for the inversion methods (see below).

Using an example of a three-site phosphate exchange reaction consisting of two reactions catalyzed by PArg[1] kinase (1st reaction) and ATPase (2nd reaction),

$$\mathrm{ADP + PArg} \underset{}{\overset{k_1}{\rightleftarrows}} \mathrm{Arg + ATP} \overset{k_2}{\rightleftarrows} \mathrm{ADP + Pi} \qquad (2)$$

k_{-1} k_{-2}

The corresponding McConnell equations (15) are :

$$dM_{ATP}/dt = -\rho_{ATP}(M_{ATP} - M_{ATP}^{\infty}) - (k_{-1}' + k_2)MATP + k_1'M_{PArg} + k_{-2}'M_{Pi} \quad (3)$$

$$dM_{Pi}/dt = -\rho_{Pi}(M_{Pi} - M_{Pi}^{\infty}) + k_2M_{ATP} - k_{-2}'M_{Pi} \quad (4)$$

where M_x is the magnetization of species x, ρ_x is the intrinsic spin-lattice relaxation rate constant of species x, M_x^{∞} is the equilibrium magnetization of species x, and k_y' is the pseudo-first order rate constant for which $k_1' = k_1[ADP]$, $k_{-1}' = k_{-1}[Arg^1]$, and $k_{-2}' = k_{-2}[ADP]$.

---

[1]Abbreviations: PArg, phosphoarginine; Arg, arginine; T_1, spin lattice relaxation time; Glc-6-P; glucose-6-phosphate; ATP_γ, ATP_α, and ATP_β, γ, α, and β phosphate of ATP; [x], concentration of x

For instantaneous perturbation of, for example, the magnetization of PArg, the initial rate of change of the other magnetizations is given by:

$$dM_{ATP}/dt|_{t=0} = -(k_{-1}' + k_2)M_{ATP}^{\infty} + k_1'M_{PArg}^{0} + k_{-2}'M_{Pi}^{\infty} \quad (5)$$

By definition, $k_2M_{ATP}^{\infty} = k_{-2}'M_{Pi}^{\infty}$ (13), hence

$$dM_{ATP}/dt|_{t=0} = -k_{-1}'M_{ATP}^{\infty} + k_1'M_{PArg}^{0} \quad (6)$$

In the saturation experiment where M_{PArg}^{0} is forced to zero, the initial slope becomes $-k_{-1}'M_{ATP}^{\infty}$. For the saturation experiment, Eq. 6 can be written in a general form, where the initial slope is directly related to the change in magnetization, ΔM,

$$d\Delta M/dt|_{t=0} = -k'M^{\infty} \quad (7)$$

where $\Delta M = M - M^{\infty}$. We have simulated the time courses of both saturation and inversion transfer experiments using the parameters from Table 1 and equations from Malloy et al. (Malloy et al., 1985). Linearity was maintained for up to 0.75 s of irradiation for the saturation method but significant deviation occurred under the same condition for the inversion method. The linearity of the initial slope of the saturation transfer time course (ΔM vs time) was verified

experimentally in this study by measuring ΔM at 3–4 time points with maximal irradiation time of 0.6 s, as described below.

In addition to *k'*, determination of the relative unidirectional fluxes of the Arg kinase reaction requires [PArg]/[ATP], which can be obtained from the fully relaxed ^{31}P NMR spectra. This requires the measurement of the intrinsic spin-lattice relaxation time (T_1^1) so that the interpulse delay can be set properly.

Male shrimp of similar size were held to their naturally dominant linear configuration in 20 mm NMR tubes and superfused (Fan et al., 1986) with filtered natural seawater thermostatted at 8 or 16 °C. In all cases, tthe shrimp tail muscle was at least 6 cm in length, which was positioned in a 2.5 cm coil such that signal contamination from other parts of the shrimp was minimized (Scheme 1). Filtered seawater was pumped from a 2 L aerated reservoir into the NMR tube at a flow rate of 15-20 mL/min from the posterior to anterior of the shrimp (the natural breathing direction for this species). The probe temperature was also controlled at 8 or 16 °C; with this arrangement, both the inflow and outflow of seawater from the NMR tube registered 8 or 16 °C on an NBS certification traceable thermometer. Under this superfusion condition, the *in vivo* ^{31}P NMR spectra of the shrimp tail muscle did not change for at least 15 hr at either temperature; all saturation transfer experiments were completed within a 12-hr period. All ^{31}P NMR experiments were performed on a Nicolet NT-200 wide-bore NMR spectrometer operated at 80.95 MHz. The intracellular pH (pHi) was calculated from a calibration curve (with pKa of 6.78) and the difference in the chemical shifts of the Pi and PArg peaks. The calibration curve was constructed with a buffer containing 0.1 M KCl and 10 mM each PArg, Pi, Glc-6-P^1, ATP, and $MgCl_2$ (Roberts et al., 1981) with chemical shifts referenced to an external capillary standard of 0.45 M methylene diphosphonate at 0 ppm. Since the temperature dependence of Pi ionization reactions is negligible between 8 and 16 °C (Weast, 1977), the Pi titration curve is assumed to be independent of the temperature.

For the saturation transfer experiments, selective saturation of the PArg or ATP_γ peaks using a DANTE pulse train (Morris and Freeman, 1978) was followed by a nonselective 90° acquisition pulse (51–56 μs). The DANTE pulse train was composed of a series of short pulses with 2-2.25 μs durations at 1–1.43 ms intervals. Three to four irradiation times ranging from 18 to 600 ms were achieved by adjusting the number of DANTE pulse trains. With this range of saturation times, the error for determination of rate constants should be less than 10%; this error was estimated from the simulated magnetization time course using the parameters from Table 1 and equation derived by Malloy et al. (Malloy et al., 1985). A similar exercise for the inversion experiment gave about 20% error for estimated rate constant. For each irradiation time course, free induction decays (FID's) with on- and off-resonance (equidistant from the resonance to which the saturation of magnetization is transferred) irradiation were collected alternately and a

total of 288 or 960 FID's were acquired by cycling through all irradiation times with 48 or 128 FID's per cycle. This procedure minimized deterioration of data quality due to spectrometer instability and any sample changes during the measurement. The extent of saturation was evaluated by comparing the areas of the ATP_γ or PArg peaks in the control spectra with that in the difference spectra, and it ranged from 97 to 100%.

For the T_1 measurement, the fast inversion recovery Fourier transform (FIRFT) method (Gupta et al., 1980) was used with a interpulse delay of 3 s, spectral width of ±2000 Hz, 2048 digitization points, and 15 variable delays (τ). For each t, 128 scans were acquired by cycling through all variable delays with 8 scans each cycle for 16 cycles. T_1 was calculated from a 3-parameter fit of the 15 data points (τ vs peak intensity) with allowance for imperfect inversion and partial saturation of signals.

Figure 44 shows a typical set of *in vivo* ^{31}P NMR saturation transfer spectra for the forward reaction in the tail muscle of live *S. ingentis*. Figure 45 shows typical spectra for the reverse reaction. From the control spectrum (Figure 1a), resonances were assigned to inorganic phosphate (Pi), phosphoarginine (PArg), and the three phosphate groups of ATP (ATP_γ, ATP_α, and ATP_β[1]). This spectral appearance is similar to those of other resting muscles of aquatic invertebrate origin (Briggs et al., 1985; Higashi et al., 1989; Thébault et al., 1987; Kamp and Juretschke, 1987; Graham et al., 1986; Thompson and Lee, 1985; Dubyak and Scarpa, 1983; Burt et al., 1976). The average pHi determined was 7.6 and was independent of the temperature (Table 1). Among intact organisms, this value was somewhat higher than that reported for another crustacean tail muscle (Thébault et al., 1987) and more similar to a mollusc muscle (Fan et al., 1991). The relatively constant pHi among different individuals suggested that they were similar in their physiological state.

The T_1 values determined at 14 °C are listed in Table 2. These values were significantly higher than those reported for scallop adductor muscle (Graham et al., 1986), crab leg muscle (Briggs et al., 1985), and crayfish tail (Butler et al., 1985), regardless of the magnetic field strength and experimental temperature used. This difference of T_1 could result from different exchange rates between Mg^{2+} and ATP, between ATP and PArg, and/or from different cytosolic properties such as "microviscosity". Making use of the measured T_1 values, we recorded relaxed ^{31}P NMR spectra, from which [PArg]/[ATP] was estimated. The mean value of this ratio was 5.0 (Table 1, footnote c), which is similar to that reported for the resting muscle of another species of shrimp (Kamp and Juretschke, 1987).

The time course of the saturation transfer for both directions was established using several short irradiation times as shown in Figure 46. The values of k_1' and k_{-1}' were calculated from the initial slopes of Figure 46 according to Equation 7. The relative fluxes were then calculated from k_1', k_{-1}', and [PArg]/[ATP]. Table 1 lists these parameters for the Arg kinase

reaction. It should be noted that $k\text{-}_1'$ at 8 °C may be more underestimated than that at 16 °C due to the partial saturation effect (cf. Figure 45 legend). In addition, the intensity ratio of ATP_β to ATP_γ remained constant in all cases, indicating that a change, if any, in free [ADP] was not detectable. Furthermore, the PArg/ATP_γ peak ratio did not vary significantly with temperature or different individual (cf. Table 1). Therefore, neither factor should contribute appreciably to the change in relative fluxes.

It is clear that neither the forward nor the reverse rate constants and fluxes exhibited a significant temperature dependence between 8 and 16 °C. Even considering the uncertainties in these experiments, the Q_{10} extrapolated for the forward and reverse reactions are at most 1.1 and 1.3, respectively. Similar temperature independence of the phosphate exchange between PArg and ATP was observed for isolated barnacle fibers from 5 to 20 °C using the ^{32}P tracer technique (Alvarez et al., 1980). However, the Q10 values in other invertebrate muscles, measured *in vivo* by ^{31}P NMR, were reported to be 2–3 (Butler et al., 1985; Briggs et al., 1985), consistent with the characteristics of the overall in vitro reaction rate of Arg kinase preparations from muscle tissues of several invertebrates (Wieser and Wright, 1979; Barman et al., 1978; Cheung, 1973; Travers et al., 1978). Furthermore, the ratio of the forward and reverse fluxes was close to unity in our study, as would be expected for the steady-state reaction of Eqn. 2 in a homogeneous medium. This result differs from the observed kinetics in crab leg muscles (Briggs et al., 1985), where it was hypothesized that compartmentation of metabolites has a large influence.

The reaction mechanism of isolated Arg kinase is of the random rapid-equilibrium sequential type (Smith and Morrison, 1969) and the rate-determining step for the enzyme (from lobster) at 12 °C has been shown to be an enzyme-product isomerization following the phosphoryl transfer (Barman et al., 1978; Nageswara Rao et al., 1976). The isomerization step was independent of the temperature over the range 12–35 °C (Barman et al., 1978). However, the equilibrium constant for the phosphoryl transfer step was strongly temperature-dependent, leading to a significant overall temperature dependence for kcat (activation energy of about 10 kcal.mole-1). Our measurement of the pseudo-first order unidirectional rates k_1' and $k\text{-}_1'$ indicated no significant temperature dependence, which can be explained in several ways. First, the enzyme from the shrimp may have a different rate-limiting step such that kcat is intrinsically temperature-insensitive. Secondly, the enzyme *in vivo* is unlikely to be operating at Vmax partly because the substrate concentrations may not be saturating the enzyme. Under this condition, the unidirectional flux will be proportional to the ratio of kcat to Km, whose temperature dependence is likely to be lower than kcat alone (Hochachka and Somero, 1984). Finally, it is possible that the Arg kinase reaction may be controlled in part by other interlinked metabolic reactions that are temperature-independent.

Regardless of the cause, this variance in temperature dependence of the Arg kinase reaction among various sources and between *in vivo* and in vitro measurements emphasizes the importance of the relationship between reaction condition and function, in addition to the well-studied structure and function, for enzymes. It is well-known that enzyme structure dictates enzyme activity, but far less is understood how the cellular and organismic environment (∫ reaction conditions) can affect enzyme activity or its regulation. Perhaps because the conditions *in vivo* are largely unknown, it has been common practice to extrapolate in vitro enzyme properties to deduce enzyme regulation *in vivo*; this is done in spite of the fact that assay conditions for isolated enzymes are not and cannot be (since they are unknown to begin with) selected based on *in vivo* reaction conditions. This report presented the different temperature dependence of Arg kinase activities observed *in vivo* for comparison to studies of isolated systems. These results –and the method used to obtain the data– contribute to an understanding of *in vivo* reaction conditions and condition/function relationship for enzymes, particularly in the numerous taxa that must live in and adapt to a changing environment.

Table 1. Intracellular pH and In Vivo Kinetic Parameters of the Arginine Kinase Reaction at Two Temperatures.

Parameter	Unit	8 °C	16 °C	Ratio 16 °/8 °C
pHi	–	7.59±0.09	7.61±0.08	
k_1'[a]	s^{-1}	0.15±0.02	0.16±0.01	1.07±0.03
$k\text{-}_1$'[b]	s^{-1}	0.60±0.14	0.50±0.13	0.83±0.40
J+[c]	s^{-1}	0.75	0.80	
J-[c]	s^{-1}	0.60	0.50	
J+/J-	–	1.25±0.44	1.60±0.52	1.28

The pH values reported are mean±1 S.D. with n = 8 for both 8 and 16 °C.

[a] rate constant for the forward reaction ADP + PArg → ATP + Arg (n = 4)

[b] rate constant (s^{-1}) for the reverse reaction ATP + Arg → ADP + PArg (n = 4).

[c] forward (J+ = k_1'$[PArg]_r$) and reverse (J- = $k\text{-}_1$'$[ATP]_r$) fluxes of the Arg kinase reaction (k_1' = $k_1[ADP]$, $k\text{-}_1$' = $k\text{-}_1[Arg]$); relative concentrations of PArg and ATP, $[PArg]_r$ (1.00) and $[ATP]_r$ (0.20) were determined from the relative peak areas of PArg and ATP_γ resonances in the relaxed *in vivo* ^{31}P NMR spectra of the tail muscle acquired with a recycle time of 23.3 s (n = 6; standard deviation = 0.02). It should be noted that this ratio did not change with temperature.

Table 2. Spin-Lattice Relaxation Times Of *In Vivo* ^{31}P NMR Resonances From The Tail Muscle Of Live Sycionia Ingentis.

Peak Assignment	T_1 (sec)
PArg	3.03
ATP_γ	2.07
ATP_α	1.32
ATP_β	1.42

Scheme 1

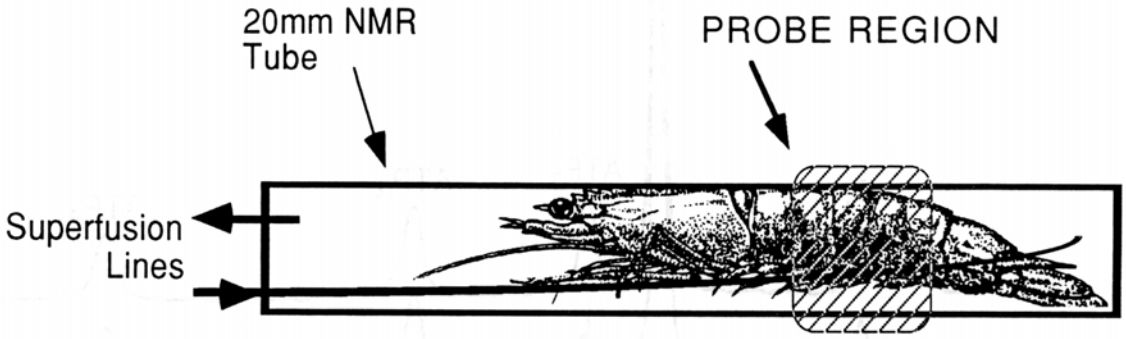

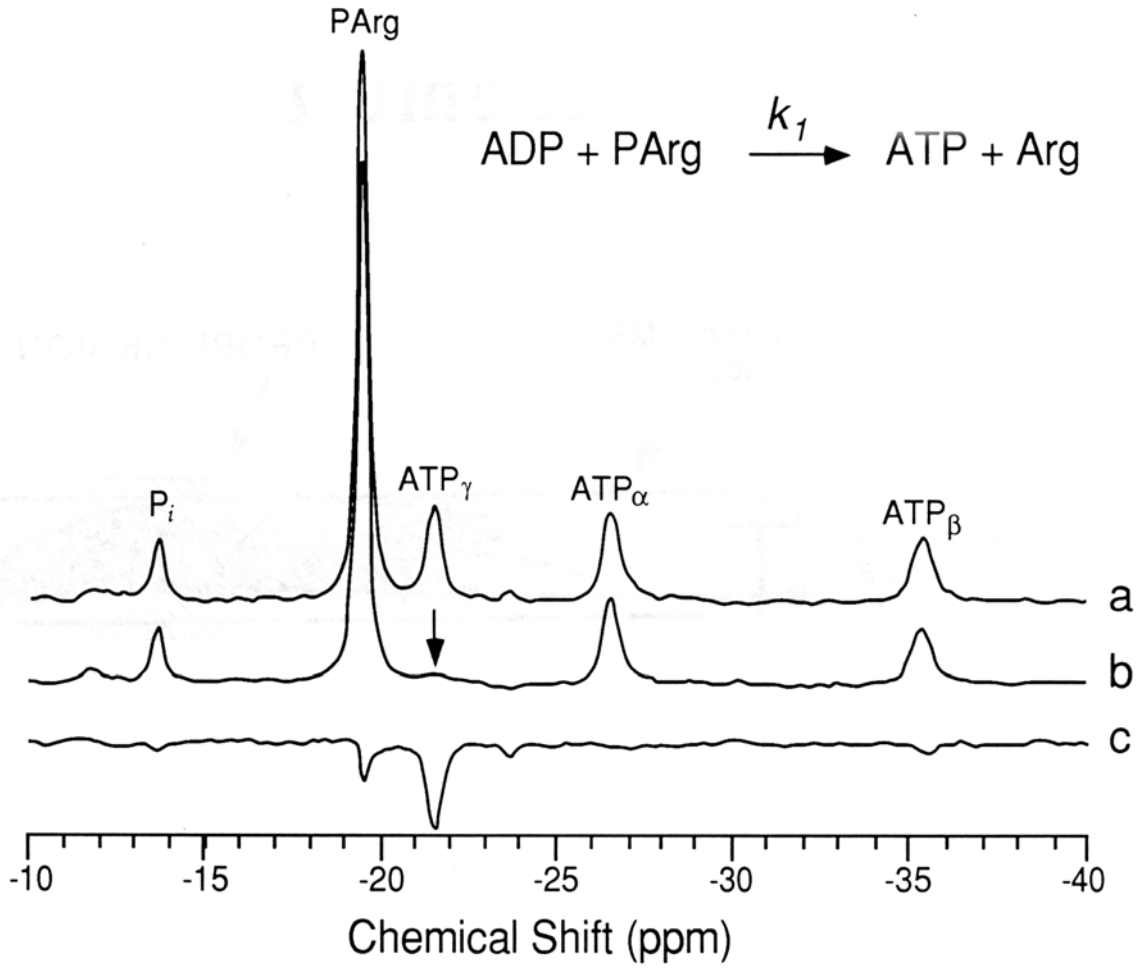

Figure 44. *In Vivo* ^{31}P NMR Saturation Transfer Spectra of the Tail muscle of Live *S. ingentis* for the Forward Reaction of Arg Kinase.

These spectra were acquired at 16 °C. Irradiation of γ-phosphate of ATP was implemented using DANTE pulse trains as described in the text. Other spectral parameters used included a spectral width of ±1500 Hz, 4096 digitization points, an irradiation duration of 549 ms, and a recycle time of 12.7 s. Spectra were processed with a line broadening factor of 10 Hz. The peaks labeled ATP_γ, ATP_α, and ATP_β correspond to γ, α, and β phosphate groups of ATP, respectively. a: off-resonance spectrum. b: on-resonance spectrum (irradiation of ATP_γ indicated by arrow). c: difference spectrum of b minus a.

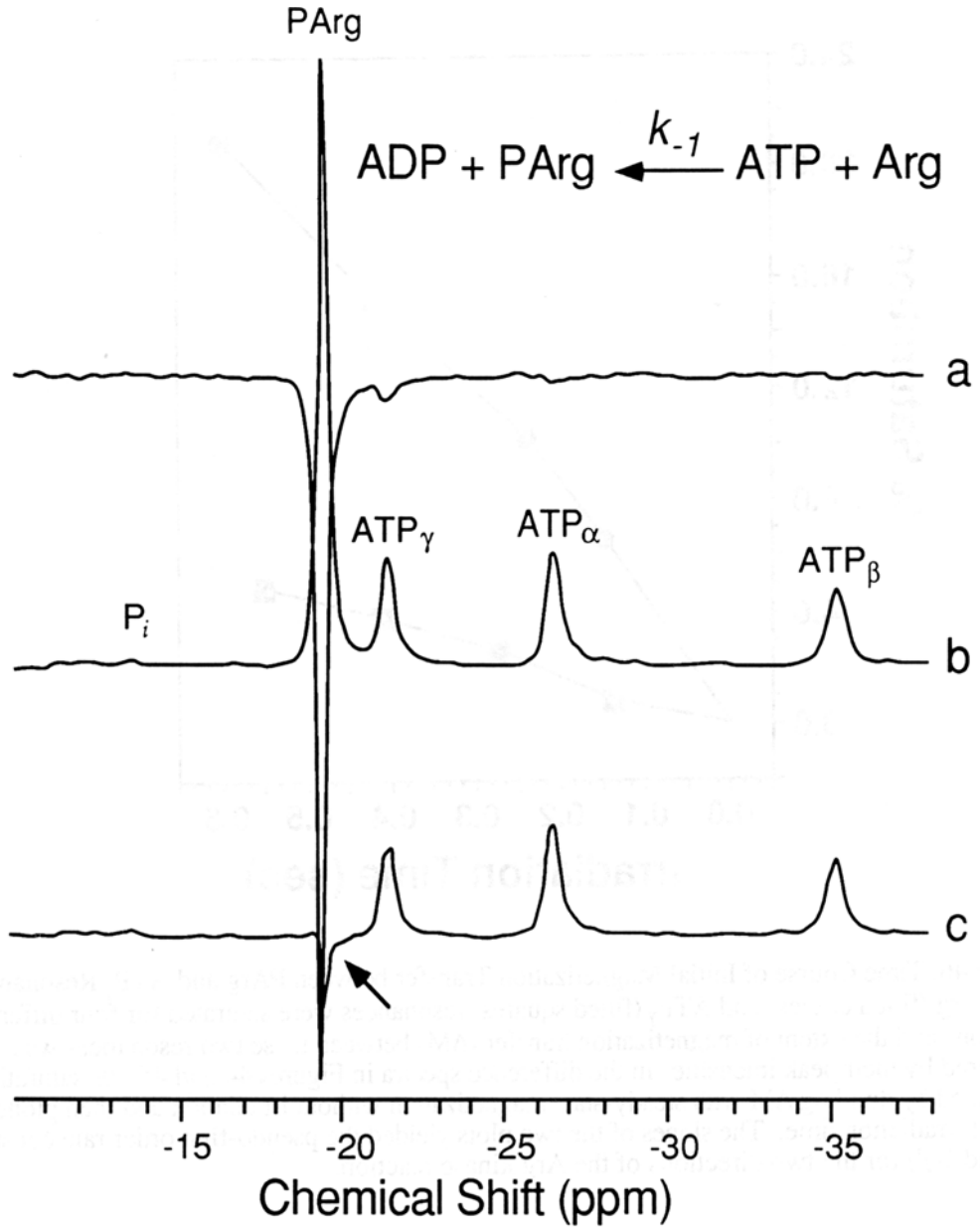

Figure 45. *In Vivo* ^{31}P NMR Saturation Transfer Spectra of the Tail muscle of Live *S. ingentis* for the Reverse Reaction of Arg Kinase.

These spectra were similarly obtained as those in Figure 44 except that a different individual was used, the PArg peak (indicated by arrow) was saturated for 240 ms, and the recycle time was 4.7 s ($2.3T_1$). Partial saturation of ATP_γ occurred with this pulse rate. However, k_{-1}' was underestimated by only about 10% as a result of this saturation effect. This error was smaller than the standard deviation listed in Table 1. In addition, the extent of underestimation of k_{-1} was greater at 8 °C than at 16 °C since T_1 should be longer and thus saturation factor larger at lower temperature. a, b, and c correspond to difference, off-resonance, and on-resonance spectra, respectively.

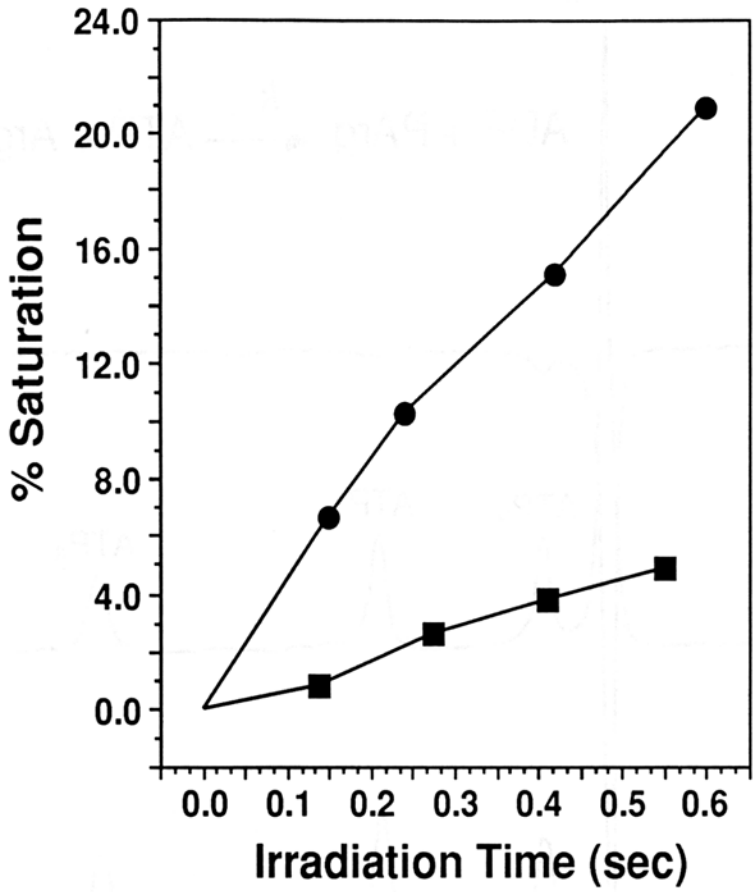

Figure 46. Time Course of Initial Magnetization Transfer between PArg and ATP_γ Resonances.

PArg (filled circles) and ATP_γ (filled squares) resonances were saturated for four different durations and the extent of magnetization transfer (ΔM) between these two resonances was measured by their peak intensities in the difference spectra in Figures 44 and 45. % saturation was calculated by dividing ΔM with steady-state magnetization without irradiation and then plotted against irradiation time. The slopes of the two plots yielded the pseudo-first order rate constants (k_1' and k_{-1}') for the two directions of the Arg kinase reaction.

Identification Of Glycerophosphorylcholine In Mussel Ovarian Extracts By Two-Dimensional NMR (*Analyt. Biochem.*, 206:251-255)

The abundance of the "phosphodiester" peak in differentiating or proliferating tissues including reproductive organs and tumors warrants further investigations of its metabolic role(s), which would require a rigorous confirmation of its identity. The assignment of this peak to glycerophosphorylcholine in ^{31}P NMR spectra of biological samples has been largely based on chemical shift, which can result in ambiguities. We employed a combination of two-dimensional ^{31}P-^{1}H heteronuclear shift correlation and ^{1}H total correlation spectroscopies to trace the spin connectivities of glycerophosphorylcholine and thus to identify its structure directly from crude ovarian extracts of mussels without ambiguities and the need for extensive purification. This approach can be applied generally to the identification of molecules containing heteroatoms in crude tissue extracts.

Introduction

Although it has been commonplace to assign ^{31}P resonances based on their chemical shifts, this assignment criterion is often unreliable because ^{31}P chemical shifts are usually sensitive to the physico-chemical environment (e.g. pH and divalent cations) of the sample matrix. To circumvent this problem, coincidence of a given resonance with that of the standard is additionally used. However, ambiguities can still result when spectral resolution is insufficient to separate overlapping resonances. Moreover, the above one-dimensional approach requires an a priori knowledge of the identity of the resonance; it falls short in identifying unknown resonances. The presence of conspicuous phosphodiester (PDE^1) resonances in both *in vivo* and extract ^{31}P NMR spectra of a variety of biological samples has been documented (Podo et al., 1987; Corbett et al., 1987; Evanochko et al., 1984; Sijens et al., 1986; Thompson and Lee, 1987; Navon et al., 1985; Koretsky et al., 1986; Freeman et al., 1983; Balaban, 1982; Alonso et al., 1989; Fan et al., 1992). In most cases, assignment of these resonances has relied primarily on chemical shifts. It was only recently that structural evidence, acquired from two-dimensional (2-D) ^{1}H NMR experiments, was provided for the presence of phospholipid catabolites (e.g. glycerolphosphorylcholine (GPC^1) and glycerolphosphorylethanolamine (GPE^1)) in frog gastrocnemius muscle (Alonso et al., 1989).

We were interested in the identity of a PDE resonance present in the *in vivo* ^{31}P NMR spectra of mussel ovaries, whose chemical shift corresponded to that of GPC. This peak has been shown in this laboratory to be a sensitive indicator for mussel oogenesis and for the perturbing effect of environmental pollutants on oogenesis (Fan et al., 1992). A similar intense

resonance was also found in the ^{31}P NMR spectra of other reproductive organs including gametes of vertebrate and invertebrate origins (Thompson and Lee, 1987; Navon et al., 1985), in mammalian tumors (Podo et al., 1987; Corbett et al., 1987; Evanochko et al., 1984; Sijens et al., 1986), and in kidneys (Koretsky et al., 1986; Freeman et al., 1983; Balaban, 1982). In the case of kidneys, an osmoregulatory role was proposed for such enrichment in renal medullas (Ullrich, 1956; Nakanishi and Burg, 1989). As for the reproductive organs and tumors, it is not clear what are the metabolic function(s) of this PDE. However, in view of its abundance in differentiating or proliferating tissues, it has been suggested that this compound may indirectly promote cell fusion and proliferation (Burt and Ribolow, 1984). Before any working hypothesis can be formulated regarding the metabolic role(s) of this PDE, its rigorous assignment is needed.

In this report, we used a combined 2-D NMR approach that employed ^{31}P-^{1}H heteronuclear shift correlation (HETCORR[1]) and ^{1}H total correlation spectroscopy (TOCSY[1]) to identify unambiguously the GPC structure from crude extracts of mussel ovaries without the need for extensive purification. Confirmation of this structure in extracts should in turn lead to a reliable assignment of the GPC resonance in *in vivo* ^{31}P spectra.

---

[1]Abbreviations: PDE, phosphodiester; GPC, glycerophosphorylcholine; GPE, glycerolphosphorylethanolamine; PCA, perchloric acid; HETCORR, heteronuclear shift correlation spectroscopy; TOCSY, total correlation spectroscopy; PC, phosphorylcholine; COSY, correlation spectroscopy.

Materials and Methods

California mussels (*Mytilus californianus*) were collected from Bodega Bay, CA and kept in flowing filtered natural seawater at 12-14°C until NMR experimentation or dissection. All standard phosphorus compounds were purchased from Sigma (St. Louis, MO, USA).

The mussel genders was assigned by histology as described previously (Fan et al., 1992). Ovarian tissues were dissected with minimum perturbations and rapidly frozen in liquid N2 and the whole procedure was completed in less than 60 s. The tissues were then lyophilized and stored at -70°C until extraction. Water-soluble phosphate metabolites were extracted with 5% perchloric acid (PCA[1]) from 0.1-0.2 g of lyophilized tissues pulverized to about 1 μm particles with a micro-dismembrator (B. Braun Melsungen AG, Melsungen, FDR) according to our previous procedure (Higashi et al., 1989; Fan et al., 1991) which was modified from Gutmann and Wahlefeld (Gutman and Wahlefeld, 1974). The final extract was lyophilized, dissolved in 0.5 ml D_2O, and adjusted to pD 7.2-7.5 for NMR analysis.

For *in vivo* ^{31}P NMR experiments, the localized gonadal spectra were acquired from live mussel individuals using a General Electric ™CSI-2 Tesla imaging NMR spectrometer

(Fremont, CA, USA) and a 3.5 cm photoetched surface probe (Fan et al., 1991; Fan and Higashi, 1989). The gonadal tissues were situated at the surface just beneath each half of the shell, which saved the more complex volume localization techniques that are often necessary for buried organs. A one-pulse experiment was implemented using a 45° nonselective pulse (15 μs), a 1 s repetition rate, a 3015 Hz spectral width, 2048 digital points, and 2048 acquisitions. The shallow tip angle minimized the signal contribution from the deeper parts of the mussel body.

For PCA extract analysis, ^{31}P NMR spectra were measured on a General Electric ™QE-300 (7 Tesla) spectrometer using a broadband 5 mm probe. A one-pulse experiment was carried out with a 90° pulse, a 1.68 s repetition rate, a 6024 Hz spectral width, 8192 digital points, and a Waltz-16 heteronuclear 1H decoupling scheme. The 2-D ^{31}P-^{1}H HETCORR spectrum of an ovarian extract was acquired from a Bruker AM-400 spectrometer (Karlsruhe, FDR) using a broadband 10 mm probe. The spectral parameters used included a 5000 Hz spectral width, a 1.5 s repetition rate, 2048 points, and a Waltz-16 ^{1}H decoupling scheme for the F2 dimension (^{31}P); a 1700 Hz spectral width, 142 points for the F1 dimension (^{1}H). For 2-D spectral processing, the F2 dimension was zero-filled to 4096 and F1 to 1024 points; both dimensions were apodized with a sine-squared bell. The 2-D phase-sensitive ^{1}H TOCSY of the same extract was obtained from a Varian (Palo Alto, CA, USA) ™Unity-600 spectrometer using a 5 mm ^{1}H probe. The spin-lock was generated using MLEV-17 (Bax and Davis, 1985) with a field strength of 10 kHz for 43.5 ms. Other spectral parameters included a 7000 Hz spectral width, a 1.94 s repetition rate, and 4800 complex points for F2 and 512 for F1 dimension. The data matrix was zero-filled to 8192 x 2048 points and a sine-squared bell was applied to both dimensions before Fourier transformation.

Results

Examples of the localized *in vivo* ^{31}P NMR spectra of a mussel ovary and testis are illustrated in Figure 1, where peaks were assigined to orthophosphate (Pi, -14.04 ppm), GPC (-16.46 ppm), phosphoarginine (PArg, -20.10 ppm), the γ-, α-, and β-phosphate resonances of ATP (ATP_γ, ATP_α, and ATP_β, -22.07, -27.19, and -35.58 ppm, respectively) based on their chemical shifts. It should be noted that the GPC peak occurred only in the ovarian spectrum, which is consistent with our earlier findings (Fan et al., 1992).

As the intensity of the GPC peak was shown by us to be sensitive to the progression of mussel oogenesis and to its perturbation by environmental pollutants (Fan et al., 1992), it is critical that the identity of this peak be confirmed by more rigorous means. Here we adopted several NMR methods to link this peak to the GPC structure (I) directly in the crude PCA extract of the mussel ovary from Figure 47. First, an authenic GPC standard was added to the ovarian extract and the ^{31}P NMR spectra of the extract before and after the addition are shown in Figure

48. It is clear that the assigned GPC peak was coincident with that arising from the standard. It should also be noted that the spectral appearance of the extract was similar to that acquired *in vivo* (cf. Figures 47 and 48) except for the broader linewidth and higher relative GPC peak intensity for the former.

Next, we employed the ^{31}P-^{1}H HETCORR method to confirm the PDE nature of the assigned GPC peak and to sort out its correlation with ^{1}H resonances as shown in Figure 49. This PDE peak was correlated with two ^{1}H resonances at 4.37 and 3.97 ppm. Two other weak PDE peaks at -15.49 and -15.96 ppm were also revealed in the HETCORR spectrum, the chemical shifts of the latter corresponded to GPE. Moreover, three phosphomonoester peaks were visible, one of which occurring at -13.09 ppm might be phosphorylcholine (PC^{1}). Finally, a PDE peak at -29.24 ppm was evident and could be assigned to the phosphate groups of UDP-glucose.

Once the connectivity between ^{31}P and ^{1}H spins was established, the phase-sensitive ^{1}H TOCSY experiment was performed using the same extract to acquire the ^{1}H-^{1}H spin correlations, thereby revealing the carbon skeleton. The ^{1}H TOCSY spectrum (Figure 50) indicated that the spin at 3.97 ppm was connected to two other ^{1}H spins (at 3.71 and 3.77 ppm) in addition to ^{31}P, which suggests that it came from the a-methylene protons of the GPC glycerol backbone while the other two were assigned as the γ-methylene and β-methine protons, respectively. The resonance at 4.37 ppm was correlated to a ^{1}H spin whose chemical shift was similar to that of the β-methine proton of the glycerol backbone. Based on its connectivity to ^{31}P spin (Figure 49) and a high chemical shift, the former resonance was assigned to the α'-methylene protons of the choline moiety while its connecting resonance belonged to the β'-methylene protons. Part of the ^{1}H spin connectivities reported here were also observed for GPC in the extracts of cell cultures (Bax and Davis, 1985) and in intact frog muscle (Sze and Jardetzky, 1990). However, in this report, we have acquired the entire scalar spin connectivities that have not been reported previously and thus provided a more rigorous assignment of GPC in tissue extracts.

Discussion

The overall similarity between the *in vivo* and extract ^{31}P NMR spectra of the mussel ovary suggests that the former was largely free of contamination from the main body of muscular tissues which exhibited a different spectral appearance from that of the ovary (Fan et al., 1992; Fan et al., 1991). The higher relative intensity of the GPC peak for extracts than for *in vivo* spectra may be in part attributed to the use of heteronuclear ^{1}H decoupling in the latter but not in the former. Decoupling of ^{31}P from ^{1}H spins would coalesce the ^{31}P multiplet of GPC into a singlet, which together with the nuclear Overhauser effect would enhance the intensity of this peak in the extract spectrum. In addition, part of the GPC pool *in vivo* may be immobilized by

binding to cell matrix, which does not contribute to the GPC signal in *in vivo* spectra. Upon extraction, this fraction could be mobilized and became observable by ^{31}P NMR in extracts.

The assignment of the GPC peak in the ovarian spectrum was substantiated by two lines of evidence in addition to the chemical shift. One came from the coincidence of this peak with that from the added GPC standard (cf. Figure 48). The other entailed the presence of a spin-spin coupling network that was consistent with the GPC structure. This included the connectivity of the ^{31}P spin to the α- and α'-methylene ^{1}H spins in the PDE moiety, of α to β to γ 1H spins in the glycerol backbone, and of α' to β' ^{1}H spins in the choline moiety of GPC (cf. Figures 49 and 50). Thus, the combination of ^{31}P-^{1}H HETCORR with high-resolution phase-sensitive ^{1}H-TOCSY (at 14.1 Tesla) provided a complete tracing of the GPC spin system in the crude ovarian extract, which could not be achieved by 1-D NMR or even 2-D magnitude-calculated correlation spectroscopy (COSY[1]) alone. Consequently, the GPC structure was identified without the need for extensive purification and avoided the ambiguity of overlapping resonances and chemical shift heterogeneity. The combined 2-D NMR techniques can be applied in general to achieve rigorous structural evidence for molecules containing heteronuclear spins from crude tissue extracts, which should in turn facilitate reliable resonance assignment of *in vivo* NMR spectra.

I

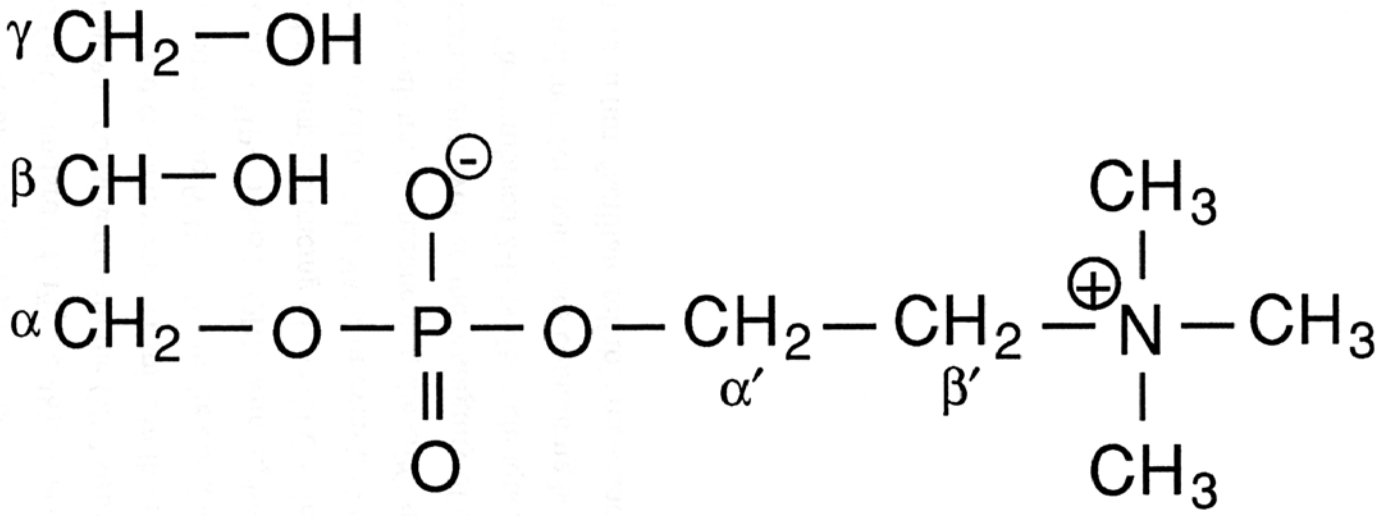

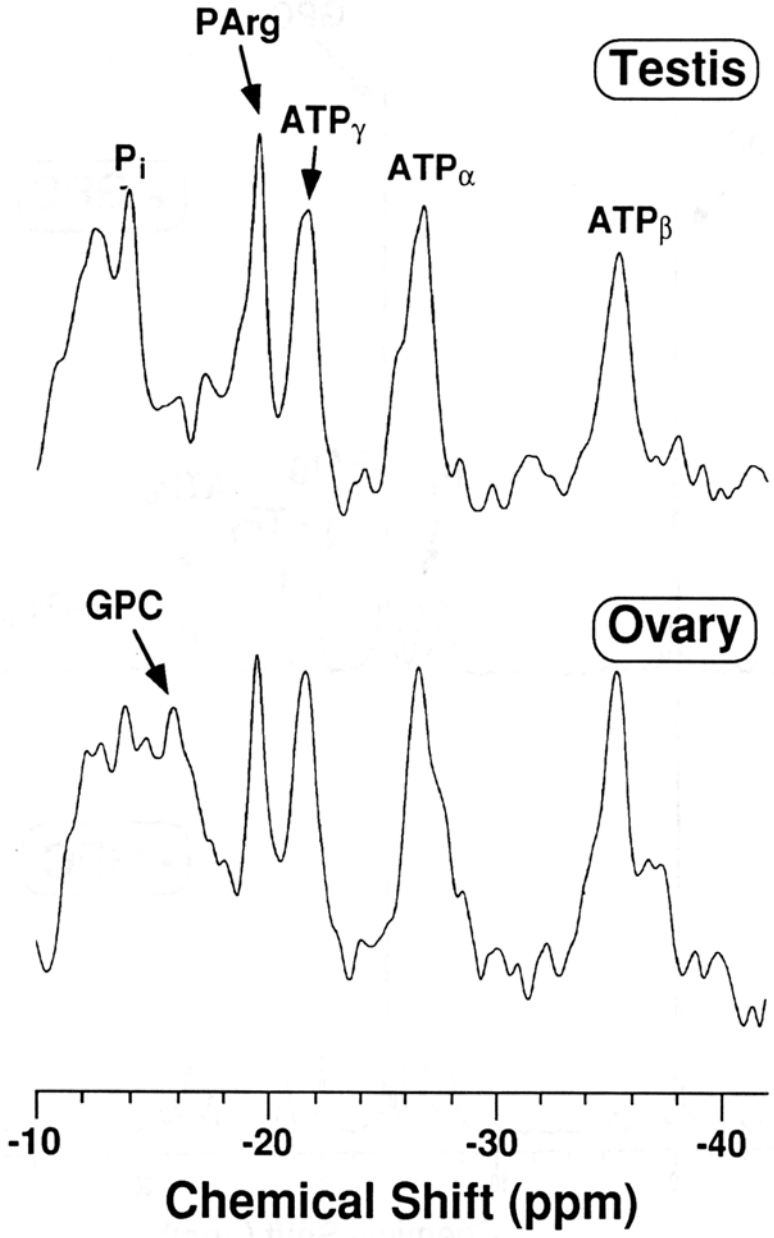

Figure 47. Localized *In Vivo* ^{31}P NMR Spectra of Mussel Testis and Ovary.

These two spectra were acquired from live male and female *M. californianus* individuals as described in Materials and Methods. A line-broadening of 20 Hz was applied before Fourier transformation to obtain the processed spectra.

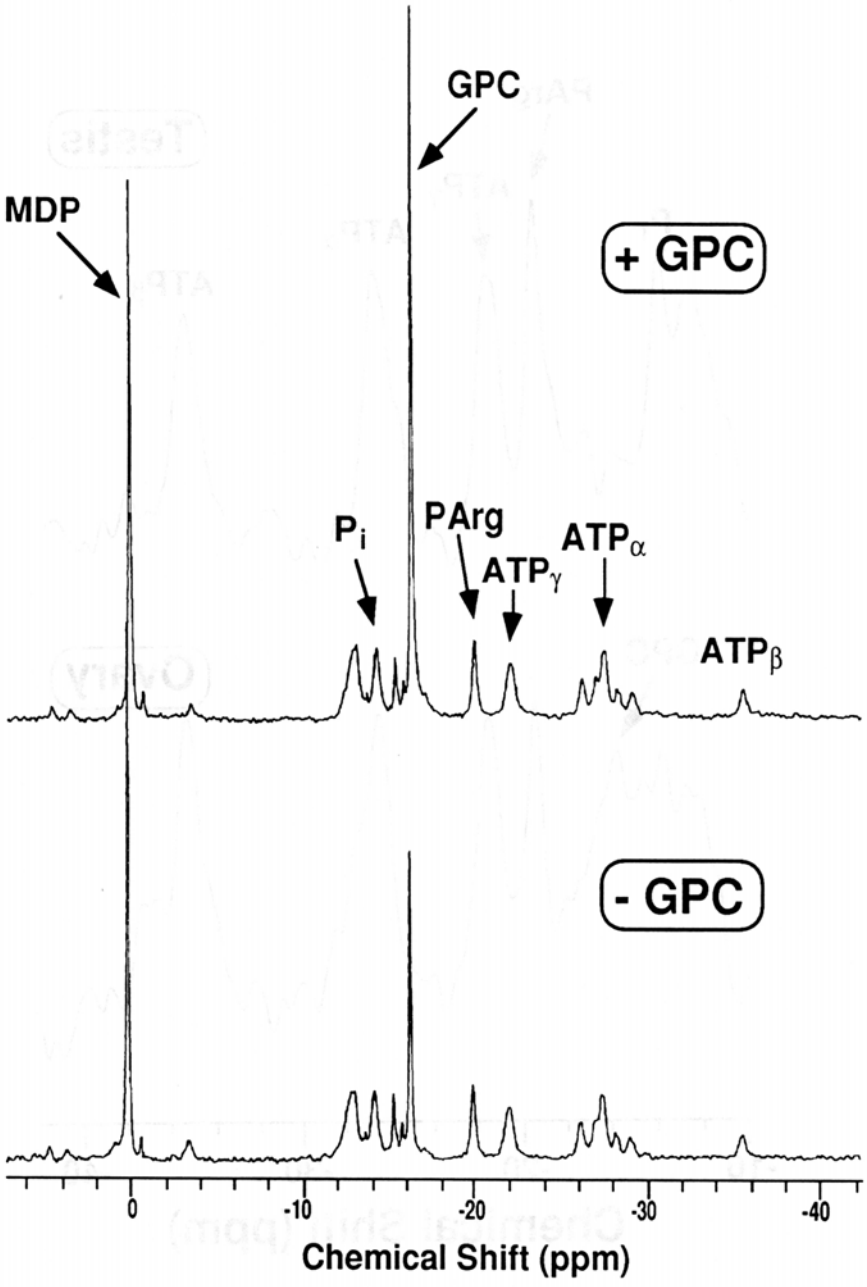

Figure 48. Comparison of ^{31}P NMR Spectra of Mussel Ovarian Extract with and without Added GPC.

The ovary from Figure 47 was dissected, extracted with 5% PCA, and analyzed by ^{31}P NMR as described in Materials and Methods. A capillary of 0.1 M methylene diphosphonate (MDP) standard was included as an external chemical shift reference (0 ppm). The spectra were processed with a line-broadening of 10 Hz.

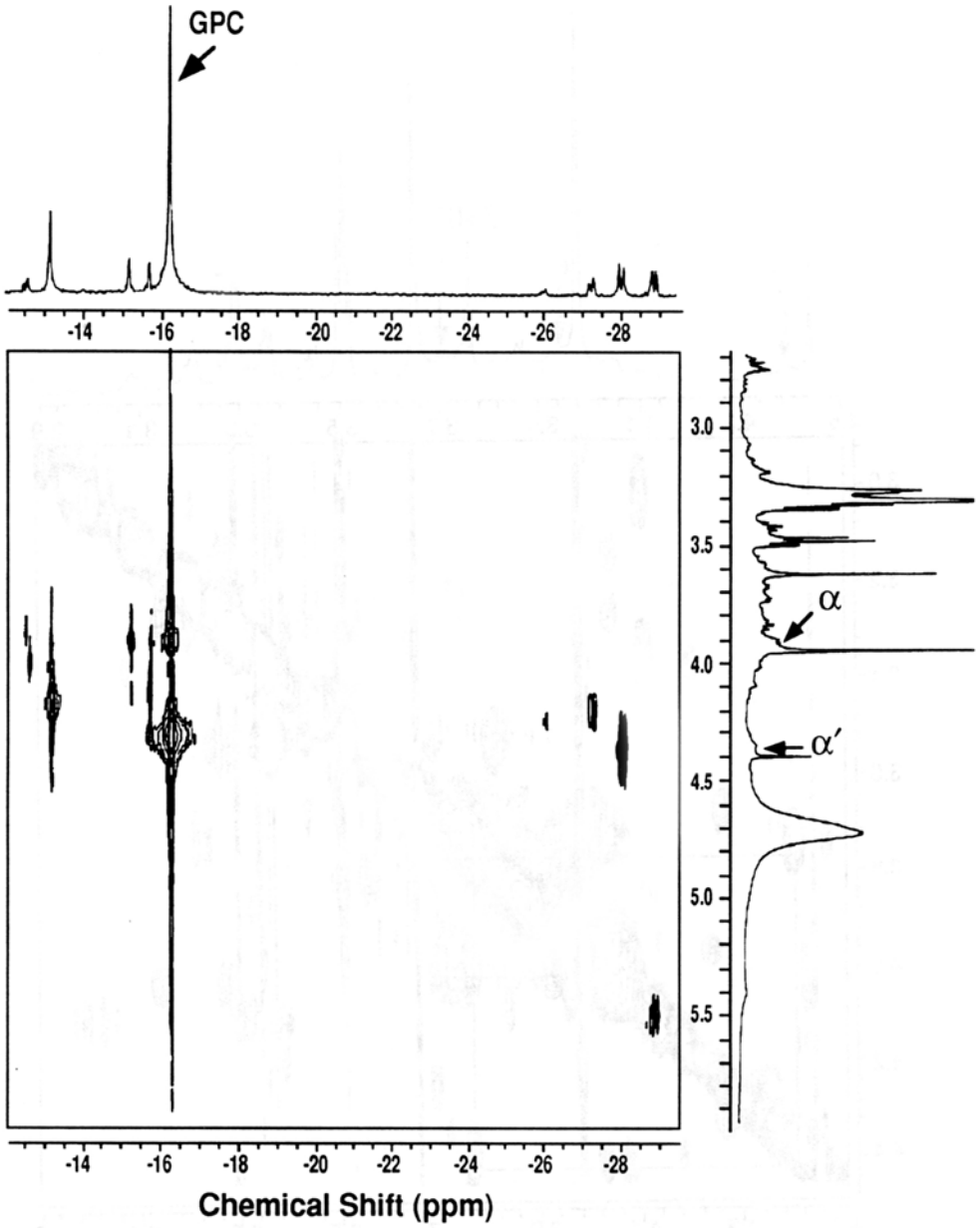

Figure 49. 2-D ^{31}P-^{1}H HETCORR Spectrum of Mussel Ovarian Extract.

A different extract from that in Figure 48 with added 50 mM EDTA was analyzed as described in Materials and Methods. The chemical shift in the F2 (^{31}P) dimension was referenced to the GPC peak while that in the F1 (^{1}H) dimension was referenced to HOD at 4.76 ppm. The α and α' spins corresponded to those denoted in Structure I. The 1-D spectra shown were corresponding high-resolution spectra instead of projections of the two dimensions.

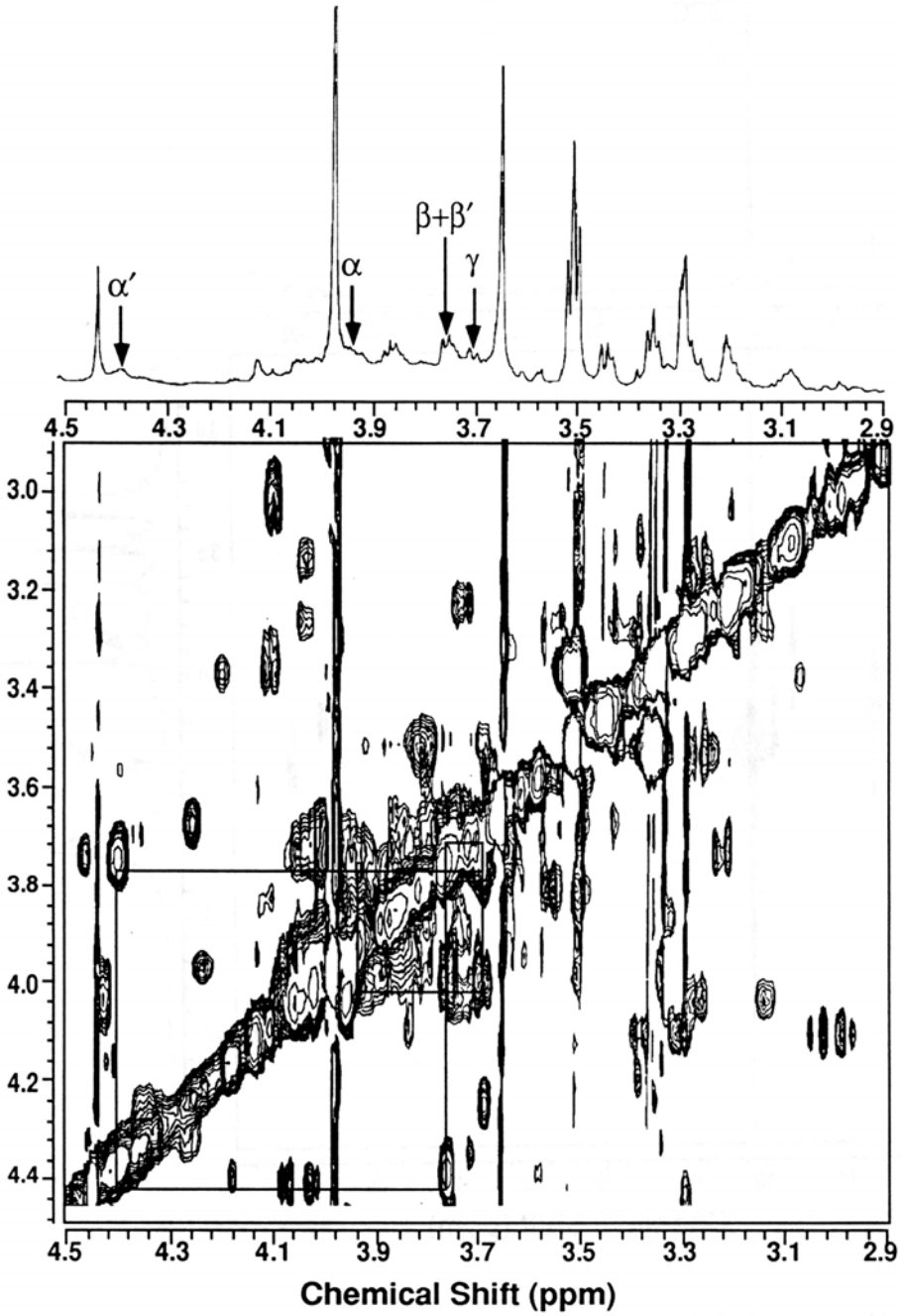

Figure 50. 2-D ^{1}H TOCSY Spectrum of Mussel Ovarian Extract.

The same extract from Figure 49 was measured as described in Materials and Methods. ^{1}H chemical shift was referenced as in Figure 49. The TOCSY spectrum is displayed along with the corresponding 1-D high resolution spectrum. The square boxes trace the spin connectivity of the glycerol and choline moieties of GPC. Labels of all spins corresponded to those denoted in Structure I.

MEASUREMENT OF PW EFFECT ON MUSSEL REPRODUCTION AND HEALTH

Use Of Noninvasive NMR Spectroscopy And Imaging For Assessing Produced Water Effects On Mussel Reproduction (In: *Produced Water: Technological/Environmental Issues and Solutions*. J.P. Ray and F.R. Engelhardt, eds., Plenum Publishing, NY)

Introduction

Perturbation of reproductive performance such as gametogenesis, can be a key factor in the decline of a species in a polluted environment since reproductive success is directly related to effects at the population level. The effects of contaminants on reproduction in indigenous marine invertebrates have been documented both in the laboratory (Kluytmans *et al.*, 1988; Hawkins *et al.*, 1989; Langston *et al.*, 1989) and in the field (Lowe, 1988; Moore, 1988; Auffret, 1988). In the Santa Barbara Channel, CA, the discharge of aqueous petroleum waste, primarily the produced water (PW[1]), has been correlated with changes in growth and gonadal-somatic indices (GSI) of mussels outplanted at the discharge site (Osenberg *et al.*, 1992). However, because other complicating environmental factors can exist in field studies, it is difficult to assign a cause-and-effect relationship between the pollution source and reproductive perturbations observed. In fact, this situation was reported for *Mytilus californianus* in an oil seep site study in the Santa Barbara Channel (Straughan, 1976). It has been suggested that the most effective approach would be to relate molecular and cellular alterations to individual-level physiological changes that lead to reproductive perturbations (Spies, 1987).

In order to assess the reproductive sucess at the biochemical level of indigenous organisms such as the California mussel (*M. californianus*), we have developed noninvasive ^{31}P NMR spectroscopy and ^{1}H NMR imaging methods to acquire unique molecular information on energy budget and detailed morphological and biophysical changes during gametogenesis. These methods were then applied to investigate the chronic effects of PW discharged into the Santa Barbara Channel, on gametogenesis in *M. californianus*.

Mytilus was utilized in this study because it is a worldwide environmental monitoring organism, and can be readily outplanted at polluted sites (Phillips, 1976; George *et al.*, 1979). Noninvasive approaches designed for repeated measurements of individuals were developed for their unique capabilities of observing chronic effects on mussels without interferences from commonly observed individual heterogeneities in reproductive performance. We have focused on the use of *in vivo* ^{31}P NMR spectroscopy for monitoring energy metabolism in mussels (Fan *et al.*, 1991) which plays a central role in gametogenesis and organismal health. This technique has rapidly become the method of choice for measuring intracellular pH, energy status, and ATP

turnover (see Gadian, 1982) in biomedical research, although its application to environmental pollution research is yet at its infancy. In view of the importance of energy balance in chronically impacted ecosystems, ^{31}P NMR should be a useful tool for assessing the individual reproductive performance.

To assist evaluation of gametogenesis, we also employed the ^{1}H NMR imaging (also known as magnetic resonance imaging, MRI[1]) technique which has been used to provide detailed anatomical features of mammals including human in medical research and diagnostics (see Morris, 1986) as well as in invertebrates such as mussels (Fan *et al.*, 1991). In this report, we demonstrated how the time course of gametogenesis was assessed by MRI in field-collected mussels, and how this information was applied to determine the impact of PW exposure on gametogenesis.

---

[1]Abbreviations: PW, produced water; MRI, magnetic resonance imaging; PCA, perchloric acid; PDE, phosphodiester; PArg, phosphoarginine; P_i, orthophosphate; [x], concentration of x.

Materials and Methods

PW was collected from an onshore plant in southern California, shipped chilled without headspace, divided into 20 ml aliquots, and kept frozen at -70°C until use. Elemental composition of PW was performed on an ARL-3510 Inductively Coupled Plasma/Atomic Emission Spectrometer using filtered (through 0.2 μm filter), acidified (5% HCl) samples. *M. californianus* was collected from Bodega Bay, CA and maintained in flowing sea water at 12-14°C until NMR measurements or dissections were conducted. The temperature of the magnet bore where the mussel was placed for NMR measurements was maintained at 14°C with recirculating cooler (Scheme 1). *In vivo* ^{31}P NMR spectroscopy was performed using a 3.0 or 3.5 cm photoetched surface NMR probe (Fan and Higashi, 1989) on a General Electric CSI-7 Tesla or a CSI-2 Tesla imaging NMR spectrometer (Fremont, CA), respectively. The surface probe arrangement allowed selective aquisition of ^{31}P NMR signals originating from the gonadal region of live mussels. Two-dimensional ^{1}H NMR images of live mussels were obtained from the CSI-2T instrument using a 3 inch birdcage imaging probe optimized for marine organisms with high conductance.

The PW exposure experiment was conducted at 14°C in a 48 hr static/renewal system for 4.5 months @ 1% (w/v) PW in Bodega Head seawater. We have chosen 1% because this is the concentration expected to occur at the discharge. For each seawater renewal, a new batch of PW kept at -70°C was thawed and added; this measure was to avoid repeated thawing or refreezing of PW. This method of PW handling did not affect toxicity to sea urchin embryos (Baldwin *et al.*,

in press). No attempt was made to control for volatization of PW constituents. The control treatment involved incubation with Bodega Head seawater for 5 months. Five mussels each were used for the exposure and the control. These mussels were fed at the static/renewal interval with a monoculture of Isochrysis galbana (Tahitian strain). At a one-month interval, all 10 mussels were subjected to ^{31}P NMR and ^{1}H MRI measurements. No fatality was observed throughout the experiment.

Following *in vivo* NMR spectroscopy and imaging, animals were dissected and their gonads subjected to both perchloric acid (PCA^1) extraction and correlative histological analysis of gametogenesis. PCA extraction was performed on lyophilized gonads which were pulverized to about 1 μm size particle to maximize extraction efficiency (Fan *et al.*, 1986). Briefly, tissues were extracted with 5% PCA, adjusted to pH 3.5 with K_2CO_3, centrifuged, and lyophilized. The lyophilized extract was dissolved in D_2O and neutralized before analysis by ^{31}P NMR on a Bruker AM-400, a General Electric Omega-300 wide-bore, or an Omega-500 NMR spectrometers. For histological examination, tissues (ovaries and testes) were fixed in phosphate buffered formalin (10%), post-fixed in 0.5% osmium tetroxide, dehydrated in a graded acetone series, and embedded in epoxy resin. Sections (1-2 μm) were stained with borate-buffered toluidine blue, and examined with light microscopy (Cherr and Clark, 1982).

Results and Discussion

In Vivo NMR Assessment of Mussel Gametogenesis: ^{31}P NMR

Using the ^{31}P NMR approach, we found that mussel ovaries and testes had several distinct differences in their phosphate metabolite composition as shown in Figure 51. A phosphodiester (PDE^1) signal (tentatively assigned as glycerophosphorylcholine) was prominent in both the *in vivo* (Figure 51A) and extract ^{31}P NMR spectra (Figure 51B) of the late-developing ovary but not in those of the late-developing testis. This was the case with at least 50 mussels examined ranging from early-developing to ripe stages. In addition, several phosphate metabolites that contributed to signals in the -27 to -30 ppm region of the extract ^{31}P NMR spectra were present in the ovary but not in the testis (Figure 51B). These metabolites are likely to be NADP(H) and UDP-glucose based on the ^{31}P NMR peak positions (Lee and Ratcliffe, 1983; Pfeffer *et al.*, 1986). We also found that several metabolites were common to both ovaries and testis, including phosphoarginine ($PArg^1$), ATP, and orthophosphate (P_i^1). Furthermore, except for PArg and P_i peak intensities, there was a close resemblance between the *in vivo* and the corresponding extract spectra, which supported that the *in vivo* spectra acquired originated largely from the gonadal tissues. The relatively higher PArg and P_i peak intensities in the extract spectra could be due to two factors: PArg may be hydrolyzed to yield P_i during extraction procedure; alternatively, part

of the increase in extract P_i peak intensity may result from mobilization of P_i fraction bound to macromolecules and therefore has become visible in the *in vivo* spectra.

The presence of the PDE signal only in the ovarian spectra provided a noninvasive way of distinguishing the gender of mussels. In addition, time course quantitation of major energy compounds such as PArg and ATP on the same individual could be utilized to detect chronic stress in situation where high variability in energy status existed.

In addition to gender distinction, the relative intensity of the PDE signal increased in ovaries from mid (**II**) to late-developing (**III**) stages and decreased from late-developing to spawned stages (**IV**) as shown in Figure 52 (see below for histological descriptions). The latter was also illustrated in the ^{31}P NMR spectra of the corresponding ovarian extracts (Figure 53). It should be noted that other phosphate metabolites including P_i, ATP, and PArg also decreased in levels after spawning (Figures 52 and 53). These results indicate that the reduction of phosphate metabolite composition in the spawned ovary was through the loss of oocytes; in particular, they suggest that PDE was associated with the oocyte and thus, could be an effective marker for oogenesis.

2-D ^1H NMR Imaging and Histology

Another noninvasive means of assessing mussel gametogenesis that we developed is 2-D ^1H MRI. Figure 54A shows the cross-section ^1H NMR images of the same three female individuals as in Figure 52, where the oogenic stages corresponded to **II**, **III**, and **IV**. The ovary (indicated by arrows) appeared as two crescent shape structures cradled against each half of the shell. It is evident from Figure 54A that the relative image density of the ovary increased from Stage **II** to **III** but decreased from **III** to **IV** (after spawning). In addition, patches of lower image density areas (*) were seen in the spawned ovary. Thus, the ovarian image density was positively correlated with the extent of oogenesis or the presence of oocytes.

These ovarian stages in Figures 52 and 54 were independently assessed by histological analysis as shown in Figure 54B. We have followed the staging criteria developed for *M. californianus* by Edwards (1985). Briefly, the Stage **I** ovary represents the early active phase of oogenesis. None of the individuals examined in this study were in this phase of ovarian development. The Stage **II** ovaries were characterized by the appearance of oocytes with multinucleolated germinal vesicles and randomly-distributed cortical granules in the cytoplasm (Figure 54B). Ripe ovaries (Stage **III**) contained distended follicles filled with eggs that either lacked nucleoli, or possessed uninucleolate germinal vesicles. In addition, a distinct band of cortical granules distributed along the periphery of the egg was evident (Figure 54B). Spawned ovaries (designated as Stage **IV** in this study) were characterized by follicles containing few eggs, along with their remnants (Figure 54B).

Likewise, the ^{1}H NMR image density of the testis was correlated with the presence of spermatocytes or spermatozoa as illustrated in Figure 55, where a pair of ^{1}H NMR images from a male individual before and right after spawning were compared. Similar to the case of the ovary, the average image density of the testis decreased and patches of low image density (indicated by *) were evident as a result of spawning. These results suggest that the developing gametes themselves were responsible for the increase in the ^{1}H NMR image density and that the patchy appearance of gonads was from spawning. The latter factor led to greatly increased standard deviations of image densities. This, together with parameters such as "patchiness" (hole count and connectivity) measurable by image analysis, could be valuable tools for evaluating gonadal heterogeneity that resulted from partial spawning.

Impact of Produced Water Exposure on Mussel Oogenesis

Applying the *in vivo* methodology described above, we have examined the chronic effect of PW exposure on mussel oogenesis in the laboratory. The PW from this discharge was unusually devoid of hydrocarbons (< 1 ppb; Higashi *et al.*, 1992) and it appeared that the inorganic fraction may be responsible for the chronic bioeffects (Higashi *et al.*, 1992). A selected elemental composition of the batch of PW used for exposure is shown in Table 1, where several trace elements including Sn, As, and Cu were present at low ppm level that could impact mussel reproduction (for more detailed composition, see Higashi *et al.*, 1992). Figure 6A and B compared the time course changes of the ovarian ^{31}P NMR spectra of PW-exposed (#4) and control (#9) individuals, respectively. One month after PW exposure, a large decrease in [PArg] occurred along with a large increase in $[P_i]$ and a smaller drop in [ATP] while the control individual exhibited little change. The opposite relationship among $[P_i]$, [PArg], and [ATP] suggest that the breakdown of PArg and ATP may have accounted for the increase in $[P_i]$. This phenomenon is usually observed when organisms are under stress. Three months after PW exposure, [ATP] and [PArg] continued to drop and [PDE] was hardly detected while a significant portion of PDE, ATP, and PArg was still present in the control individual. Finally, no further major compositional changes in the phosphate metabolites occurred in the PW-exposed individual after 4.5 months. In contrast, a large decrease in [PArg] and [ATP], a moderate decrease in $[P_i]$, and the disappearance of PDE signal were observed for the control individual after 5 months. These changes in the control individual were consistent with the occurrence of spawning where the loss of oocytes was associated with a large decrease in the concentrations of phosphate metabolites (*cf.* Figures 52 and 53).

In addition, according to histological examination, ovaries from the exposed individuals were dominated by connective tissues and dense granular materials with very few normal oocytes within the follicles (Figure 57A). This appearance was more characteristic of degenerating rather

than spawned gonads. In contrast, the control ovary appeared to have undergone spawning prior to the end of the experiment based on the presence of empty follicles and a low count of normal oocytes (*cf.* Figures 57A and 54B).

Moreover, impact of PW on oogenesis was evident in the ^{1}H NMR images of the exposed individuals relative to those of the control. As shown in Figure 57B, a dramatic decrease in the ovarian image density was observed for the individual (#2) after exposure to PW for 4.5 months . The control individual also exhibited a decline in the ovarian image density but to a lesser extent (result not shown). With repeated image measurements on the same individual, the time course changes in the ovarian image density was established, which is shown in Figure 58. The pattern of change in ovarian image density of two PW-exposed individuals clearly differed from that of the control; the former two declined progressively with time while the latter increased prior to a sudden drop. Together with the evidence acquired from ^{31}P NMR and histology, these patterns of change were consistent with a degeneration of oogenesis in PW-exposed individuals and with occurrence of spawning in the control. Therefore, chronic PW exposure in the laboratory appeared to perturb energy balance in mussel ovary and caused a regression in mussel oogenic activities.

Although preliminary, these results indicated that the noninvasive NMR methodologies that we have developed could be applied to explore the long-term effects of pollutants on reproduction and organismal health in the laboratory. Similar approach could also be extended to investigate effects in field outplant studies. In either case, the added advantage of this approach is that a clear relationship could be discerned without the need for a large number of samples because the same individual is moniotred both before and after the exposure and detailed time course changes can be established.

Conclusion

This study demonstrated that the noninvasive NMR approaches (^{31}P NMR spectroscopy and ^{1}H NMR imaging), together with correlative histological analysis, provided reliable assessments of gender-specific gametogenesis in mussels. Specifically, *in vivo* ^{31}P NMR revealed a specific phosphodiester indicator for oogenesis, in addition to providing information on gonadal energy budget. In a complementary fashion, ^{1}H NMR imaging enabled the distribution density of developing gametes across the entire gonad to be monitored.

When applied to follow the effect of PW exposure on mussel, both methods revealed the dynamics of chronic ovarian perturbations on the same individual, thus eliminating interferences arising from intrinsic heterogeneities in oogenesis of this species. Consequently, reliable conclusions could be drawn from a much smaller sample size. The changes observed suggest that PW exposure perturbed ovarian energy balance and caused ovarian degeneration in *M.*

californianus. To the best of our knowledge, this is the first direct demonstration of perturbations in reproduction of organisms chronically exposed to PW under controlled laboratory conditions. However, it should be kept in mind that as produced water composition may vary from batch to batch and that the results reported here were derived from one batch only, a general conclusion of the impact of produced water cannot be drawn. Nevertheless, such study, together with the fractionation approach employed by Higashi *et al.* (1992), can lead to the identification of active constituents in PW and help establish a cause-and-effect relationship between PW and observed bioeffects.

More importantly, how such laboratory studies relate to the decreased GSI and growth observed for field-outplanted mussels (Osenberg *et al.*, 1992) await further investigations. To help answer this question, an outplant experiment is underway that utilizes the same noninvasive approaches to explore the relationship between PW discharge and reproductive development in field-exposed mussels.

Table 1. Elemental Composition of Produced Water Employed for Mussel Exposure.

	Element														
	S	Ca	Na	Sn	As	Zn	Pb	Cu	Ni	Mn	Al	Ba	Cr	Cd	Fe
ppm	10	168	9900	0.2	0.5	0.02	<0.1	0.06	0.04	0.06	0.09	70	0.4	<0.1	0.74

Scheme 2

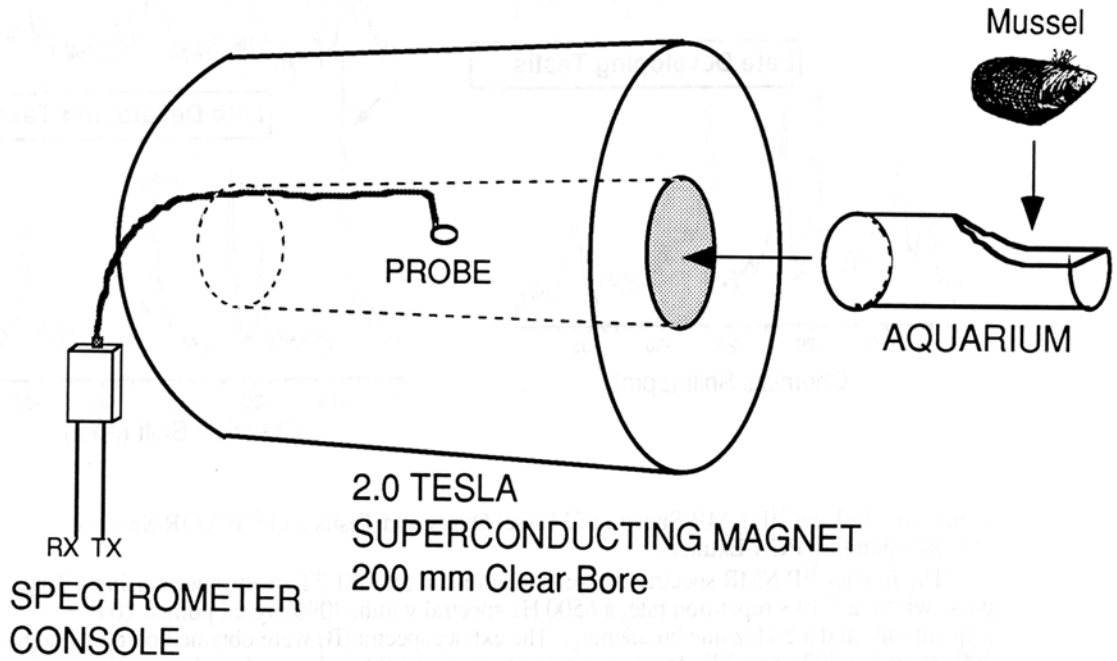
Mussel
PROBE
AQUARIUM
RX TX
SPECTROMETER
CONSOLE
2.0 TESLA
SUPERCONDUCTING MAGNET
200 mm Clear Bore

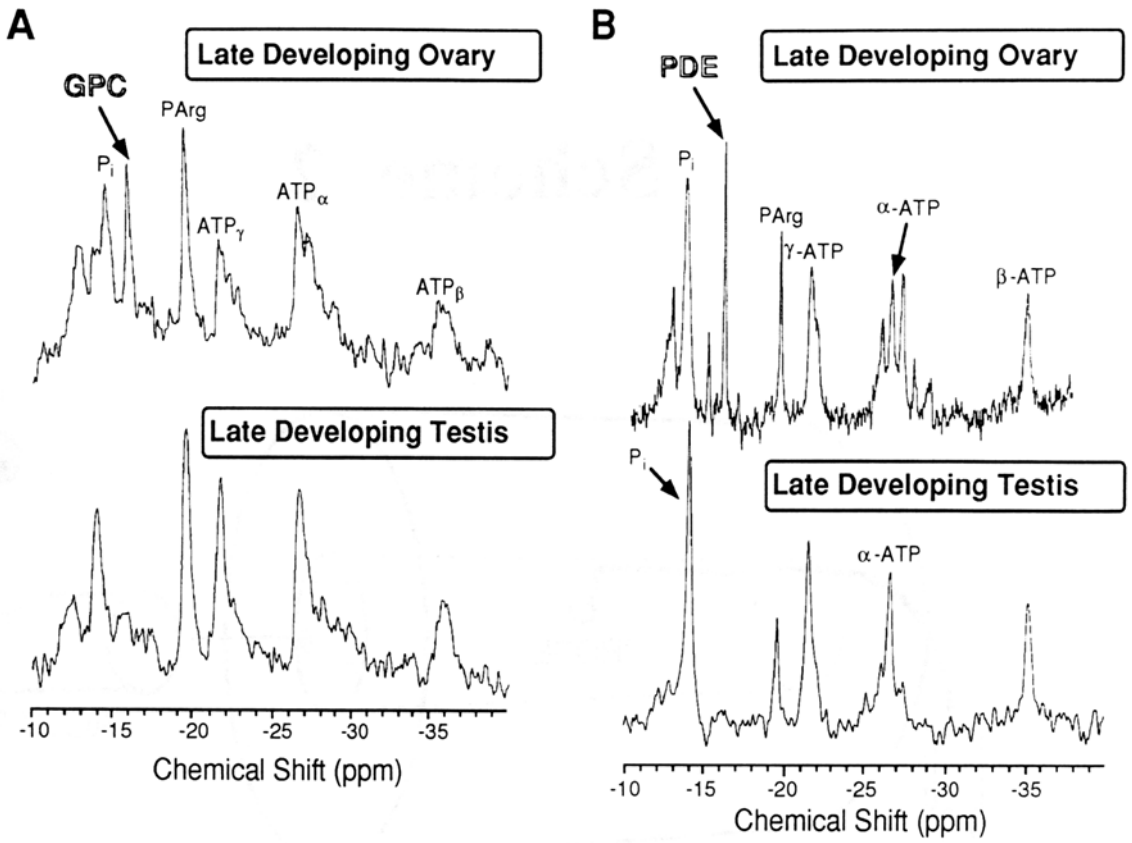

Figure 51. *In Vivo* ^{31}P NMR Spectra of Mussel Ovary and Testis and ^{31}P NMR Spectra of Corresponding PCA Extracts.

The *in vivo* ^{31}P NMR spectra (A) were acquired on the CSI-7T spectrometer using a 30 μs pulse width, a 1.13 s repetition rate, a 6500 Hz spectral width, 4096 digital points, 2048 acquisitions, and a 20 Hz line broadening. The extract spectra (B) were obtained on the Omega-500 (ovary) and Omega-300 (testis) spectrometers using a 90° pulse angle, a 1 s repetition rate, a 9000 Hz spectral width, 4096 digital points, 2048 acquisitions, and a 10 Hz line broadening. Peak assignment is as follows: orthophosphate (P_i); phosphodiester (PDE); phosphoarginine (PArg); γ-ATP, α-ATP, and β-ATP, γ, α, and β-phosphate of adenosine triphosphate (ATP).

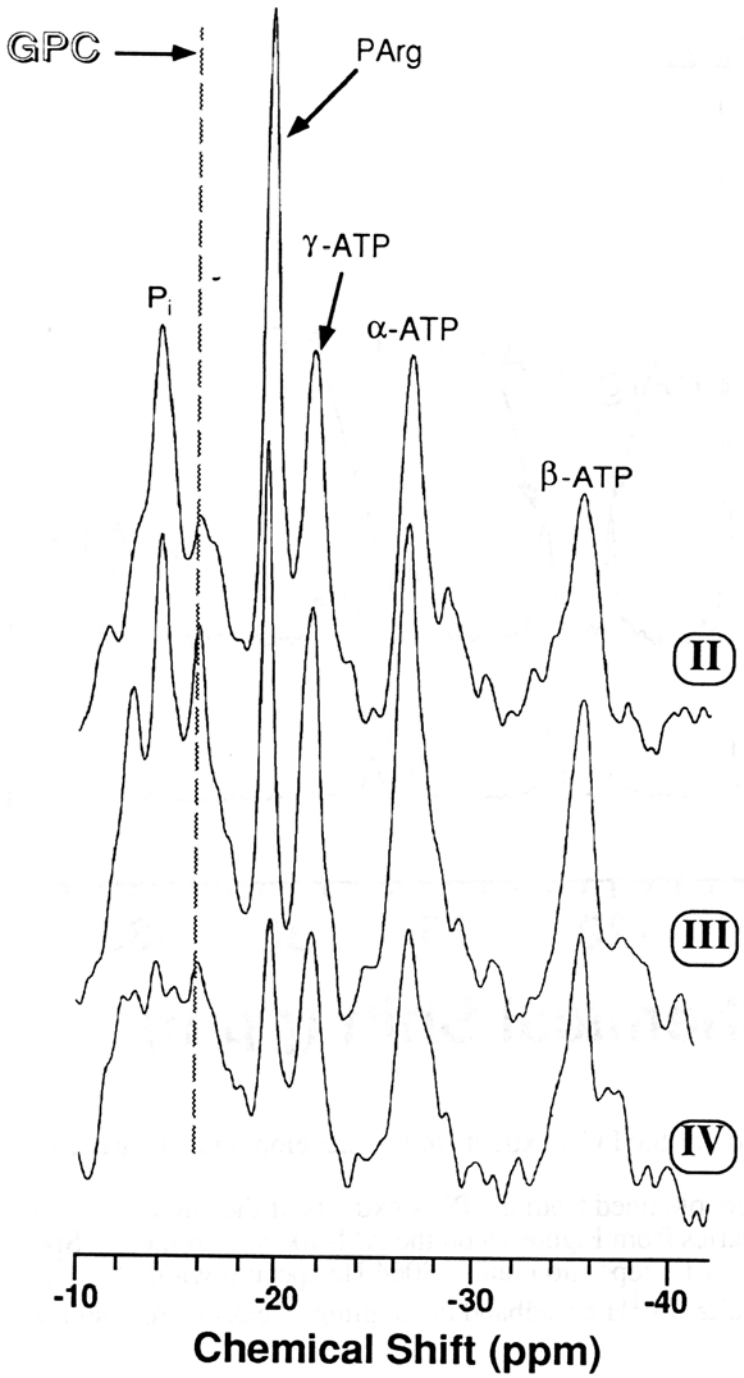

Figure 52. *In vivo* ^{31}P NMR spectra of mussel ovary in three different gametogenic states.

These spectra were acquired on the CSI-2T spectrometer using a 45° pulse angle to minimize signal contribution from other parts of the mussel body. Other spectral parameters included a 1 s repetition rate, a 3015 Hz spectral width, 2048 digital points, 2048 acquisitions, and a 20 Hz line broadening. Peak assignment is the same as that in Figure 47. **II**, **III**, and **IV** represent mid-developing, late-developing, and partially spawned ovaries (see text for stage descriptions).

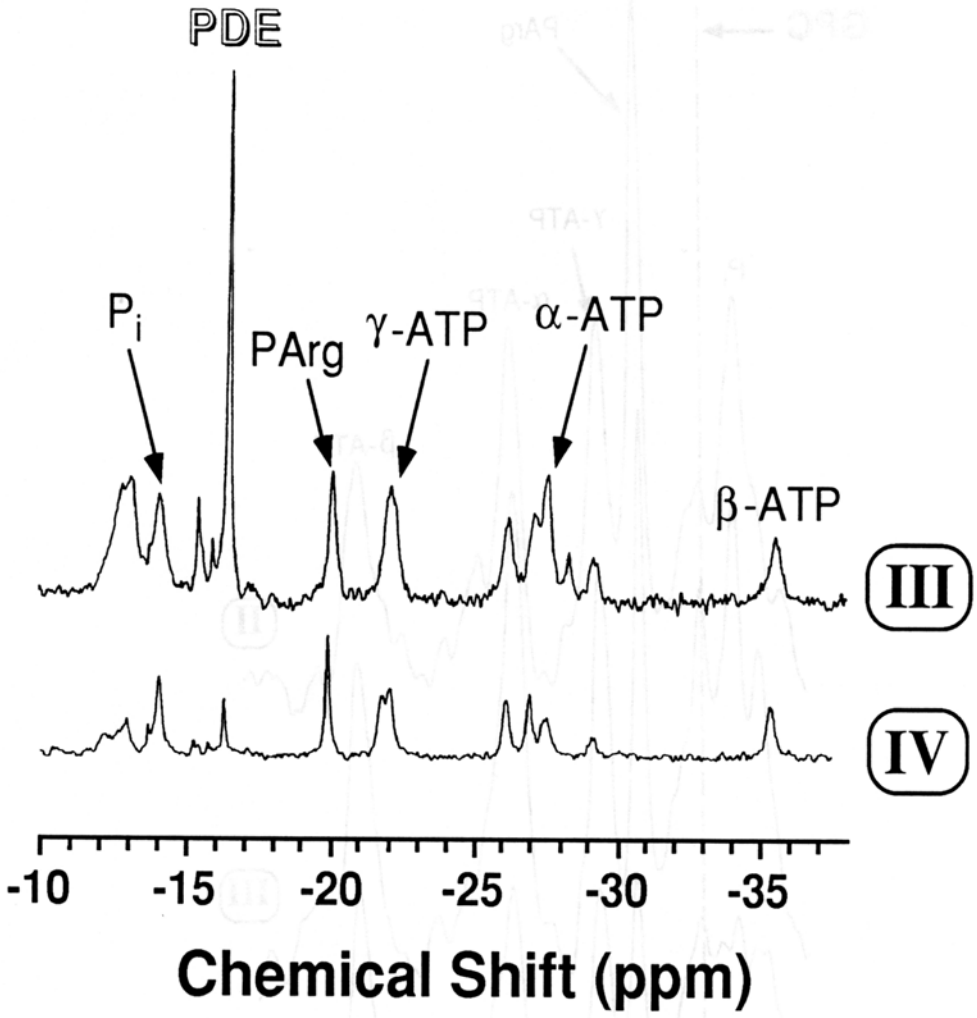

Figure 53. ^{31}P NMR spectra of the PCA extracts of late-developing and partially spawned ovaries.

These two spectra were obtained from the PCA extracts of the late-developing (**III**) and partially spawned (**IV**) ovaries from Figure 48 on the AM-400 spectrometer. Spectral parameters included a 90° pulse angle, a 1 s repetition rate, a 8064 Hz spectral width, 8192 digital points, and 2048 acquisitions with Waltz-16 ^{1}H broadband decoupling. Peaks were assigned as in Figure 47.

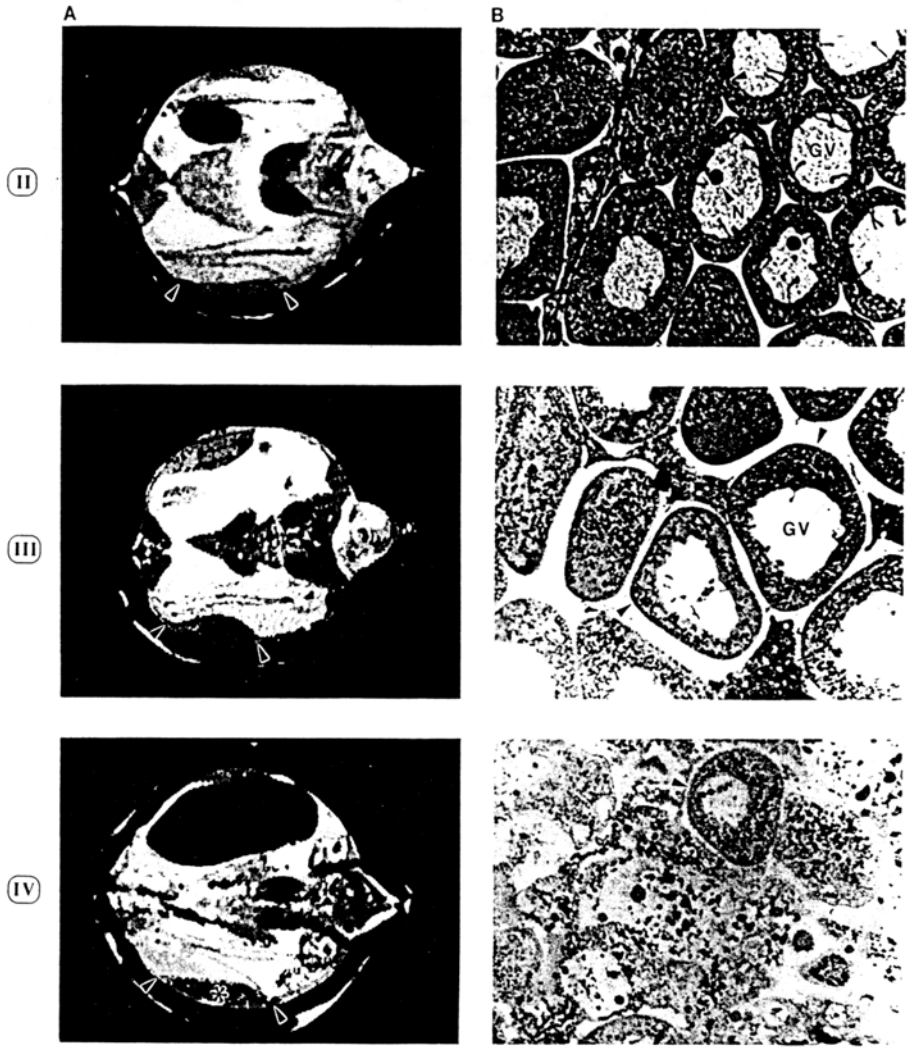

Figure 54. 2-D ^{1}H NMR images and histomicrographs of ovaries in different gametogenic states.

The ^{1}H NMR images (A) of corresponding ovaries from Figure 48 were acquired on the CSI-2T spectrometer using a multislice spin-echo pulse sequence that allowed simultaneous acquisition of 8 slices . Each image slice was 2 mm thick and 5 mm apart with a digital resolution of 256x256. The spin-echo delay (TE = 120 ms) was chosen to optimize the image contrast between the ovary and the rest of the mussel tissues. In the examples shown, the ovary (indicated by arrows) appeared as two crescent shape structures lined against each half of the shell. The asterisk indicates patches of lower density areas. The oogenic stages were assessed independently by histological analysis of the corresponding ovaries (B). The three histomicrographs shown are at 450-fold magnification. The Stage **II** ovary contained oocytes with distinct germinal vesicles (GV), multiple nucleoli (N), and randomly-distributed cortical granules (arrows). The Stage **III** ovary possessed mature eggs with either one or no nucleolus and a distinct layer of cortical granules along the periphery of the egg (arrows). The Stage **IV** (partially spawned) ovary was characterized by a few intact eggs (arrow) and remnants of resorbing oocytes.

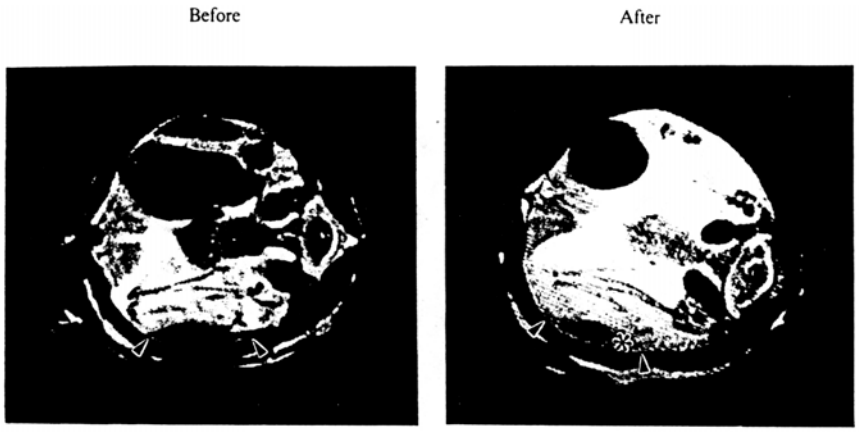

Figure 55. 2-D ^{1}H NMR images of a male mussel before and after spawning.

The ^{1}H NMR images were obtained similarly as in Figure 50. The same individual was scanned both before and right after spawning was induced. Ovarian tissues are indicated by arrows. Patches of low image density areas (indicated by *) were evident in the ovarian image acquired after spawning.

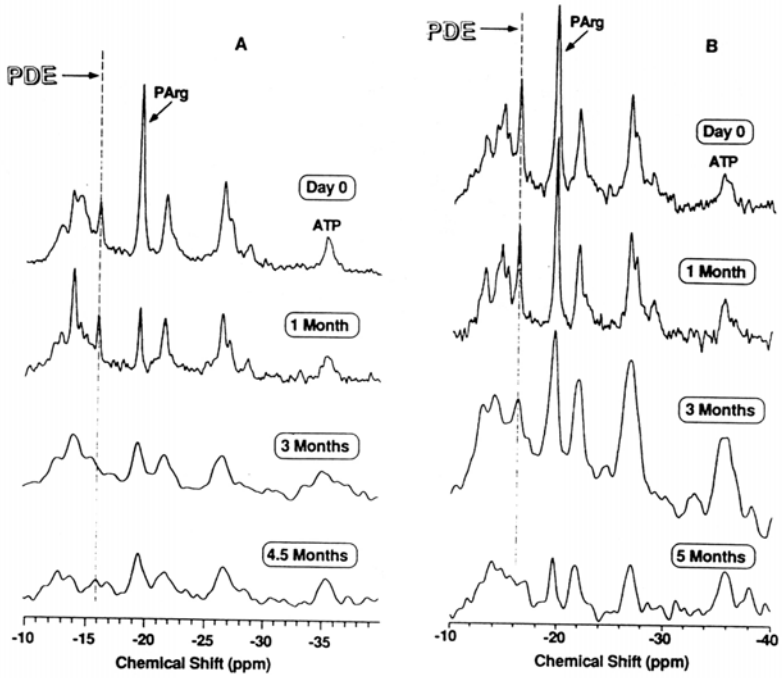

Figure 56. Time course changes in *in vivo* ^{31}P NMR spectra of ovaries from two female mussels under PW and control treatments.

The treatment conditions were as described in Materials and Methods. For the first one month treatment, ^{31}P NMR spectra were acquired on the CSI-7T spectrometer using the same parameters as in Figure 47 while those acquired thereafter were from the CSI-2T instrument using the same parameters as in Figure 48. The acquisition parameters used for these two instruments were adjusted to give comparable ^{31}P NMR spectra of the ovaries. A: PW-exposed ovary; B: Control ovary.

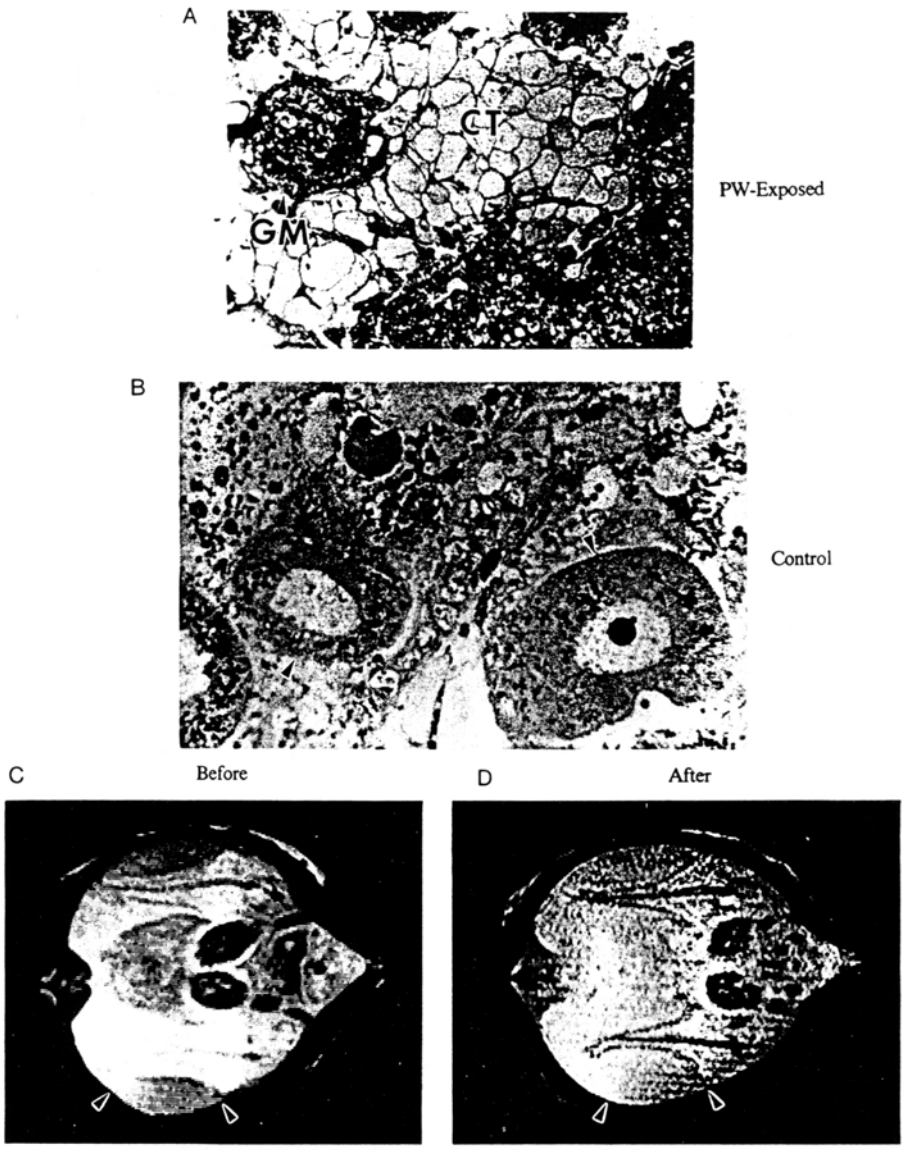

Figure 57. 2-D ^{1}H NMR images of a PW-exposed female and histomicrographs of ovarian sections from mussels under PW and control conditions.

Treatment conditions were as described in Materials and Methods. The two micrographs (A) shown are at 450-fold magnification. The PW-exposed (#2) and the control individuals (#9) were those from Figure 56. Degenerating oocytes, connective tissues (CT), and dense granular material (GM) were evident in the PW-exposed ovary while a few intact eggs (arrows) and remnants of resorbing oocytes were seen in the control ovary. The pair of NMR images (B) shown were acquired from #2 before and after the exposure as described in Figure 50. Ovarian tissues are indicated by arrows.

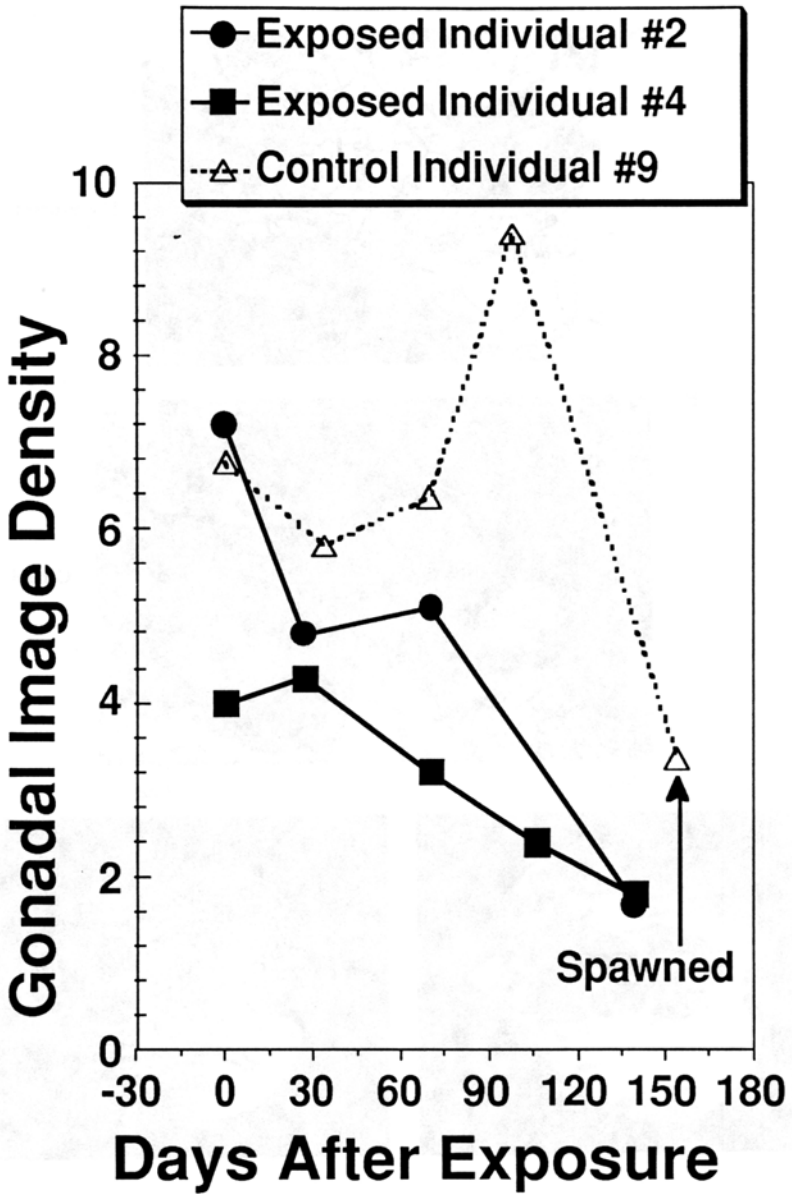

Figure 58. Time course change in the ^{1}H NMR image density of ovaries from mussels under PW exposure and control conditions.

The treatment protocol was as described in Materials and Methods and the NMR image acquisition was the same as in Figure 4. The ovarian image density was obtained by digitizing the NMR images into a microcomputer via a high-resolution video camera, followed by image analysis using the "Image" program developed by the National Institute of Health. The relative image density is defined as the ratio of the image density of the ovary to that of the body water. By taking this ratio, any systematic error associated with image aquisition and digitization was minimized. The closed symbols and open triangles represent PW-exposed and control individuals, respectively.

REFERENCES

Abed, M. and Crawford, B.J. (1986) Can. J. Zool., 64:1436-1443.

Allen NS, Allen RD (1978). Ann Rev. Biophys. Bioeng. 7: 497-526

Alonso, J., Arús, C., Westler, W.M., and Markley, J.L. (1990) Magn. Reson. Med. 15, 142-151.

Alonso, J., Arús, C., Westler, W.M., and Markley, J.L. (1989) Magn. Reson. Med. 11, 316-330.

Alvarez, R., M. Luxoro, V. Nassar-Gentina, and G. Szklarz (1980) Quart. J. Exp. Physiol. 65, 199-205.

Amemiya, S. (1989). Dev. Growth Differ., 31:131-145.

Anderson BS, Hunt JW (1988). Mar. Environ. Res. 26: 113-134

Arsenault, L.A., Ottensmeyer, F.P., and Heath, I.B. (1988). J. Ultrast. Molec. Struct. Res., 98:32-47.

Auffret, M., (1988). Mar. Ecol. Prog. Ser. 46:101-107.

Barman, T.E., F. Travers, R. Bertrand, and G. Roseau (1978) Eur. J. Biochem. 89, 243-249.

Barrow, K.D., Jamieson, D.D., and Norton, R.S. (1980) Eur. J. Biochem. 103, 289-297.

Balaban, R.S. (1982). In: Biochemistry of Kidney Function (Morel, F., ed.), pp. 337-351, Elsevier, Amsterdam.

Baldwin, J.D., M.C. Pillai, and Cherr, G.N.(1992). Mar. Biol., 114: 21-30.

Bayne, B. L. (1971) Comp. Biochem. Physiol. 40A, 1065-1085.

Bayne, B.L., Bayne, C.J., Carefoot, T.C., and Thompson, R.J. (1976) Oecologia (Berl.) 22, 229-250.

Bax, A. and Davis, D.G. (1985) J. Magn. Reson. 65, 355-360.

Boehm, P.D. (1987). In: Boesch, D.F. Rabalais, N.N. (eds.) Long-Term Environmental Effects of Offshore Oil and Gas Development. Elsevier Applied Science, p. 233-286

Boon-Niermeijer, E.K., Tuyl, M., VanderScheur, H. (1986). Int. J. Hyperthermia, 2:93-105

Booth, C.E., McDonald, D.G., and Walsh, P.J. (1984) Mar. Biol. Lett. 5, 347-358.

Briggs, R.W., G.K. Radda, and K.R. Thulborn (1985) Biochim. Biophys. Acta 845, 343-348.

Brindle, K.M. (1988) Prog. NMR Spectr. 20, 257-293.Burke, R.D., Tamboline, C.R. (1990). Dev. Growth Differ., 32(5):461-471

Burt, C.T., T. Glonek, and M. Barany (1976) J. Biol. Chem. 251, 2584-2591.

Burt, C.T., Glonek, T., and Bárány, M. (1976). J. Biol. Chem. 251, 2584-2591.

Burt, C.T. and Ribolow, H.J. (1984) Biochem. Med. 31, 21-30.

Busa, W.B., Crowe, J.H., and Matson, G.B. (1982) Arch. Biochem. Biophys. 216, 711-718.

Butler, K.W., R. Deslauriers, Y. Geoffrion, J.M. Storey, K.B. Storey, I.C.P. Smith, and L. Caltabiano, M.M., Koestler, T.P., Poste, G., Greig, R.G. (1986). J. Biol. Chem., 28:13381-13386

"CRC Handbook of Chemistry and Physics", 57th Edition (1977) R.C. Weast, ed., p.D-152, CRC Press, Cleveland.

Cavanaugh, G.M. (1956). Formulae and methods of the Marine Biological Laboratory Chemical Room. (6th ed.), G.M. Cavanaugh, ed. pp.55-86. Woods Hole: Marine Biological Laboratory.

Charters AC, Neushul M (1979). Aquatic Botany 6: 67-78

Cherr, G.N. and Clark, W.H., Jr., (1982). Develop. Growth Different. 24:341-352.

Cherr, G.N., Yudin, A.I., and Katz, D.F. (1990). Dev. Growth Differ., 32:353-365.

Cherr, G.N., J. Shoffner-McGee, and Shenker, J.M. (1990). Environ. Toxicol. Chem., 9:1137-1145.

Cherr, G.N., R.G. Summers, J.D. Baldwin, and Morrill, J.B. (1992). Micr. Res. Tech., 22: 11-22.

Cheung, A.C.-F. (1973) Arch. Biochem. Biophys. 154, 28-39.

Cole K (1968). Can J Bot 46: 777-782

Coleman, N. (1973) Comp. Biochem. Physiol. 45A, 393-402.

Coleman, N. and Trueman, E.R. (1971) J. Exp. Mar. Biol. Ecol. 7, 295-304.

Cooper JA (1987). J Cell Biol 105: 1472-1478

Corbett, R.J.T., Nunnally, R.L., Giovanella, B.C., and Antich, P.P. (1987) Cancer Res. 47, 5065-5069.

Cresti ME, Pacini E, Ciampolini F, Sarfatti FG (1977). Planta 136: 239-247

Crise-Benson, N. and Beson, S.C. (1979). W. Roux Arch.186:65-70.

de Vooys, C.G.N. and de Zwaan, A. (1978) Comp. Biochem. Physiol. 60, 343-347.

de Zwaan, A., Kluythmans, J.H.F.M., and Zandee, D.I. (1976) Biochem. Soc. Symp. 41, 133-168.

de Zwaan, A. and Wijsman, T. C. M. (1976) Comp. Biochem. Physiol. 54B, 313-324.

de Zwaan, A. (1977) Oceanogr. Mar. Biol. Ann. Rev. 15, 103-187.

Davies, D.D., Grego, S., and Kenworthy, P. (1974) Planta 118, 297-310

Debec, A., Courgeon, A.-M., Maingourd, M., Maisonhaute, C. (1990). J. Cell Sci. 96:403-412

Deysher LE, Dean TA (1984). Mar Biol 93: 1720-1723

Doonan JH, Jenkins GI, Cove DJ, Lloyd CW (1985). Eur J Cell Biol 41: 157-164

DeSimone, D. and Spiegel, M. (1986). Roux Arch. Dev. Bio. 195:433-444.

Dubyak, G. R. and Scarpa, A. (1983) Biochemistry 22, 3531-3536.

Edwards, E.L., (1985). Technical Report Series, Humboldt State University, CA., pp. 57.

Ellington, W.R. (1983) J. Exp. Zool. 227, 313-317.

Ellington, W.R. (1985) Mol. Physiol. 7, 155-164.

Ellington, W.R. (1983) J. Exp. Zool. 228, 431-444.

Evanochko, W.T., Sakai, T.T., Ng, T.C., Krishna, N.R., Kim, H.D., Zeidler, R.B., Ghanta, V.K., Brockman, R.W., Schiffer, L.M., Braunschweiger, P.G., and Glickson, J.D. (1984) Biochim. Biophys. Acta 805, 104-116.

Fan, T.W.-M., R.M. Higashi, and A.N. Lane (1986) Arch. Biochem. Biophys. 251, 674-687.

Fan, T.W.-M. and Higashi, R.M., Lane, A.N., and Jardetzky, O., (1986). Biochim. Biophys. Acta 882:154-167.

Fan, T. W.-M., Higashi, R.M. & Lane, A.N. (1988) Arch. Biochem. Biophys. 266, 592-606.

Fan, T. W-M. and Higashi, R.M. (1989) Anal. Chem. 61, 636-638.

Fan, T.W.-M., R.M. Higashi, and J.M. Macdonald (1991) Biochim. Biophys. Acta 1092, 39-47.

Fan, T.W-M., R.M. Higashi, G.N. Cherr, and Pillai, M.C. (1992). In: Produced Water: Technological/Environmental Issues and Solutions. J. P. Ray and F.R. Engelhardt, eds. Plenum Press, New York. pp. 403-414.

Franke WW, Herth W, van der Woude WJ, Morre DJ (1972). Planta 105: 317-341

Freeman, D., Bartlett, S., Radda, G., and Ross, B. (1983) Biochim. Biophys. Acta 762, 325-336.

Gadian, D.G. (1982) Nuclear Magnetic Resonance and Its Applications to Living Systems, pp.29-34, Clarendon Press, Oxford.

Gadian, D.G., Radda, G.K., Dawson, M.J., and Wilkie, D.R. (1982) in Kroc Foundation Series (Nuccitelli, R. and Deamer, D. W., eds.), Vol. 15, pp.61-77.

Galileo, D.S. and Morrill, J.B. (1985). J. Morphol., 185:387-402.

Garlick, P.B., Radda, G.K., and Seeley, P.J. (1979) Biochem. J. 184, 547.

Garman, G.D., M.C. Pillai, and Cherr, G.N. (1991). Proc. of 12th annual SETAC Meeting, Seattle, WA. pp. 222

Gilkey, J.C. and Staehelin, A. (1986). J. Electron. Microsc. Tech. 3:177-210.

Gehlen, H (1954) Z. Phys. Chem. 203, 125.Gerhardini GL, North WH (1972). Proc 7th Int Seaweed Symp pp. 172-180

Goff LJ, Coleman AW (1984). Dev Biol 102: 173-194

Graham, R. A., Ellington, W. R., and Chih, C. P. (1986) Biochim. Biophys. Acta 887, 157-163.

Gunning BES, Wick SM (1985). J Cell Sci Suppl 2: 157-179

Gunther, A.J., Davis, J.A., O'Connor, J.M., Phillips, D.J.H., Kramer, K.S., Richardson, B.J. (1990). "Status and Trends Report on Dredging and Waterway Modification in the San Francisco Estuary", San Francisco Estuary Project.

Gupta , R.K., J.A. Ferretti, E.D. Becker, and G.H. Weiss (1980) J. Magn. Reson. 38, 447-452.

Gutmann, I. and Wahlefeld, A.W. (1974) in Methods of Enzymatic Analysis (Bergmeyer, H. U., ed.), pp.1586-1587, Academic Press, New York.

Hamer, D.H. (1986). Ann. Rev. Biochem. 55: 913-951

Harkey, M.A., Whiteley, A.H. (1980). Wilhelm Roux's Archives, 189:111-122

Hascall, G.K. (1980). J. Ultrastruct. Res. 70:369-375.

Hawkins, A.J.S., Rusin, J., Bayne, B.L., and Day, A.J., (1989). Mar. Environ. Res. 28:253-257.

Hay, E.D. (1984). In: Trelstad, R.L. (ed.) The role of extracellular matrix in development. A.R. Liss, Inc. New York, p. 1-31

Hayes, C.E., Edelstein, W.A., Shenck, J.F., Mueller, O.M., and Eash, M. (1985) J. Magn. Reson. 63, 622-628.

Heinegard, D. and Paulsson, M. (1984). In: Extracellular matrix biochemistry. K. Piez and A.H. Reddi eds. Elsevier, New York, pp. 277-324.

Hensel W (1984). Planta 162: 404-414

Hensel W (1985). Protoplasma 129: 178-187

Hepler PK, Palevitz BA (1974). Ann Rew Plant Physiol 25: 309-362

Heslop-Harrison J, Heslop-Harrison Y (1989). J Cell Sci 93: 299-308

Heslop-Harrison J, Heslop-Harrison Y (1991). Phil Trans R Soc Lond B pp. 225-235

Heslop-Harrison J, Heslop-Harrison Y, Cresti M, Tiezzi A, Moscatelli A (1988). J Cell Sci 91: 49-60

Higashi, R.M., Fan, T.W.M., and Macdonald, J.M. (1989) J. Exp. Zool. 249, 350-356.

Higashi, R.M., Cherr, G.N., Bergens, C.A., Fan, T.W-M., Crosby, D.G. (1992). In: Produced Water: Technological/Environmental Issues and Solutions. J. P. Ray and F.R. Engelhardt, eds. Plenum Press, New York. pp. 223-233.

Hochachka, P.W. and G.N. Somero (1984) "Biochemical Adaptation", Princeton University Press, Princeton.

Hoult, D.I., Busby, S.J.W., Gadian, D.G., Radda, G.K., Richards, R.E., and Seeley, P.J. (1974) Nature 252, 285-287.

Huheey, J.E. (1972) Inorganic Chemistry: Principles of Structure and Reactivity, pp.212-213, Harper & Row, New York.

Johnson, W.S. Hooper, G.R. Holdaway, B.F. and Rasmussen, H.P. (1976). Micron 7:305-306.

Kamp, G. and H.P. Juretschke (1987) Biochim. Biophys. Acta 929, 121-127.

Katow, H. and Solursh, M. (1979). J. Exp. Zool. 210:561-567.

Katsuta J, Shibaoka H (1988). Plant Cell Physiol 29: 403-413

Kawabe, T.T., Armstrong, P.B., and Pollock, E.G. (1981). Dev. Biol. 85:509-515.

Keller, R. and Winklbauer, R. (1990). Sem. in Dev. Biol., 1:25-37.

Kelley, P.M., Schlesinger, M.J. (1982). Molec.cell. biol. 2: 267-274

Kersey YM, Hepler PK, Palevitz BA, Wessels NK (1976). Proc Natl Acad Sci USA 73: 165-167

Kiermayer O, Fedtke C (1977). Protoplasma 92: 163-166

Kim, K.S., Kim, Y.K., Naftolin, F., Markert, C.L. (1987). In: McLachlan, J.A., Pratt, R.M., Markert, C.L. (eds.) Developmental toxicology: mechanisms and risk. Cold Spring Harbor Laboratory, Cold Spring Harbor, p. 123-136 (Banbury Rep. No. 26)

Kluytmans, J.H., Brands, F., and Zandee, D.I., (1988). Mar. Environ. Res. 24:189-192.

Konat, G., Offner, H., Mellah, J. (1984). Experimentia, 40: 303-304

Koretsky, A.P., Wang, S., Klein, M.P., James, T.L., and Weiner, M.W. (1986) Biochemistry 25, 77-84.

Kropf DL, Maddock A, Gard DL (1990). J Cell Sci 97: 545-552

LaClaire JW II (1987). Planta 171: 30-42

Lane, M.C., Solursh, M. (1988). Dev. Biol. 127:78-87

Lane, M.C., Solursh, M. (1991). Dev. Biol. 143:389-397

Langston, W.J., Bebianno, M.J., and Mingjiang, Z., (1989). Mar. Environ. Res. 28:195-200.

Lee, R.B. and Ratcliffe, R.G., (1983). J. Exp. Bot. 34:1222-1244.

Lerch, K. (1980). Nature, London 284 :368-370

Levyns MR (1933). *Ag*. Ann Bot 47: 349-353

Lindinger, M.I., Laurén, D.J., and McDonald, D.G. (1984) Mar. Biol. Lett. 5, 371-381

Lloyd CW (1982) The cytoskeleton in plant growth and development. pp. 457. Academic Press, New York

Lowe, D.M., (1988). Mar. Ecol. Prog. Ser. 46:91-100.

Luft, J.H. (1971). Anat. Rec. 171:369-416.

Luning K, Neushul M (1978). Mar Biol 45: 297-309.

Luoma, S., Phillips, D. (1988). Mar. Pollut. Bull. 19 :405-413

Malloy, C.R., A.D. Sherry, and R.L. Nunnally (1985) J. Magn. Reson. 64, 243-254.

Mascarenhas JP, Lafountain J (1972). Tissue and Cell 4: 11-14

McCarthy, J.F., Shugart, L.R. (1990). In: McCarthy, J.F., Shugart, L.R. (eds.) Biomarkers of environmental contamination, Lewis Publishers, Boca Raton, Florida, CRC Press, p.3-14

McClay, D. and Ettensohn, C. (1987a) In: Genetic Regulation of Development. 45th Symposium Soc. Dev. Biol., W. Loomis, ed. pp. 111-128.

McClay, D. and Ettensohn, C. (1987b). Ann. Rev. Cell Biol., 3:319-345.

McMahon, R.F. (1988) Amer. Zool. 28, 97-114.

Meindl U (1983). Protoplasma 118: 75-90

Meyer, R.A., Brown, T.R., Krilowicz, B.L., and Kushmerick, M.J. (1986) Am. J. Physiol. 250, C264-274.

Mineyuki Y, Furuya M (1986). Protoplasma 130: 83-90

Monne, L. and Harde, S. (1951). Arkiv for Zoologi, 1(28):463-469.

Monne, L. and Slautterback, D.B. (1950). Exp. Cell Res. 1:477-491.

Moore, M.N., (1988). Mar. Ecol. Prog. Ser. 46:81-89.

Morejohn LC, Fosket, D (1986). Science 224: 874-876

Morrill, J.B. and Santos, L.L. (1985). In: The Cellular and Molecular Biology of Invertebrate Development, R. Sawyer and R. Showman, eds., No. 15, Belle Baruch Library in Marine Science, Univ. S. Carolina Press, Columbia, S.C.

Morrill, J.B. (1986). Meth. in Cell. Biol 27:263-293.

Morris, G.A. and R. Freeman (1978) J. Magn. Reson. 29, 433-462.

Motomura T (1990). J Phycol 26: 80-89

Motomura T (1991). J Phycol 27: 248-257

Murata, F., Suzuki, S., Tsuyama, S., Suganuma, T., Imada, M., and Furihata, C. (1985). Histochem. J. 17:967-980.

Nageswara Rao, B.D., D.H. Buttlaire, and M. Cohn (1976) J. Biol. Chem. 251, 6981-6986.

Nagai R, Rebhun LI (1966). J Ultrastruct. Res 14: 571-589

Nakai Y, Ushiyama R (1978). Can J Bot 56: 1206-1211

Nakanishi, T. and Burg, M. B. (1989) Am. J. Physiol. 257, C795-C801.

Navon, G., Gogol, E., and Weissenberg, R. (1985) Arch. Androl. 15, 153-157.

Neff, J.M. (1987). In: Boesch, D.F., Rabalais, N.N. (eds.) Long-Term Environmental Effects of Offshore Oil and Gas Development, Elsevier Applied Science, New York, p. 469- 538

Neff, J.M., Rabalais, N.N., Boesch, D. (1987). In: Boesch, D.F., Rabalais, N.N. (eds.) Long-Term Environmental Effects of Offshore Oil and Gas Development, Elsevier Applied Science, New York, p. 149-173

Nemer, M., Travaglini, E.C., Rondinelli, E., D'Alonzo, J. (1984). Develop. Biol., 102(2): 471-482

North W (1971). Nova Hedwigia 32: 1-600

Nothnagel EA, Barak LS, Sanger JW, Webb WW (1981). J Cell Biol 88: 364-372

Nakatsuji, N. (1984). Amer. Zool. 24:615-627.

Nichols, B.A., Chiappino, M.L., and Dawson, C.R. (1985). Invest. Ophthalmol. Visual. Sci. 26:464-473.

Pearse, A.G.E. (1968) Histochemistry: theoretical and applied. Little, Brown, and Company, Boston.

Pfeffer, P. E., Tu, S.-I., Gerasimowicz, W.V., and Cavanaugh, J.R., (1986). Plant Physiol. 80:77-84.

Podo, F., Carpinelli, G., Di Vito, M., Giannini, M., Proietti, E., Fiers, W., Gresser, I., and Belardelli, F. (1987) Cancer Res. 47, 6481-6489.

Oakley BR, Morris NR (1980). Cell 19: 255-262

Osenberg, C.W., Schmitt, R.J., and Canestro, D., (1992). In: "Produced Water: Technological/Environmental Issues and Pollution", J.P. Ray and F.R. Englehardt, eds., in press.

Ott DW (1992). In: Menzel D (ed) The cytoskeleton of the algae. CRC Press, Boca Raton, Florida, pp 255-272

Papenfuss G F (1942). Am J Bot 29: 15-24

Perdue TD, Parthasarathy MV (1985). Eur J Cell Biol 39: 13-20

Picton JM, Steer MW (1982). J Theor Biol 98: 15-20

Pillai MC, Baldwin J D, Cherr GN (1990). J Cell Biol 111: 415a

Rebhun, L.I. (1974). In: Principles and techniques of electron microscopy: biological applications. Vol.2. M.A. Hayat, ed. Van Nostrand Reinhold Co., New York, pp. 2-49.

Roberts, J.K.M., N. Wade-Jardetzky, and O. Jardetzky (1981) Biochemistry 20, 5389-5394.

Roccheri, M.C., DiBernardo, M.G., Giudice, G. (1981a). Dev. Biol. 83:173-177

Roccheri, M.C., Sconzo, G., DiBernardo, M.G., Albanese, I., DiCarlo, M., Giudice, G. (1981b). Acta. Embryol. Morphol. Exper. 2:91-99

Roccheri, M.C., LaRosa, M., Ferraro, M.G. Cantone, M., Cascino, D., Giudice, G., Sconzo, G. (1988). Cell. Differ. 24:209-214

Sanders, B. (1990). In: McCarthy, J.F., Shugart, L.R. (eds.) Biomarkers of Environmental Contamination, Lewis Publishers, CRC Press, Boca Raton, FL., p. 165-191

Sandström, J. (1982) "Dynamic NMR Spectroscopy", Ch.2, Academic Press, London.

Schlesinger, M.J., Collier, N.C., Agell, N., Bond, U. (1989). In: Pardue, M.L., Feramisco, J.R., Lindquist, S. (eds.) Stress-Induced Proteins, Alan R. Liss, N.Y.p. 127-148

Sconzo, G., Roccheri, M.C., DiCarlo, M., DiBernardo, M.G., Giudice, G. (1983). Cell Differ. 12:317-320

Sconzo, G., Roccheri, M.C., La Rosa, M., Oliva, D., Abrignani, A., Giudice, G. (1986). Cell Differ., 19:173-177

Shapiro, A.Z. (1981) Sov. J. Mar. Biol. 7, 132-136.

Shihira-Ishikawa I (1987). Jap J Phycol (Sorui) 35: 251-258

Sijens, P.E., Bovée, M.J., Seijkens, D., Los, G., and Rutgers, D.H. (1986) Cancer Res. 46, 1427-1432.

Smith, E. and J.F. Morrison (1969) J. Biol. Chem. 244, 4224-4234.

Solursh, M. (1986). In: Developmental Biology: A comprehensive synthesis. Vol.2. L. Browder ed. Plenum, New York, pp. 391-431.

Somorjai (1985) Eur. J. Biochem. 149, 79-83.

Speigel, E., Burger, M.M., and Speigel, M. (1983). Exp. Cell Res. 144:47-55.

Speigel, E., Howard, L., and Speigel,M. (1989). J. Morph. 199:71-92.

Strathmann, M.F. (1987). Reproduction and Development of Marine Invertebrates of the Northern Pacific Coast. University of Washington Press.

Straughan, D. (1976). American Petroleum Institute, Washington, D.C., p.119 Publ. #4280

Steer MW, Steer JM (1989). New Phytol 111: 323-358

Sturgess, J.M., Mitranic, M.M., and Moscarello, M.A. (1978). J. Microscopy, 114:101-105.

Subjeck, J.R., Shyy, T.-T. (1986). Cell. Physiol.19:C1-C17

Sugiyama, K. (1972). Dev. Growth Differ. 14:63-73.

Summers, R.G., Morrill, J.B., Nislow, C., Yudin, A. and Cherr, G. (1987). J. Cell Biol., 105:85a.

Sze, D.Y. and Jardetzky, O. (1990) Biochim. Biophys. Acta 1054, 181-197.

Taketani, S., Kohno, H., Yoshinaga, T., Tokunaga, R. (1989). Fed. Europ. Biochem. Soc., 245(1,2):173-176

Talbot, P. and DiCarlantonio, G. (1984). Gamete Res. 10:127-142.

Thébault, M.T., .P. Raffin, and J.Y. Le Gall (1987) Biochem. Biophys. Res. Comm. 145, 453-459.

Thompson, S.N. and Lee, R.W.K. (1985) J. Parasit. 71, 652-661.

Tiwari SC, Polito VS (1988). Protoplasma 147: 100-112

Travers, F., R. Bertrand, G. Roseau, and N. Van Thoai (1978) Eur. J. Biochem. 88, 523-528.

Turley, E.A., Brassel, P., and Moore, D. (1990). Exp. Cell Res. 187:243-249.

Ugurbil, K. (1985) J. Magn. Reson. 64, 207-219.

Ullrich, K.J. (1956) Pflügers Arch. ges. Physiol. 262, 551-561.

Venema G, Koopmans A (1961). Cytologia 27: 11-24

Viarengo, A., Pertica, M., Mancinelli, G., Zanicchi, G., Orunesu, M. (1980). Comp. Biochem. Physiol., 67C:215-218

Wagner, G. and K. Wüthrich (1979) J. Magn. Reson. 33, 675-678.

Williamson RE (1986). Plant Physiol 82: 631-634 Walsh, P.J., McDonald, D.G., and Booth, C.E. (1984) Mar. Biol. Lett. 5, 359-369.

Wieser, W. and E. Wright (1979) Hoppe-Seyler's Z. Physiol. Chem. 360, 533-542.

Welch, W.J., Feramisco, J.R., Blose, S.H. (1985). Ann. N.Y. Acad. Sci., 455:57-67

Welch, W.J., Mizzen, L.A., Arrigo, A.-P. (1989). In: Pardue, M.L., Feramisco, J.R., Lindquist, S. (eds.) Stress-Induced Proteins, Alan R. Liss, New York, p. 187-202

Wessel, G.M., Marchase, R.B., McClay, D.R. (1984). Dev. Biol. 103:235-245

Wessel, G.M., McClay, D.R. (1987). Dev. Biol. 121:149-165

Widdows, J., Bayne, B L., Livingstone, D.R., Newell, R.I E., and Donkin, P. (1979). Comp. Biochem. Physiol. 62A, 301-308.

Wijsman, T.C.M. (1976). J. Comp. Physiol. 107, 129-140.

Wijsman, T.C.M. (1975). in Proc. 9th Europ. Mar. Biol. Symp., pp.129-149.
Wilson L, Meza I (1973). J Cell Biol 58: 709-718
Wolpert, L. and Mercer, E.H. (1963). Exp. Cell Res. 30:280-300.
Yudin, A.I., Cherr, G.N., and Katz, D.F. (1988). Cell Tissue Res. 251:555-564.
Zurburg, W., de Bont, A. M. T., and de Zwaan, A. (1982). Mol. Physiol. 2, 135-147.
Zs-Nagy, I. and Ermini, M. (1972). Comp. Biochem. Physiol. 43B, 593-600.